UNIVERSITAT POLITÈCNICA DE VALÈNCIA

DEPARTAMENT D'ENGINYERIA QUÍMICA I NUCLEAR

DOCTORAL THESIS

DEVELOPMENT, ASSESSMENT AND APPLICATION OF COMPUTATIONAL TOOLS FOR DESIGN SAFETY ANALYSIS OF LIQUID METAL COOLED FAST BREEDER REACTORS

Author:

Aurelio Lázaro Chueca

Director:

PhD Sebastián Martorell Alsina

Supervisor at JRC-IET:

PhD Luca Ammirabile

May 2014

Idilio atómico y uránico-melancólico / Atómica melancolía

Salvador Dalí

***Abstract*:**

Nuclear energy has been identified as a potential contributor to reduce the greenhouse effect gases emissions and consequently it should play an important role in the electricity production mix of every country. Developing countries can also find in nuclear energy the solution to power their expected growth. The current fleet of nuclear reactors is based on a technology designed in the early stages of the nuclear power development and presents as major concerns its associated nuclear waste disposal, its high safety requirements and its financial hurdles.

The Generation IV International Forum (GIF) is an international R&D platform with the objective to coordinate the envisaged efforts needed to develop a new generation of nuclear reactors. The organisation has identified a selection of nuclear designs with potential to meet the highest technological objectives; improved fuel management capabilities, higher reliability and safety standards and economic competitiveness regarding any other energy source.

Among these designs, Liquid Metal cooled Fast Breeder Reactors (LMFBRs) stand out due to its potentiality to achieve the ambitious goals presumed for the new generation of nuclear reactors. The Sodium Fast Reactor (SFR) and Lead Fast Reactor (LFR) are the preferred technologies due to their benign thermo-mechanical and chemical coolant characteristics.

In order to assess the compliance of the proposed designs with the highest safety standards it is needed to apply computational tools able to simulate the system behaviour under conditions that may overtake the reactor safety limits from the early stages of its design process. These computational tools should also be detailed enough to take into account the particular phenomena related with fast reactors including three-dimensional effects that may occur during certain transients.

The objective of the research work in this PhD thesis has been to develop, assess and apply advanced computational tools and models for the design basis analysis of liquid metal cooled fast breeder reactors.

The first part of the thesis outlines the development of a one-dimensional thermal-hydraulic model of the European Sodium Fast Reactor (ESFR) design with point kinetic neutronic feedback, which has been benchmarked with its peers in the framework of the FP7-CP-ESFR project, using a state-of-the-art thermal-hydraulic system code TRACE. The model is applied to analyse the system behaviour withstanding the most severe Design Basis Accident initiator identified in the safety assessment of the design, the Unprotected Loss of Flow (ULOF) transient. The same process is applied to develop an equivalent model of the Lead Fast Reactor (LFR) demonstrator called ALFRED in the framework of the FP7-CP-LEADER project.

The last and most important part of the research work focuses on the development and application of the extension of the one-dimensional model into a three-dimensional thermal hydraulic model, which is coupled with a spatial neutronic model that upgrades the point kinetic neutronic feedback used previously. The coupled TRACE-PARCS system codes are used. These coupled tools allow performing calculations with a higher detail level, and especially, reproducing asymmetric phenomena, such as the coastdown of single primary and secondary pumps or the withdrawal of a peripheral control rod bank, demonstrating the unique capability

of the code to simulate such transients and the capability of the design to withstand them under safety limits.

The final chapter of the PhD thesis presents the conclusions and main contributions of the research work and envisage topics for further research.

Key-words: Generation IV, Sodium Fast Reactor, ESFR, CP-ESFR, Lead Fast Reactor, ALFRED, LEADER, Multi-physics, Thermal-hydraulics, Neutronics, Asymmetric transients, ULOF, UTOP, TRACE, PARCS.

Resumen:

La producción eléctrica de origen nuclear tiene la destacada ventaja de no conllevar emisiones de gases de efecto invernadero y por lo tanto contribuye a limitar la huella antropogénica en el medio ambiente si forma parte de la producción eléctrica global. Los países en vías de desarrollo también pueden encontrar en la energía nuclear la solución tecnológica con la que potenciar su esperado crecimiento.

La generación actual de reactores nucleares está basada en una tecnología diseñada durante las primeras fases del desarrollo de la energía nuclear y todavía no ha superado alguno de sus inconvenientes tales como la gestión de los residuos radiactivos, los elevados requisitos de seguridad y sus inconvenientes financieros.

La "Generation IV International Forum" es una plataforma de investigación y desarrollo internacional con el objetivo de coordinar los esfuerzos prospectivos necesarios para desarrollar una nueva generación de reactores nucleares. Esta organización ha identificado una serie de diseños de reactores nucleares potencialmente capaces de alcanzar los más altos objetivos tecnológicos exigibles a ésta tecnología, como son una gestión avanzada de los residuos, una aumentada seguridad y fiabilidad y competitividad económica con respecto a cualquier otro medio de generación eléctrica. Entre estos diseños destacan los que son objeto de estudio en esta tesis, los reactores rápidos refrigerados por metales líquidos.

Para asesorar el cumplimiento de los diseños propuestos con estos elevados objetivos de seguridad es necesaria la aplicación de herramientas computacionales capaces de simular el comportamiento de la planta nuclear en condiciones que pueden superar los límites de seguridad establecidos y que deben considerarse desde las fases más tempranas del diseño. Estas herramientas computacionales deben tener también el suficiente grado de detalle para simular los fenómenos particulares que acontecen en los diseños propuestos y los efectos tridimensionales que pueden surgir en transitorios con componentes asimétricas.

El objetivo de este trabajo de investigación ha sido el de desarrollar, asesorar y aplicar estas herramientas y modelos computacionales para el análisis de seguridad de diseños innovadores de reactores rápidos reproductores refrigerados por sodio y plomo.

La primera parte de la tesis expone los desarrollos del modelo termohidráulico unidimensional con respuesta neutrónica de cinética puntual del prototipo de reactor rápido avanzado refrigerado por sodio "European Sodium Fast Reactor" usando un código puntero de modelado termohidráulico como el código TRACE. Este modelo fue contrastado con sus modelos equivalentes en el marco del proyecto europeo CP-ESFR dentro del programa FP7. El modelo se aplicó para analizar la seguridad del sistema para soportar el accidente base de diseño potencialmente más dañino identificado en los estudios preliminares de seguridad del reactor, el transitorio desprotegido de pérdida de refrigerante. Un proceso análogo se aplicó para desarrollar un modelo equivalente del prototipo de reactor rápido refrigerado por plomo ALFRED en el marco del proyecto europeo CP-LEADER.

La última y más importante etapa del proceso de investigación se centró en la extensión del modelo termohidráulico unidimensional del reactor de sodio ESFR a un modelo termohidráulico tridimensional acoplado con el modelo de neutrónico espacial que sustituye a la aproximación basada en cinética puntal anteriormente utilizado, para ello se utilizó el código de acoplamiento TRACE-PARCS.

Estos modelos acoplados realizan simulaciones con un elevado nivel de detalle al implicar cálculos multifísicos y permite la simulación de fenomenología asimétrica dadas sus capacidades tridimensionales. Esto supone un paso adelante respecto del estado de la herramientas de este tipo aplicadas a reactores avanzados y permite el análisis de transitorios no estudiados hasta el momento tales como la parada de una única bomba en el circuito primario y secundario o la extracción de barras de control situadas en posiciones periféricas.

Los últimos capítulos de esta tesis doctoral exponen los resultados del análisis de dichos transitorios demostrando la capacidad de los modelos para simularlos y la capacidad del diseño para soportarlos bajo los límites de seguridad establecidos.

El capítulo final expone las conclusiones y aportaciones científicas relevantes del trabajo de investigación desarrollado. También se indican los posibles objetivos de investigación futura a los que este trabajo puede servir como base.

Palabras-clave: Generación IV, Reactor Rápido de Sodio, ESFR, CP-ESFR, Reactor Rápido de Plomo, ALFRED, LEADER, Multi-físico, Termohidráulica, neutrónica, transitorios asimétricos, ULOF, UTOP, TRACE, PARCS

Resum:

La producció elèctrica d'origen nuclear té el destacat avantatge de no comportar emissions de gasos d'efecte hivernacle i per tant, contribueix a limitar l'empremta antropogènica en el medi ambient, si forma part de la producció elèctrica global. Els països en vies de desenvolupament també poden trobar en l'energia nuclear la solució tecnològica amb la qual potenciar el seu esperat creixement.

La generació actual de reactors nuclears està basada en una tecnologia dissenyada durant les primeres fases del desenvolupament de l'energia nuclear i encara no ha superat inconvenients tals com la gestió de residus radioactius, els elevats requisits de seguretat i els seus inconvenients financers.

La "Generation IV International Forum" es una plataforma d'investigació i desenvolupament internacional amb l'objectiu de coordinar els esforços necessaris per a desenvolupar una nova generació de reactors nuclears. Aquesta organització ha identificat una sèrie de dissenys de reactors nuclears potencialment capaços d'assolir els més alts objectius tecnològics exigibles a aquesta tecnologia com son, una gestió avançada dels residus, una augmentada seguretat i fiabilitat i competitivitat econòmica respecte a qualssevol altre medi de generació elèctrica. Entre aquests dissenys destaquen aquells que són objecte d'estudi en aquesta tesi, els reactors ràpids refrigerats per metalls líquids.

Per a garantir el compliment del objectius de seguretat dels dissenys proposats, és necessària l'aplicació d'eines computacionals capaces de simular el comportament de la planta nuclear en unes condicions en les que és probable que es superen els límits de seguretat establerts i que han de considerar-se des de les fases més primerenques del disseny. Aquestes eines computacionals han de tindre també el suficient grau de detall per a simular els fenòmens particulars que esdevenen en els dissenys proposats i els efectes tridimensionals que poder sorgir en transitoris amb components asimètrics.

L'objectiu d'aquest treball d'investigació ha sigut el de desenvolupar, assessorar i aplicar aquestes eines i models computacionals per a l'anàlisi de seguretat de dissenys innovadors de reactors ràpids reproductors refrigerats per sodi i plom.

La primera part de la tesi exposa els desenvolupaments del model termohidràulic unidimensional amb resposta neutrònica de cinètica puntual del prototip de reactor ràpid avançat refrigerat per sodi "European Sodium Fast Reactor", ESFR, utilitzant un codi punter de modelat termohidràulic, el codi TRACE. Aquest model fou contrastat amb els seus models equivalents en el marc del projecte europeu CP-ESFR dins del programa FP7. El model es va aplicar per a analitzar la seguretat del sistema per a suportar l'accident base de disseny que potencialment té majors conseqüències identificat en els estudis preliminars de seguretat del reactor, el transitori desprotegit de pèrdua de refrigerant. Un procés anàleg es va aplicar per a desenvolupar un model equivalent del prototip de reactor ràpid refrigerat per plom, anomenat ALFRED, en el marc del projecte europeu CP-LEADER.

L'última i més important etapa del procés d'investigació es va centrar en l'extensió del model termohidràulic unidimensional del reactor de sodi ESFR a un model termohidràulic tridimensional acoblat amb el model neutrònic espacial que substitueix a l'aproximació basada

en cinètica puntual anteriorment utilitzat, per a això s'utilitzà el codi d'acoblament TRACE-PARCS.

Aquests models acoblat realitzen simulacions amb un elevat nivell de detall al implicar càlculs multi físics i permet la simulació de fenomenologia asimètrica, donades les seues capacitats tridimensionals. Açò suposa un pas endavant respecte del estat de les eines d'aquest tipus aplicades a reactors avançats i permet l'anàlisi de transitoris no estudiats fins al moment tals com l'aturada d'una única bomba en el circuit primari i secundari o l'extracció de barres de control situades en posicions perifèriques.

Els últims capítols d'aquesta tesi doctoral exposen els resultats de l'anàlisi dels esmentats transitoris demostrant la capacitat dels models per a simular-los i la capacitat del disseny per a suportar-los sota els límits de seguretat establerts.

El capítol final exposa les conclusions i aportacions científiques rellevants del treball d'investigació desenvolupat. També s'indiquen els possibles objectius d'investigació futura als que aquest treball pot servir com base.

Paraules-clau: Generació IV, Reactor Ràpid de Sodi, ESFR, CP-ESFR, Reactor Ràpid de Plom, ALFRED, LEADER, Multi físic, Termohidràulica, Neutrònica, Transitoris Asimètrics, ULOF, UTOP, TRACE, PARCS.

This research work has been done in the frame of a collaboration between the

Joint Research Centre – Institute for Energy and Transport

and the Universitat Politècnica de València.

A mi familia

Index

Figures

Tables

1. Introduction

1.1 Background

From a techno-economic perspective, energy is not only a simple commodity, it is the commodity that allows us to make use of any other good produced by the human being. Nowadays, the development of a robust and reliable energy sector, able to promote a sustainable and secure energy solution is pivotal to every economic, environmental and developmental issue. The world needs low-carbon, efficient and reliable energy services to meet its long-term needs for economic growth and development. Similarly, developing countries need modern and reliable energy production systems able to sustain their expected growth. For that reason, it is a challenge for the human being to find energy sources able to power our continuous and increasing needs.

We have developed means to convert the energy of the sun into electric power, namely, thermal and photoelectric installation and windmills. Unfortunately, these renewable energy sources present the disadvantage that it is difficult to generate large quantities of electricity as those produced by traditional sources with the need to reduce the amount of energy we use or to build more energy facilities. Another disadvantage of renewable energy sources is linked to the reliability of supply: key renewable energy sources such as solar and wind energy rely on the weather for its source of power which is affected by much variability and whose predictability is still poor, particularly in the short term. In addition the current cost of renewable energy technology is far higher than traditional electricity generation since it is a new technology and as such has extremely large capital cost. For these reasons, conventional fossil and nuclear energy sources remain those that allow us to have energy in a discretionary way.

However, the climate change characterized by the climate system's warming trend likely caused by anthropogenic greenhouse gas (GHG) emissions can strongly limit the use of fossil fuels in the near future. In fact energy-related greenhouse gas emissions are the dominant contributor to climate change and are projected to further increase in the following years. Current patterns of energy production and consumption are more and more unsustainable and threaten the environment on both local and global scales. Reducing greenhouse gas emissions from the burning of fossil fuels is at the heart of current efforts to address climate challenge.

In this respect nuclear energy has demonstrated its reliability in providing a constant, competitive and carbon- free production of electricity during its more than 60 years of industrial experience. So, in principle it could play an important role in the current and future national

energy mixes. Nevertheless, nuclear power still has to overcome important drawbacks such as nuclear waste management, proliferation risk, economic feasibility and, especially, safety concerns. To this respect new designs have been studied that could theoretically provide a higher level of safety than current LWR while assuring a sustainable use of nuclear energy.

The Generation IV International Forum (GIF) [GenIV, 2002] is an international initiative with the objective of setting a common roadmap for the R&D efforts needed to conceive a new generation of nuclear reactors that will excel in its waste management capabilities, enhanced safety standards and economic competitiveness. Among the proposed designs, liquid metal cooled reactors stand out due to their potentiality to reach the challenging objectives defined in the initiative and also due to the existing past experience in related projects.

Ensuring that these designs reach the highest safety standards require the development and validation of methods and tools to be applied to this innovative technology. There is a need to generate an entire methodology to assess these new designs, covering from modelling guidelines to regulatory framework and for that the use of validated computations tools is essential.

These computational tools should receive the legacy of their peers applied to the current reactor technology but should be adapted to the peculiar characteristics of fast reactors.

This thesis is a contribution to such a purpose.

1.1.1 The Generation IV International Forum

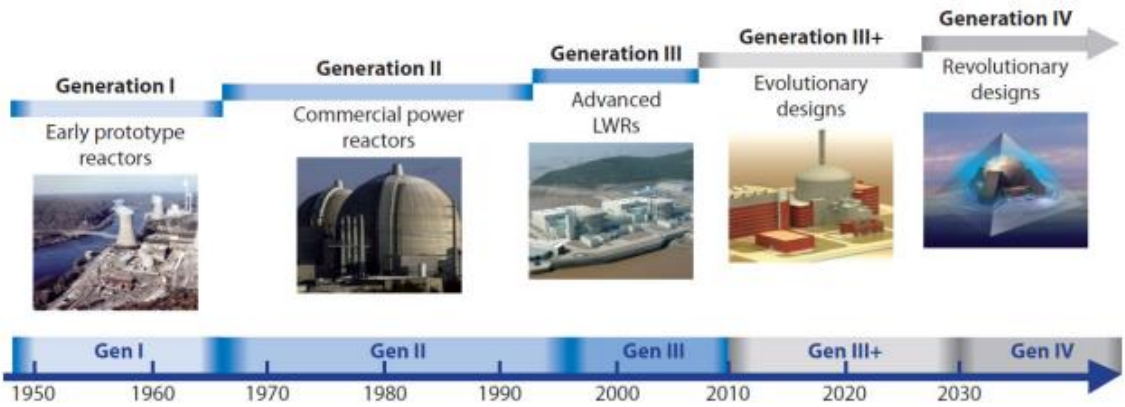

Figure 1: Evolution of the nuclear power technology generations [GenIV, 2002]

The Generation IV International Forum is an international initiative to define the R&D needs for developing a new generation of nuclear reactors.

This organisation is composed by 13 countries (Argentina, Brazil, Canada, China, Euratom, France, Japan, Republic of Korea, Russia, Republic of South Africa, Switzerland, United Kingdom

and United States). The objective of such organisation is to agree on a framework for international cooperation in research towards the development of a future generation of nuclear energy systems that can be licensed, constructed and operated. These nuclear energy systems are designed to meet the following goals [GenIV, 2014]:

- Sustainability: The designs should provide sustainable energy production making a more efficient use of the nuclear fuel and at the same time notably reduce the long term stewardship burden.
- Safety and reliability: These designs will excel in safety and reliability, having a very low likelihood and degree of reactor core damage and no need for offsite emergency response.
- Economic competitiveness. The designs should have a clear life-cycle cost advantage and a low financial risk compared with other energy sources.

For those challenging purposes different countries decided to share their particular expertise in a pool where synergies between the different national research programmes could arise. The first objective was to define the different reactor technology envisaged to be able to reach these challenging goals. With almost a hundred different designs being scrutinized, six reactor concepts were finally selected:

- Gas-Cooled Fast Reactor System
- Lead-Cooled Fast Reactor System
- Molten Salt Reactor System
- Sodium-Cooled Fast Reactor System
- Supercritical-Water-Cooled Fast Reactor System
- Very-High-Temperature Reactor System

Currently, GIF is organising the initiatives to convert those concepts into feasible designs to have them available for deployment by 2030, when a great share of the current nuclear power plant fleet will be near the end of their operative phase.

1.1.2 Liquid metal cooled fast breeder reactors

This thesis is focused on the safety assessment of a particular type of the aforementioned designs: the Liquid Metal Cooled Fast Breeder Reactors. These reactor designs use liquid metal coolants, sodium and lead, to extract the nuclear generated power. Their physical properties (i.e. thermal conductivity, heat capacity and boiling point) justify their use as a coolant. In addition to this, the particular nuclear properties of these materials (i.e. atomic mass) are essential to reach a high energy neutronic spectrum in the core that will allow breeding.

Breeding is the name of the mechanism that takes place when a fertile isotope U238, which is the predominant isotope of natural uranium (>99%), is converted into a fissile isotope Pu239

that produces fission reactions. The degree of conversion that takes place in a reactor is defines the breeding ratio [WalRe,1981].

$$CR = \frac{fissile\ material\ produced}{fissile\ material\ destroyed}$$

A breeder reactor is such nuclear system with CR>1. To reach that threshold it is necessary to have an optimal neutronic economy, which means that the ratio between the number of neutrons emitted and the number of neutrons absorbed should be as high as possible. This ratio increases remarkably for high energy reactions as Figure 2 shows. This is the rationale behind fast neutron reactors designs.

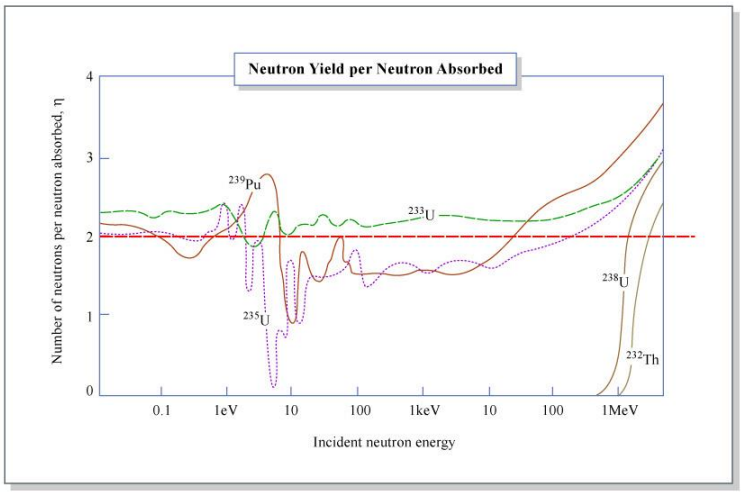

Figure 2: Neutrons yield per neutron absorbed

Consequently, fast breeder reactors allow the production of fissile material at least at the same ratio that fissile material is consumed. This would allow to have a sustainable, carbon-free energy source with a reactor fleet able to operate with an efficient use of the nuclear fuel and lowering the amounts of highly radioactive content of the nuclear waste.

1.1.3 LMFBR history. The past experience

The idea of fast breeder reactor is not new, on the contrary, it was conceived in the early stages of the nuclear technology development. This first fast reactor, called Clementine, was built in Los Alamos National Laboratory in USA in 1946. A few years later, Enrico Fermi and Walter Zinn fostered the first fast breeder reactor, the *Experimental Fast Breeder Reactor – I* (EBR-I) in 1951, becoming the first nuclear plant in history to generate electricity.

The EBR-I experimental facility constituted also the first Sodium Fast Reactor (SFR) to be built. It was followed up by the EBR-II [Sackett, 1997], which entered into operation in 1964 and operated until 1994. These two have been the two main projects carried out in the USA.

In Europe, France has been the country most determined to develop LMFBRs. The first of the kind was called *Rapsodie* prototype. It began its operation in 1967 and last until 1983. It was continued by the *Phenix* [Sauvage, 2005] prototype, which began its operation in 1974 and was shutdown in 2009. It was a pool type sodium reactor with an electrical power output of 250MW. During these years produced 20 billion kWh of electricity and was loaded with 51 fuel cycles. The construction of the first full power LMFBR started in 1977 with the *SuperPhenix* plant. It reached full power operation in 1986. The plant faced a range of technical and political drawbacks that forced its shutdown in 1998.

Japan has been the main actor for the LMFBRs development in Asia. Its first experimental facility was Joyo plant, which became critical in 1977. It was upgraded to an irradiation test facility which is still in operation. Japan´s LMFBRs programme continued with the Monju [Matsuura et al, 2007] facility. It was a loop type SFR prototype reactor designed to generate 280MWe. It reached the first criticality in 1994 and supplied electrical power one year after. It suffered a sodium leakage accident that caused the programme suspension. It was restarted in 2010 but it was discontinued few months later as a consequence of the Fukushima accident.

The Soviet Union also showed interest in LMFBRs development. In 1956, the BR-1 prototype with a thermal power of 100W reached criticality. It was upgraded with BR-2 (100kW) and BR-10 (10MW). The BN-350 was the first Soviet full scale SFR built in 1973 with an electrical output of 350MW. The BN-600 [Buksha et al, 1997] was a pool type SFR reactor completed in 1979 with an electrical power of 600MW. Currently, the reference design is the BN-800 [Saraev et al, 2012].

The operational experience of Lead Fast Reactors (LFR) is much shorter that the experience achieved with SFR technology. LFR designs were used by the Soviet Union as nuclear reactors for submarine propulsion. Nevertheless, in the 1990s Russia renewed its interest in LFR technology with its application to civil purposes.

The Sustainable Nuclear Energy Platform (SNTP) [SNETP, 2009] is a European organisation gathering together 75 members from 19 European countries involved in nuclear technology research. This organisation has prioritised and coordinated the R&D European initiatives in three designs, the Sodium-cooled Fast Reactor (SFR), the Lead-cooled Fast Reactor (LFR) and the Gas-cooled Fast Reactor (GFR). The organisation has defined also a roadmap for the development of such technologies. This roadmap is shown in Figure 3.

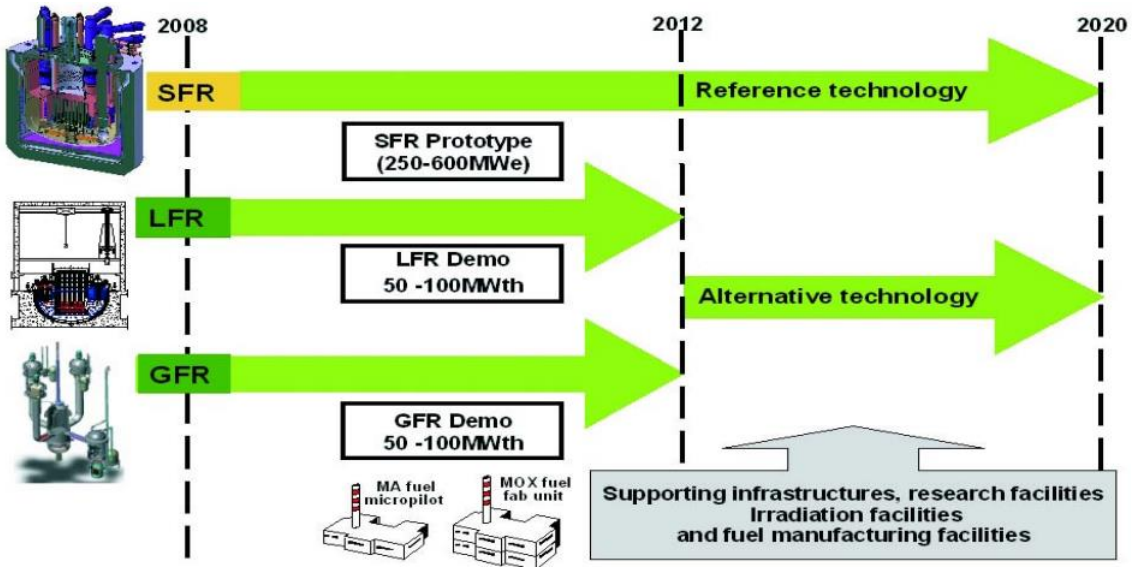

Figure 3: Fast reactor technology roadmap [SNETP, 2009]

1.2 Nuclear Safety in Liquid Metal Fast Breeder Reactors

A nuclear facility as any industrial installation is, in case of accident, a potential source of harm to humans, environment as well as a possible loss of investments. Therefore, any installation should be secured with the highest safety standards that ensure its uncompromised safety.

Nuclear power plants are designed to maintain their integrity and performance for a bounding set of normal operational events as well as abnormal events that are expected to occur or might occur at least once during the lifetime of the plant. In addition, they are designed to maintain performance of safety functions for a set of Design Basis Accidents (DBA) which involve failures that are possible but unlikely to occur during the plant lifetime [IAEA, 2012]

The so-called Beyond Design Basis Accidents (BDBA) comprises those accidents which are postulated and physically possible but not considered in the design due to the extreme low probability of occurrence.

For obvious reasons intrinsic to the nuclear technology it is not possible to test such transients on a plant scale. Rather separate and integral experimental facilities [Wolfert et al, 1988] are built on smaller scale to investigate the phenomenology of such transients in order to extrapolate the results at plant level. In this respect the development of computational tools that are validated against those experiments and hence are able to perform reliable simulations of the behaviour of the plant during those transients is essential.

The outcomes of these transient simulations are then compared with a set of deterministic design criteria that will allow to evaluate if the design is able to withstand those credible accidents. If any of the considered key safety working variables of the plant is over the figures of merit established in the design criteria the design should be modified.

An initial classification of the transients to be considered in the safety assessment of the design of fast reactors consists in dividing them between protected and unprotected transients. The protected transient implies the successful operation of the plant protection system when called upon to function while the postulated unprotected transient will lead the plant to evolve without the intervention of any protection system.

The postulated transients can be classified based on the nature of the cause that generates the accident. In this respect, we can consider the following classification;

- Reactivity transient. These transients are triggered by a variation of the core reactivity, which can be caused by the incorrect withdrawal of a control rod, the spurious ejection of a control rod, a core loading error, a reduction of the coolant inlet temperature, the addition of a moderator, voiding the core with gas or variations in the core geometry.
- Cooling accidents. These transients are triggered by a variation in the cooling capability, which can be caused by a pump failure (the so called Loss of Flow (LOF) accidents), valve failure, the loss of primary coolant, leak in the intermediate heat exchangers or the failure in the decay heat removal system or a failure of the diagrid.
- Sub-assembly cooling accidents. These transients are triggered by a local variation of the cooling capability due to the incorrect position of a sub-assembly, the inlet or outlet blockage of a sub-assembly, a local blockage or cooling defects of a subassembly or the pin failure and its damage propagation within the sub-assembly and the core.
- Accidents outside the core. This category includes; fuel handling accidents, coolant-water reaction in the steam generators, fires or radioactive releases.
- Internal and external hazards induced accidents. This category includes natural occurrences such as fires, earthquakes, tsunamis, floodings…, airplanes, missiles, explosions, gas releases.

For any of these transients the design has to demonstrate that it is able to keep the plant in safe conditions and without exceeding any of the safety parameters as defined in the safety assessment of the design.

1.3 Purpose, objectives and methodology of the research

The purpose of this research work is to develop, assess and apply advanced computational tools and models for the design basis analysis of liquid metal cooled fast breeder reactors.

These computational tools and models should be able to perform more reliable and accurate simulations of the system behaviour under postulated transients triggering accident scenarios that may threaten the plant integrity. These accident scenarios involve complex thermal-hydraulic and neutronic phenomena for which a three-dimensional multi-physics approach is essential to reach a complete and exhaustive understanding of the processes taking place.

The LMFBRs are considered among the proposed systems in the Generation IV International Forum as well as in the European Sustainable Nuclear Industrial Initiative (ESNII) in support of the SET-Plan. Therefore, this analysis is a potential contributor to the optimisation process of the proposed designs.

The design of the two LMFBR systems proposed in GIF, the SFR and LFR, have been identified in the framework of two European research projects. These designs are the European Sodium Fast Reactor (ESFR) developed in the FP7 CP-ESFR project [Vasile et al, 2011] and the LFR prototype ALFRED developed in the FP7 LEADER project [LEADER, 2010].

The approach followed to reach the objectives of the research was:

1. Review of the state-of-the-art on advanced computational tools and to identify the most suitable ones to be adapted for multi-physic safety analysis of LMFBR designs. The TRACE system code developed by the Nuclear Regulatory Commission (NRC) was identified as the tool to perform the thermal-hydraulics studies. The spatial neutronic deterministic code PARCS was selected to supply the neutronic response of the system.
2. Adapt the selected codes to the LMFBR technology. While these codes were essentially developed for LWR technology the fundamental equations remain also valid for other coolants than water provided that *ad-hoc* correlations and methods specific to LMFBR technology are implemented in the codes.
3. One-dimensional model development of the SFR design. Framed in the Collaborative Project on the European Sodium Fast Reactor design (CP-ESFR) a one dimensional model of the ESFR design was developed for the adapted TRACE system code. The results of the simulations performed with this model were compared with the equivalent ones developed by other organisations also partners of the project as a benchmarking to proof the consistency of the results.
4. One dimensional model development of a LFR design. Framed in the Collaborative Project LEADER (CP-LEADER) a one dimensional model of the ALFRED design was also

developed. The results were also benchmarked with equivalent models of the other organisations participating in the project.

5. Upgrade of the SFR design into a three-dimensional thermal-hydraulics model. The one-dimensional model developed for the ESFR design was upgraded to take into account three-dimensional thermal-hydraulic phenomena that may take place in the system during the transients. This innovative model allows the analysis of asymmetrical thermal-hydraulic transients, which were not feasible with the one dimensional model. Since there is no equivalent 3-D model, the results were benchmarked with the one dimensional model results limited to the symmetric transient considered.
6. Development of a spatial kinetic core model. All the models developed until this point include a point kinetics neutronic feedback. This approach is satisfactory for one dimensional thermal-hydraulic models due to the symmetric restriction, but in order to have a three-dimensional multi-physic perspective of the system evolution during the analysed transients a consistent thermal-hydraulics and neutronic spatial profile is required. For that reason a three-dimensional neutronic model of the core was developed for the ESFR core design for the spatial kinetics code PARCS taking as input the representation of the core materials in terms of a Cross Section (XS) set.
7. Thermal-hydraulic and neutronic coupling scheme. After the neutronic model of the core demonstrated to provide accurate result for static calculation, the next step towards an integrated multi-physic dynamic calculation tool was the online coupling between the thermal-hydraulic and the neutronic calculation feedback. This is done by mapping the thermal-hydraulic model nodes with the neutronic model ones in such a way that the thermal-hydraulic calculation takes into account the power profile generated by the neutronic calculation and this last one takes into account the thermal conditions of the coolant and core materials during the analysed transient.
8. Assessment of the coupled calculations. After the idea was technically implemented it was checked against the previous calculations to prove the capability of this multi-physics platform to perform symmetrical transient calculations.
9. Asymmetrical transients. After the platform was benchmarked and proved the capability to perform symmetric transients it was ready to be used to take advantage of its unique capability to perform asymmetrical accidental cases. Different transients involving asymmetric effects were calculated to assess the system response to accommodate the localised effect that they may trigger.
10. Safety Assessment of the designs. With the simulations performed by the generated computational tool and models in its different stages a first approach to the safety assessment of the design can be done. Since all the transients considered were in unprotected conditions, the results obtained can be used to define the unleashing values and grace times for the protection systems design.

1.4 Thesis structure

This thesis is structured as follows:

Chapter 1

The current first chapter is an introduction, providing the background and rationale on which the doctoral work was performed including a description of the approach followed as well as of the structure of the thesis.

Chapter 2

The second chapter includes the state-of-the-art of the LMFBR designs considered. It gives an overview of the technology insights and safety principles. The recent and current research projects that foster this thesis are also described.

The chapter also includes a brief description of the computational tools used and a detailed report on the modifications performed on their source code in order to adapt them to the LMFBR requirements.

Chapter 3

The third chapter gives a detailed explanation of the methods and tools used in this thesis. This chapter includes a detailed explanation of the thermal-hydraulic models of the SFR and LFR plant designs developed for TRACE system code including the point kinetic neutronic scheme to take account of the neutronic feedback in the calculation. This chapter also describes the insight of the extension of the SFR thermal-hydraulic model into a three-dimensional model.

A complete neutronic model description for the neutronic code PARCS including the cross-section set generation using the Monte Carlo based code SERPENT follows including the description of the coupling scheme used to interconnect the thermal-hydraulic and neutronic model.

Chapter 4

The fourth chapter describes in detail the results obtained with the developed one dimensional SFR (ESFR) and LFR (ALFRED) models to simulate a set of transient postulated in the design basis safety assessment in unprotected conditions.

This section includes the different benchmarking exercises to test the consistency of the models.

Chapter 5

The fifth chapter includes the extension of the one-dimensional model of the ESFR into a three-dimensional model and the coupling with the spatial neutronic model.

The chapter includes the benchmark against the one-dimensional model performed for symmetrical cases and the asymmetrical transients simulated.

The chapter also shows the added value of the multi-physics platform, the simulation of three asymmetrical transients (the asymmetric coastdown of primary and secondary single pumps and the asymmetric withdrawal of a control rod). The analysis of the results of the asymmetrical calculations in terms of the safety analysis of the design is also indicated.

Chapter 6

The sixth chapter summarizes the research work done including a detailed analysis of the objectives fulfilled and the consequences that arise from it. This chapter also includes a first safety analysis of the considered designs.

Finally, a number of indications is given about possible further developments based on the achievements of this thesis.

2. State of the art

This chapter outlines the technological framework for which the research work has been developed. It covers from an overview of the technical basis of fast breeder reactors to the description of the latest designs developed in recent international research projects.

This section also deals with an overview of the computational tools used to perform the safety studies along with the modifications implemented in order to adapt them to liquid metal cooled fast reactor technology.

2.1 The technology: Liquid Metal Fast Breeder Reactors. Design considerations.

As mentioned in the introduction, Liquid Metal Fast Breeder reactors are nuclear reactors operating with a fast neutronic spectrum.

The availability of a fast spectrum allows both breeding and transmutation capabilities. Fertile U238 can produce fissile material at least at the same ratio at which it is consumed while long-life minor actinides can be “burnt” into shorter-life waste lowering down of the amount and toxicity of the nuclear waste.

These features are expected in a new generation of nuclear reactor designs characterized by a level of safety that is higher than in current light water reactors. The importance of the safety objectives has become overriding in the aftermath of the Fukushima-Daichi accident.

The safety assessment of such designs is crucial to ensure that the expected high level of safety is achieved. This becomes particularly complex when innovative concepts are assessed. Current international R&D efforts are taking place to develop, integrate and harmonize methodologies of the safety assessment practices to be applied to these innovative nuclear designs [SARD3.5, 2012].

The next sections briefly describe the fundamentals of this technology including design safety principles and design considerations together with the specific plant designs this thesis deals with.

2.1.1 Fundamentals of the technology.

In a very simplistic approach we can consider the fundamentals of a technology as the suitable materials and its distribution and interaction to reach the purpose of the design. In this sense, we can identify as fundamental material of a fast breeder reactor design the coolant used (in this case only liquid metal coolants are considered), fuel materials, cladding materials and control materials.

2.1.1.1. The Coolant

The subject of this research work are nuclear reactors cooled by liquid metals, in particular Sodium and Lead. The choice of the coolant for a fast breeder reactor has a very important effect in the overall plant layout design [WalRe, 1981]. The coolant influences the neutronic design and conditions the selection of materials and systems (cladding material, pumps, heat exchangers…).

The principal objective of the coolant is to convey the heat from where it is generated (the core) towards where it is converted into a more suitable energy form, returning eventually to the core, which closes the thermodynamic cycle. Further to this objective, the selected coolant has to optimise some other properties, such as; thermal properties, neutronic behaviour, hydraulic characteristics and metallic compatibility.

From the thermal perspective the coolant is required to remove the very high power that is generated in the core (energy density four times higher than in a LWR). For that reason a high heat transfer coefficient is advisable. Another important thermal property of a fluid, with a very strong impact in the design and consequent safety studies, is the boiling temperature. The coolant void fraction is a major contributor for the neutronic behaviour of the system. Indeed, the abrupt change in the void fraction caused by the coolant boiling creates important neutronic perturbations with remarkable effects in the core performance. Consequently, for safety reasons, coolant boiling should be avoided in LMFBRs.

The following table (Table 1) shows the main thermal properties of different metal coolants. The characteristics of water are provided for the sake of reference.

Property	Na	NaK	Hg	Pb	H2O
T_{melt} (^oC)	98	18	-38	328	0
T_{boil} (^oC)	880	826	357	1743	100
Cp (kJ/(kg ^oC))	1.3	1.2	0.14	0.14	4.2
k (W/(m ^oC))	75	26	12	14	0.7
h (W/(m^2 ^oC))	36000	20000	32000	23000	17000
Rel. Pump Power	0.93	0.93	13.1	11.5	1

Table 1: Comparison of thermal properties for various liquid metals [WalRe, 1981]

It is important to remark the very high boiling temperature of lead (1743 ^{o}C), which confers the LFR designs an increased robustness against loss of coolant accidents.

From the neutronic perspective, the coolant has to allow high energy neutronic spectrum, what means that should not moderate the neutrons produced in the fission reactions.

In addition, the coolant should have low neutronic absorption. In fast reactors, the neutron economy is of special importance, since there is a need of ¨free¨ neutrons for breading and transmutation purposes. Thus, the neutronic absorption should be minimised. This low neutronic absorption cross section would also limit the coolant activation.

Another point to consider is the hydraulic behaviour of the coolant. It is a factor that remarkably affects the efficiency of the plant since part of the energy extracted from the core should be used to pump the coolant for its cooling down. The hydraulic characteristics of the coolant also affect the capability of the system to evolve into natural circulation in the hypothetical case in which the pumps stop working (the so-called loss of flow transients).

Finally, the compatibility of the coolant with other materials in contact with it is essential to secure the long term reliability of the system. Indeed, the coolant will be in direct contact with the material composing the cladding, the pipes and the heat structures in severe thermal conditions that may lead to material degradation, which should be avoided.

Among the possible liquid metal coolants available, both sodium and lead stand out due to their good balance of the aforementioned characteristics. As shown in the introduction, sodium has been selected in most of the LMFBR developed so far due to its excellent thermal properties, relatively low pumping power needs and excellent compatibility with other metals. Nevertheless, its major disadvantages are the highly exothermic chemical reaction with air and water and relatively low boiling temperature. On the contrary, lead and lead-bismuth coolants don´t react with air and water and present much higher boiling temperatures. On the other hand, their compatibility with other metals is much worse and corrosion processes can be expected to appear, which could limit the long term system reliability.

2.1.1.2. System Designs

This section presents an overview of the basic technology options [WalRe, 1981] to be considered within the design phase of the different reactor systems. This overview will introduce the design options taken in the sodium and lead cooled reactor concepts that are presented in the next sections of this chapter.

Core and Blanket

There are two basic choices regarding the distribution of the fertile material within the core. The first one, is the so called homogeneous configuration. In this configuration all assemblies containing pure fertile fuel are located in the axial and radial regions, called the axial and radial blanket respectively. This creates a uniform mixture of fissile and fertile fuel material throughout the core. The alternative is the heterogeneous core that combines fissile and fertile assemblies through the core layout. This configuration yields to higher breeding ratios and reduced sodium void effect, but it complicates the fuel managing capabilities in large cores.

Fuel assembly

With the aim to minimize the fissile concentration in the LMFBRs a tight fuel lattice that maximizes the fuel volume fraction in advisable. A triangular lattice arrangement (Figure 4) allows higher fuel volume fraction than a square one, which are frequently used in LWR. That is the reason why most of the LMFBRs designs include hexagonal fuel assemblies.

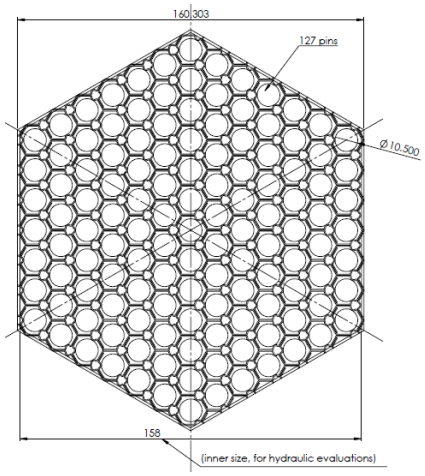

Figure 4: LMFBRs typical fuel assembly

Vessel internals

The first design option to define the primary system layout is the position of the core. The core structure can be hanged from the top of the reactor vessel or can lay at the base of the vessel with core support structures. This option is highly dependent on the size of the core and the coolant physical properties since buoyancy effects play an important role. The designs shown in the following sections present each of these two options.

Since the primary system is not pressurized the mechanical loads of the vessel are lower than in LWR. Indeed, the expected thickness of the vessel wall of a LMFBR is around 30 mm, so much lower than the typical value for a pressurized LWR (300 mm).

The assemblies are slotted in the position holes throughout the core support structure. Control rods enter from the top of the core.

In the most typical LMFBR configuration, the coolant flows from the lower part of the vessel (cold pool) through the core until reaching a big sodium pool placed in the upper part of the vessel (hot pool). The coolant enters into the heat exchangers to transfer the heat to the secondary loop and reaches the pumps where it is ejected into the cold pool again.

System heat transfer

The features to implement the heat transfer within the system in a LMFBR is also highly dependent on the coolant choice. The safety concerns linked to the strong exothermal chemical sodium-water reaction impose the presence of an intermediate heat exchange loop in sodium fast reactor designs. This configuration is justified even without choosing water as the turbine fluid driver. A tube rupture, even with an inert gas, may trigger an accident scenario if this gas enters the core due to the positive reactivity caused by the density change.

The layout scheme of this configuration is shown in Figure 5.

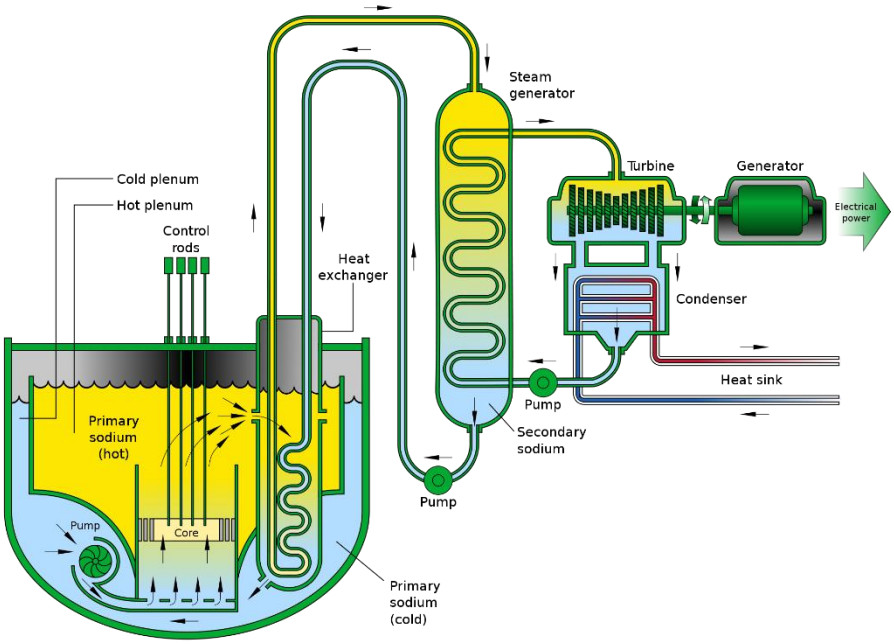

Figure 5: Sodium Fast Reactor layout scheme [GenIV, 2002]

On the contrary, in lead fast reactors the fact that the water-lead chemical reaction is limited and the strong buoyancy effect due to the high lead density makes the scenarios described above very unlikely. That is the reason why lead fast reactor designs don't include an intermediate heat exchange loop.

The layout scheme of this configuration is shown in Figure 6.

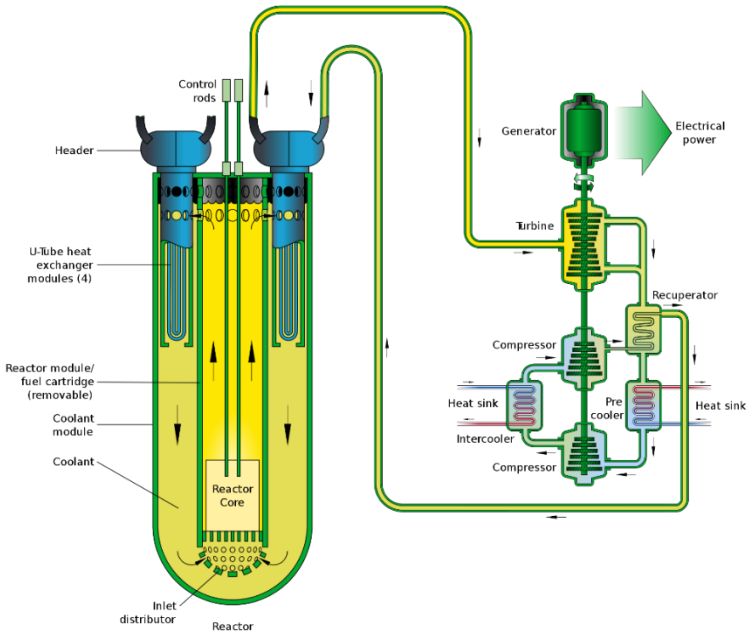

Figure 6: Lead Fast Reactor layout scheme [GenIV, 2002]

There are also two different configurations for the primary system. In the pool-type system configuration all the primary components (core, primary pumps and heat exchangers) are contained in a coolant pool within the primary vessel. In the loop-type configuration the heat exchangers and primary pumps are located outside the primary vessel and interconnected with the rest of the system by pipes.

The main advantages of the pool-type reactor are:

- Reduced primary leaking and pipe rupture probability
- Higher sodium inventory and, therefore higher thermal inertial, in the primary system is (about three times higher than in the loop type)- This results in smoother transients, and consequently enlarging grace times and dumping thermal effects all over the system
- The cover gas system is simpler since the only free surface needed is the free surface of the primary vessel

The main advantages of the loop-type reactor:

- Simpler maintenance and flexibility for system modifications;
- Reduced neutron shielding to prevent the activation of the secondary circuit;

- Simpler vessel structural design;
- Enhanced natural circulation due to system layout (differences in vertical elevation) and defined coolant flow path;
- Easier load-following possibilities due to reduced thermal inertia;

Figure 7 illustrates the difference between the two systems showing the scheme of both of them applied to a SFR.

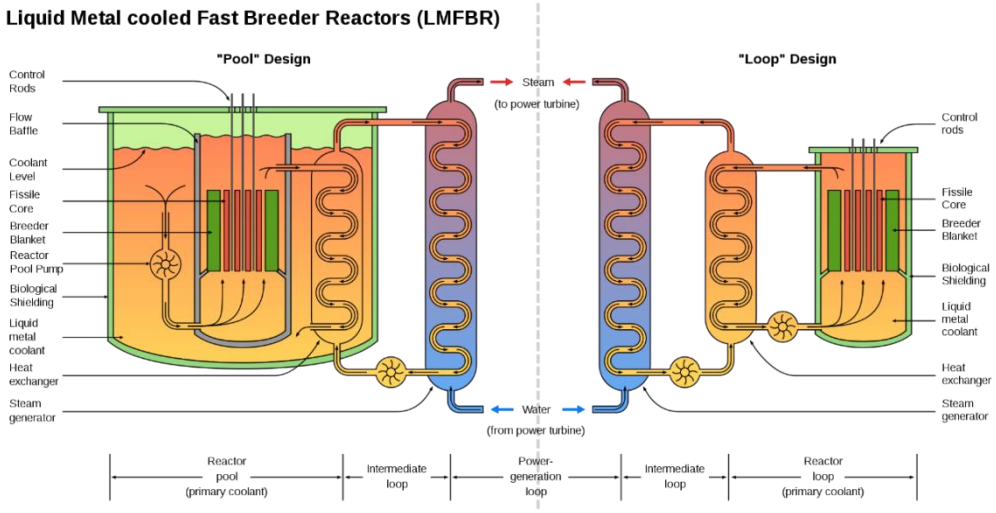

Figure 7: Difference between pool-type (left) and loop-type (right) for a SFR design

2.1.2 The ESFR design

The plant design [Genot, 2009 and Blanchet, 2009] is based on an industrial sodium cooled pool reactor of 1500 MWe. The reactor has three coolant systems: a primary sodium coolant system, an intermediate sodium coolant system, and a steam-water, turbine-condenser coolant system. The pool-type primary system includes the core, three mechanical primary pumps (PP) and six Intermediate Heat Exchangers (IHX), (Figure 8). Six Decay Heat Removal systems (DHR) connected to six Direct Reactor Cooling loops (DRC) are also present to ensure decay heat removal of the reactor upon shut down. The coolant flows upward through the reactor core into the upper sodium pool (plenum) of the main vessel. From the upper plenum the sodium flows downward through the intermediate heat exchanger and discharges into a lower sodium pool. The vertically oriented primary pumps draw the coolant from the lower pool and discharge it into the core inlet plenum. The secondary system consists of six intermediate loops, each equipped with one Intermediate Heat Exchanger (IHX) on the reactor side and six modular sodium/water Steam Generators (SG) of 100 MWth power capacity each.

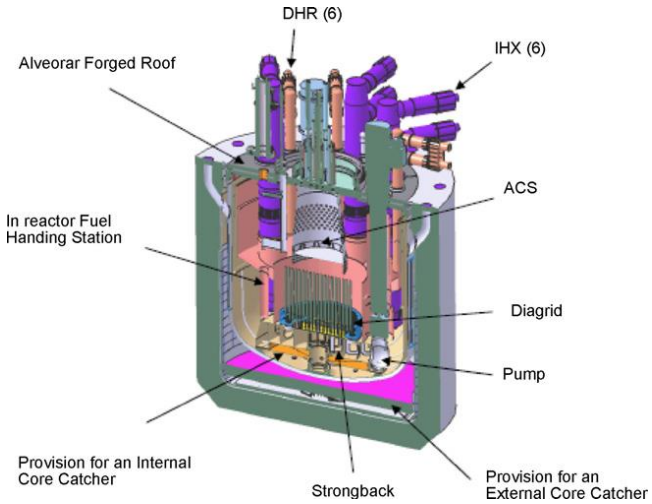

Figure 8: ESFR pool-primary vessel scheme [Vasile et al, 2011]

The tertiary system consists therefore of 36 separate circuits. This configuration is the so-called modular configuration and enhances the safety of the system by limiting the effects of a possible sodium water reaction caused by a steam tube rupture.

The SFR oxide core layout consists of an inner and outer fuel region with different Pu mass content in order to flatten the radial core power profile at end of cycle. There are 225 inner fuel sub-assemblies and 228 outer fuel sub-assemblies. The control rod system is composed of 9 DSD (Diverse Shutdown Device) and 24 CSD (Control and Shutdown Device). The CSD rod absorber contains natural boron carbide whereas the DSD rod absorber contains enriched boron carbide. The reflectors consist of three rings of assemblies with two additional rows of dedicated assemblies or alternative devices such as steel blocks for shielding.

The fuel sub-assembly consists of a hexagonal wrapper tube that contains a triangular arrangement of 271 fuel pins with helical wire wrap spacers. The fuel pin consists of (U,Pu)O2 pellets in ODS steel cladding. The fissile zone is 1 m high. The lower blanket is filled with steel pellets.

In general terms the ESFR core is flat (“pancake” design) to provide good thermal-hydraulic properties and to enhance neutron leakage in order to reduce the sodium void effect. The breeding gain is about 1.04.

The core radial layout is shown in Figure 9 and the core axial layout is shown in Figure 10.

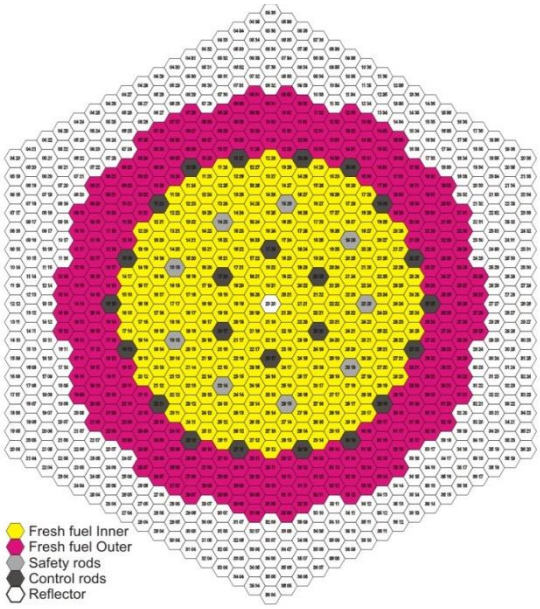

Figure 9: Oxide core radial layout [Vasile et al, 2011]

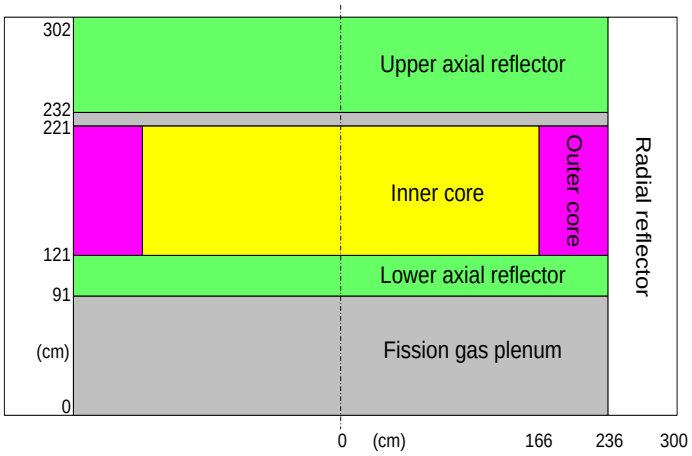

Figure 10: Oxide core axial layout [Vasile et al, 2011]

The main reactor parameters in nominal conditions are listed in Table 2

Variable	
Reactor Power (MWth)	3600
Number of FA	453
Number of pins per FA	271
Fuel pin outer clad diameter (mm)	10.73
Fuel pin inner clad diameter (mm)	9.73
Fuel pellet outer diameter (mm)	9.43
Fuel pellet inner diameter (mm)	2.4
Cladding material	ODS Steel
Fuel Pellet material	(U,Pu)O2
Average Burn-up (GWd/tHM)	100
Core average plutonium factor (%)	15.7
Core inlet temperature (˚C)	395
Average core structure temperature (˚C)	470
Average fuel temperature (˚C)	1227
Total primary massflow rate (Kg/s)	19535
Primary Na inventory (m3)	2612.8
Total secondary massflow rate (Kg/s)	15330
Secondary Coolant temperature at IHX inlet (˚C)	525
Secondary Coolant temperature at IHX outlet (˚C)	340
Water temperature at SG inlet (˚C)	240
Water temperature at SG outlet (˚C)	490
Steam Pressure (MPa)	18.5

Table 2: Main thermodynamic variables of the ESFR design [Vasile et al, 2011]

The optimised core

One of the main work packages of the CP-ESFR project was dedicated to the core design [Blanchet et al, 2009]. During the first part of the project the reference oxide core proposed in the design was studied to improve its performance, particularly in the area of safety and minor actinides management. This core was described in the dedicated project deliverable [Blanchet et al, 2009].

In the later stage of the project, this reference core design was modified in order to optimise its safety characteristics, namely by decreasing the total positive sodium void reactivity feedback [Sunderland, 2012]. The void reactivity effect is the combination of three phenomena; the hardening of the neutron spectrum (positive effect), the increase in neutron leakage (negative effect), and reduced neutron capture (positive effect). Therefore, a reduction of the positive void effect reactivity can be achieved by either increasing neutron leakage or by neutron spectrum softening.

An increase of neutron leakage from the core region can be achieved through modifications in the core geometry (usually by adopting a “pan-cake” geometry of the active core region at the expense of the general neutron economy). Extensive studies determined a set of core design modifications that optimised the total sodium void reactivity (becoming less positive). Among the most efficient design solutions identified there is an enlarged sodium plenum above the active core region in combination with an absorber layer above the sodium plenum (to reduce neutron backscattering from the reflector region above the plenum. Figure 11 shows the combined effect of different upper plenum thickness of the absorber and boron layers. It can be observed that the sequential increase of the layer’s thickness converge to an asymptotic value of reactivity reduction slightly over 800 pcm. The pair of values selected was 60 cm for the sodium plenum and 30 cm for the boron layer. These modifications implied a considerable increase in the sub-assembly length that was compensated by reducing the upper axial reflector width [Sunderland, 2012].

Figure 9 shows the axial distributions of the fuel assembly in the optimised version (referred to as OO – optimized oxide core).

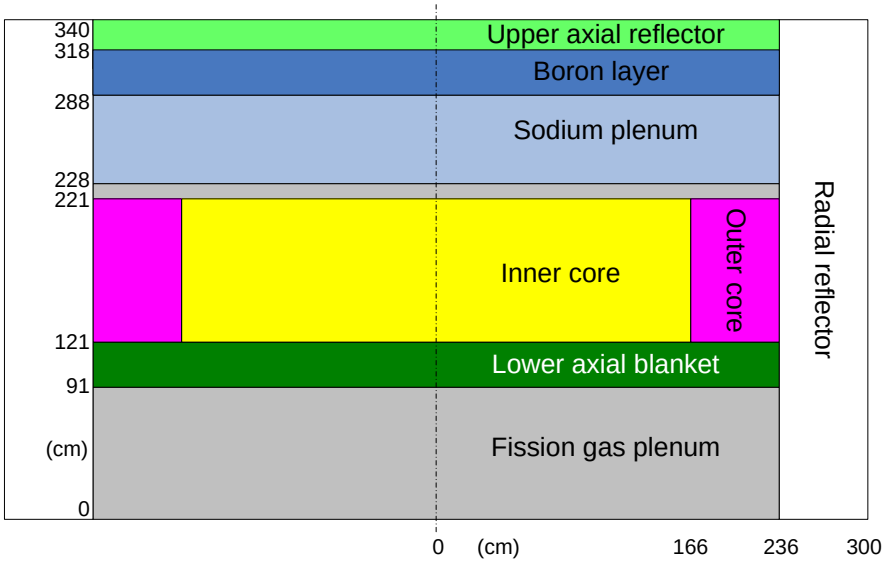

Figure 11: Core configuration in the Optimised Oxide core [Mikitiyuk, 2012]

With these modifications the cumulative value of the positive void reactivity feedback effect was considerably decreased. Table 3 shows the different reactivity coefficients for both the reference and the optimised core configuration [Mikityuk,2012].

Reactivity Coefficients	REFERENCE CORE	OPTIMISED CORE
Doppler constant KD (pcm)	-1191	-1169
Cool. exp. A.Core (pcm/K)(Inner/Out-I/Out-II)	0.400/0.100/0.05	0.142 / 0.134/0.05
Cool.exp. Na Plenum.(pcm/K) (Inner/Out-I/Out-II)	no plenum	-48.18181818
Fuel expansion (pcm/K)	-0.1754	-0.153
Cladding expansion (pcm/K)	0.1485	0.137
Diagrid expansion (pcm/K)	-0.5515	-0.847
Control rod expansion coefficient (pcm/mm)	-8.474	-8.474

Table 3: Comparison of the main neutronic for the reference core and the optimised core

After the introduction of the upper sodium plenum other design options were investigated sequentially, taking into account the various accumulative effects. In this line, the lower axial blanket was substituted by a fertile blanket composed of depleted uranium dioxide and AmO_2.

2.1.3 The ALFRED prototype

The ALFRED design consists in a pool type 300 MWth power lead cooled reactor. As justified in the previous section, this design does not have the intermediate circuit by including the eight steam generators in the primary vessel.

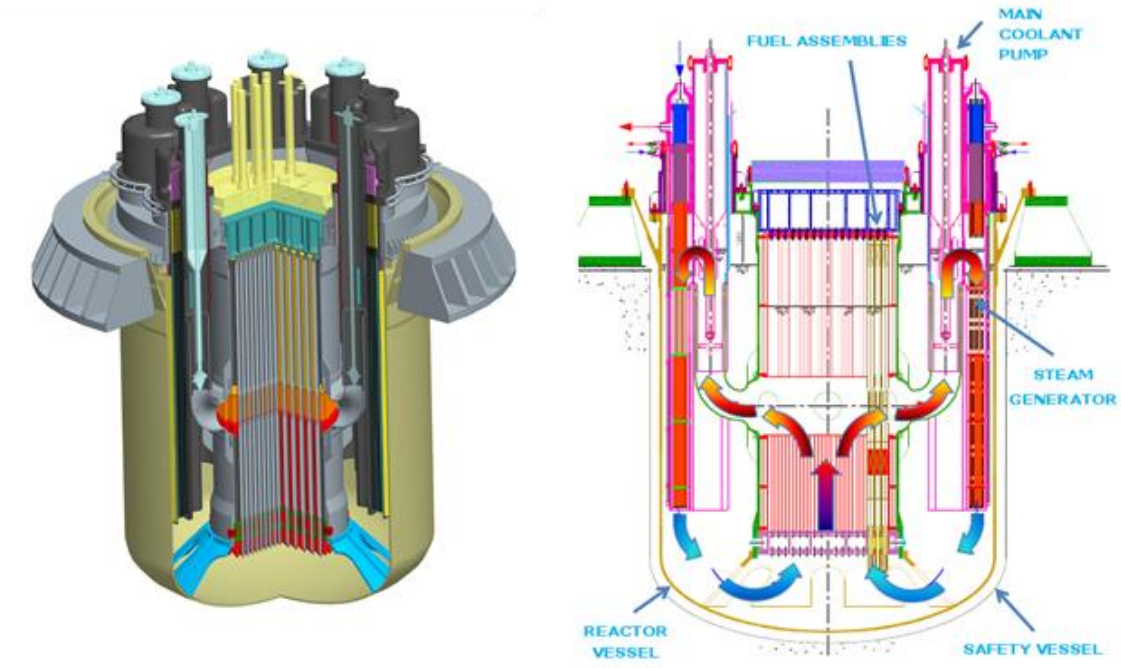

Figure 12: ALFRED primary vessel [Bandini et al, 2013]

The fuel is contained in hexagonal wrapped assemblies extended to the cover gas to simplify fuel handling. Eight mechanical pumps are placed in the hot collector conveying the flow towards the primary side of the eight steam generators where it is cooled down before arriving to the low vessel cold pool.

The temperature shift in the core is of 80°C, between 400°C and 480°C. The secondary loops reach 180 Pa in nominal conditions with a shift of 115 °C between 335°C and 450°C. The relatively high working temperature provides the system with a high overall efficiency, higher than 42%.

These eight steam generators are distributed symmetrically around the primary vessel. Their layout is bayonet type with an intermediate medium between the lead side and the water/steam side, which contributes to the mitigation of a possible tube rupture accident.

The main thermal variables along with the core design parameters are listed in Table 4.

Parameter	Unit	Values
Thermal power	MW	300
Active height	cm	60
Pellet hollow diameter	mm	2
Pellet radius	mm	4.5
Gap thickness	mm	0.15
Clad thickness	mm	0.6
Pin diameter	mm	10.5
Wrapper thickness	mm	4
Distance between 2 wrappers	mm	5
Lattice pitch (hexagonal)	mm	13.86
Pins per FA	-	127
Inner vessel radius	cm	165
Inner / Outer FAs number	-	57 / 114
Inner / Outer enrichment	atom%	21.7% / 27.8%
$(Pu+^{241}Am) / (Pu+^{241}Am+U)$		
Mass inventory of actinides:	tons	
BOC - U / Pu / Minor Actinides		5.27 / 1.78 / 0.038
EOC - U / Pu / Minor Actinides		5.19 / 1.74 / 0.043
Fuel residence time	month	60
Number of batches	-	5
Cycle length	month	12
Dk_{eff} swing	pcm	≈ -2600
BoC/EoC k_{eff} (with CR extracted)	-	1.025 / 0.999
Grace time for the cladding failure (ULOF)	minutes	30

Table 4: Main design parameters for the ALFRED design [LEADER,2012]

2.2 Safety Principles

Besides sustainability considerations, one of the fundamental goals that drive the conception of a new nuclear reactor technology generation is the achievement of high safety levels.

Currently, important R&D efforts focus to develop, integrate and harmonize methodologies of safety assessment practices to be applied to these innovative nuclear designs [SARD3.5, 2012]. The SARGENIV project financed within the 7th Framework Programme of the European Commission works in this direction.

One of the main objectives of this project was to elaborate in feasible terms a methodology to develop and assess the enhanced safety characteristics that the GenIV designs aim to.

A particular task (Task 3.5) established the way to achieve an enhanced safety design through a number of objectives tailored for such a purpose, namely:

- Reduce the number of abnormal/accidental events and reduce the potential of escalations to accident situation by enhancing the plant capability to control them.
- Reduce, as far as reasonably practicable, the core damage frequency and any other reactivity release.
- Reduce the impact of external hazards and malevolent acts.
- Reduce the radiological impact as much as reasonably achievable by design provisions of any operating, incidental/accidental, decommissioning and dismantling activities.
- Ensuring that radiological consequences of abnormal events do not exceed radiological consequences of normal operation.
- Ensure that accidents without severe core damage induce no off-site radiological impact.
- Reduce the potential radioactive releases from accidents with severe core damage. Accidents with severe core damage which lead to early or large releases should be practically eliminated. For any other one, there should be no need for off-site measures.
- Enhancing the effectiveness of the independence between all the levels of defence-in-depth.
- Ensure that the safety and security measures are designed and implemented in an integrated manner.
- Ensure effective management for safety from the design state.

These objectives, which are much more conservative than the ones achieved by the current nuclear power plant generation, should be obtained following the subsequent principles;

- Defence in depth: It is based in the implementation of different levels of protection, including successive barriers preventing the release of radioactive material. It provides an overall strategy of safety measures and features of nuclear power plants. The strategy is divided in levels with different objectives and consequences in case of failure.
- Barriers. Physical barriers between the material and the environment should be identified and their integrity should be maintained as far as reasonably practicable. There should be independency between different barrier levels, this means that the failure of a barrier should not jeopardise the integrity of the following barrier.
- Fundamental safety functions. These are functions that shall be ensured for all plant states, namely:
    - Control of reactivity
    - Removal of heat from the reactor and from the fuel store
    - Confinement of the radioactive material, shielding against radioactive and control of planed radioactive releases.
- Practical elimination: The design should be such that plant states that could lead to high radiation doses or large radioactive releases are practically eliminated. Practical elimination means that it is either physically impossible for the conditions to occur, or at least extremely unlikely to arise.
- ALARA/ALARP: (*As low as reasonably achievable / practicable)* The objective of this principle is that, in addition to meeting the normal requirements of good practice in engineering, further safety or risk reduction measures for the design or operation of the facility should be sought and implemented unless the proposed measures are grossly disproportionate.
- Built-in rather than added-on. This principle states that the safety measures and features should be intrinsic to the design.
- Complementarity of deterministic and probabilistic approaches. This principle states the need to integrate deterministic and probabilistic information into the decision making process.

With the definition of the objectives to achieve and the principles that should lead the designers to reach those objectives, the next step is to define a methodology of the safety assessment process.

The IAEA NS-G1.2 [IAEA, 2001] defines the safety assessment as ¨*the systematic process carried out throughout the design process to ensure that all the relevant safety requirements are met by the proposed design of the plant*¨ … ¨*The design and safety assessment are part of the same iterative process conducted by the plant designer which continues until a plant solution meets all the requirements…*¨.

In an early stage of the procedure the following steps can be identified;

1. Identification of the challenges to the safety functions
2. Identification of the mechanism (postulated initiating events)
3. Creation of families of initiating events and selection the one considered as representative and envelop for the family
4. Design of the provision needed for each representative initiating event of each family
5. Safety analysis: deterministic and probabilistic safety analysis.

The purpose of this thesis is to contribute to the safety assessment process of the design by a deterministic analysis of a set of postulated transients identified in an early stage of the safety assessment process. This means, taking as an input the outcomes of the second and third point of the aforementioned methodology contribute the fifth step analysing the plant response after the corresponding initiating event.

According to the IAEA glossary [IAEA, 2007] an initiating event is ¨a*n event identified during design as capable for leading to anticipated operational occurrence or accident conditions. The primary causes of postulated initiating events are human induced or natural events*¨. They shall include all foreseeable failures of structures, systems and components of the plant, as well as operating errors and possible failures arising from external and internal hazards.

It is appropriate to categorise the reference postulated initiating events according to the estimated frequencies of the groups of initiating events that they cover and complement the engineering judgement and probabilistic studies. The most common classification [EUR, 2001] is;

- Design Basis Conditions 1 (DBC1): DBC1 consist of different transients necessary to operate the plant. Among these transients should be considered
    - Power operation
    - Start up and shutdown
    - Load following

- Design Basis Conditions 2 (DBC2): DBC2 transients consist of anticipated operational occurrences. These are the corresponding initiating events that might occur several

times during the plant life (cumulative frequency of occurrence higher than 10^{-2} reactor^{-1} year^{-1}) , such as:

- Protected reactivity insertion as a runaway of a group of control rods (TOP)
- Acceleration of primary/secondary pumps from 30% load
- Loss of feed water on all SGs
- Doubling core by-pass flow

- Design Basis Conditions 3 (DBC3): DBC3 transients consist of accidents with a cumulative frequency higher than 10^{-4} reactor^{-1} year^{-1}, such as:
  - Protected coastdown of all primary pumps (loss of flow transients: LOF)
  - Protected loss of offsite power (LOOP)

- Design Basis Conditions 4 (DBC4): DBC4 consists of accidents with a cumulative frequency lower than 10^{-4} reactor^{-1} year^{-1}, such as:
  - All unprotected transients (the shutdown system is assumed to fail when called upon)
  - LIPOSO (break of a pipeline joining the primary pump with the core grid plate)

DBC3 and DBC4 accidents correspond to initiating events that are not expected to occur during the life-time of the plant but analysed to assess the potential consequences.

In addition to the DBC transients, safety evaluations become necessary for transients being allocated to so called Design Extension Conditions (DEC). These kinds of analyses need specific approaches for demonstrating that consequences of even extremely low probability events, or event sequences, are limited to the plant itself and do not pose a safety problem to the surrounding area. Computational tools including fuel mechanic model for these kinds of analyses are partly different from the ones used for consequence analyses of transients belonging to DBC events.

The criteria considered to evaluate the consequences triggered by each of the categories of postulated events should be pondered according to their expected frequency of occurrence. The IAEA glossary [IAEA, 2007] defines ¨acceptance criteria¨ as ¨*specific bounds on the value of a functional indicator or condition indicator used to assess the ability of a structure, system or component to perform its design function*¨.

Even though it is a concept highly dependent on national particular legal and regulatory infrastructures, there are some generic characteristics that should be common to all of them. In this sense the following generic criteria can be fixed for the different categories of postulated initiating events described in the previous section.

In general terms, the acceptance criteria common to all DBC and DEC are;

- A postulated initiating event should not propagate to a more serious one
- If a postulated initiating event triggers an emergency shutdown, the core should remain subcritical during the entire scenario

The DBC1 and DBC2 postulated initiating events are the ones related with a higher frequency of occurrence. Thus, the acceptance criteria to be applied to them should have the highest requirements. Thus, examples of acceptance criteria in this category are;

- The integrity of the barriers should not be challenged.
- No fuel damage is expected
- No loss of safety equipment is expected

For DBC3 postulated initiating events, which correspond with infrequent events, the criteria is reduced.

- The damage of the first barrier should be limited. The integrity of the other ones should not be challenged.
- No fuel damage is expected

For DBC4 and DEC, categories which correspond to extremely unlikely events that are not supposed to happen during the lifetime of the plant, the acceptance criteria is the loosest;

- The damage of the first barrier should be limited. The integrity of the other ones should not be challenged.
- Fuel damage should be limited

The definition of the safety objectives, principles to follow, identification of the postulated initiating events that may challenge the reactor integrity and the definition of the acceptance criteria that the different system should comply with in the different plant states are part of the deterministic safety assessment process of a nuclear system design. The other part is the substantiation of that a certain design reaches such safety requirements.

According to the R&D agenda of the SNETP (Sustainable Nuclear Energy Technology Platform) [SNETP, 2009] and GIF there is a need to develop computational tools to ensure the safety of new reactor concepts. These computational tools should provide a reliable and accurate way to simulate conditions that may threat the reactor safety. Accident scenarios in a Nuclear Power Plant (NPP) involve 3D phenomena that these tools should be able to simulate.

The strategy followed in this research work has been based in the adaptation of the computational tools verified, validated and extensively used in LWR safety analysis to the specific phenomena that takes place in LMFBRs. These codes are introduced in the next section along with the necessary modifications performed to them.

2.3 The codes

In order to effectively contribute to the safety assessment of the design the selection of reliable computer codes able to simulate the behaviour of the different plant systems during accidental transient is of great importance.

For the purpose of this research work the NRC flagship system code TRACE was selected to perform the thermal-hydraulic simulation of the LMFBR. The spatial neutron kinetic code PARCS was selected to provide the three-dimensional reactivity feedback which calculate and distributes the generated power throughout the core.

In this section the fundamentals of each of these code together with the ones used for benchmarking purposes are described. The modifications performed in order to adapt them to the specific characteristics of LMFBRs are also described.

2.3.1 TRACE

2.3.1.1 Code description

The TRACE (TRAC-RELAP Advanced Computational Engine) code is the latest of a series of best-estimate system codes developed by the U.S. Nuclear Regulatory Commission for the analysis of steady-state and transient thermohydraulic-neutronic behaviour in light water reactors [NRC, 2007]. The models used include multidimensional two-phase flow, non-equilibrium thermodynamics, generalized heat transfer, reflooding, level tracking and neutron kinetics. The official version doesn't support biphasic liquid metals but adaptations and modifications made by various European organizations, in particular PSI, allow this code now to be applied also for SFR analysis under sodium boiling conditions [Chenu A.-Th, 2011]. The FRED code [Mikityuk, K. et al, 2011] coupled to TRACE was used at Paul Scherrer Institute (PSI) to simulate the evolution of thermal and stress-strain conditions in fuel rods.

2.3.1.2 Code modifications

TRACE and PARCS system codes are mainly developed to perform transient calculations of LWRs. Nevertheless, they can be applied to LMFBR technology system provided that some modifications are introduced in their source codes to implement particular correlations specific for liquid metal coolants.

The heat transfer coefficient affects the heat transfer capability of all in-vessel and core structures (cladding, wrapper, control rods, sub-assembly, etc.) as well as all heat exchangers (intermediate HX and steam generators). Liquid metals have a much lower Prandlt number than water, which means that the ratio between the heat transfer due to thermal conductivity and to convection is much higher for liquid metals. The correlations to take into account this effect differ substantially from the built-in code water correlations, so their replacement become a prerequisite.

A modification of the Ushakov's correlation [Mikityuk, 2009] was proposed for simulation of the heat transfer to the developed sodium flow in tube bundles:

$$Nu = 7.55x - \frac{20}{x^{13}} + \frac{0.041}{x^2} Pe^{0.56+0.19x} \quad (1)$$

where Nu is the Nusselt number, x is the pitch-to-diameter ratio and Pe is the Peclet number. This equation can be applied for x from 1.3 to 2.0 and Pe up to 4000.

The Philipponneau correlation (Philipponneau, 1992) was proposed to be used for calculation of the MOX fuel thermal conductivity:

$$\lambda = \left(\frac{1}{1.320\sqrt{x + 0.0093} - 0.091 + 0.038B + 2.493 \cdot 10^{-4} T} + 88.4 \cdot 10^{-12} T^2\right) \cdot \frac{1 - P}{1 + 2P} \quad (2)$$

where λ is the thermal conductivity (W/mK), x is the deviation from the stoichiometry, B is fuel burnup (at%), T is the fuel temperature (K), P is the fractional porosity.

A parametric study was performed using the TRACE/FRED code in order to derive for the ESFR project a dependence of the fuel-clad gap conductance on the local linear heat generation rate. The following correlation was derived and recommended for all participants (Figure 13):

$$hgap = \min\left(3\left(1000 - LHGR + \left(\frac{LHGR}{10}\right)^2 + \left(\frac{LHGR}{100}\right)^3\right), 23000\right) \quad (3)$$

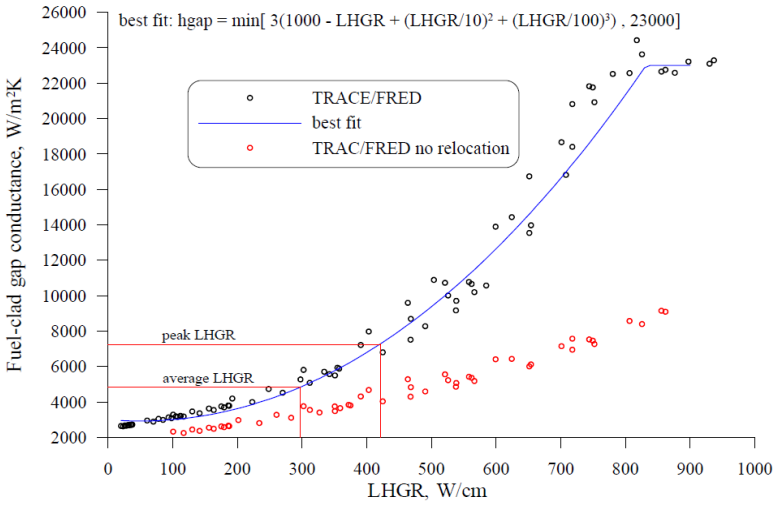

Figure 13: Fuel gap conductance ESFR [Lassmann et al, 1987]

where *hgap* is the gas gap heat conductance (W/m^{2}K) and *LHGR* the local linear heat generation rate (W/cm). The *hgap* value is limited from above by 23000 W/m^{2}K, corresponding to the closure of the gap [Lassmann et al, 1987].

Specific pressure drop correlations [Chenu et al, 2011] may have an impact on the calculation, especially in those transients where natural circulation processes are important. Nevertheless, they were not implemented by all the partners as no natural convection transients were assessed or benchmarked within this current project, but these effects are to be considered in further developments.

TRACE code contains built-in sodium coolant thermal properties, so they have been considered valid for the purpose of this work. On the contrary TRACE code doesn´t include pure lead thermal properties, but lead-bismuth one. So, in order to reduce the uncertainty in the calculations, the specific pure lead thermal properties were implemented in the source code [Lázaro A et al - L, 2013].

These thermal data was provided by research organisation leading the LFR technology research, namely, ANSALDO and the Italian National Research Institute ENEA. These data were derived from experimental tests. This research work included the analysis of such data ant its comparison with the available bibliography.

An exhaustive comparison of the main thermal properties was performed between the lead-bismuth correlations embedded in the TRACE source, the ones extracted from the abovementioned data, and the ones proposed in the OECD/NEA Handbook for lead and lead-bismuth eutectic [NEA, 2007]. Some physical quantities (as saturation temperatures and pressures) appeared to be nearly identical, so they were left unmodified. Others, for which remarkable differences had been observed, were substituted, namely: the derivative of the internal energy over time, Figure 14.

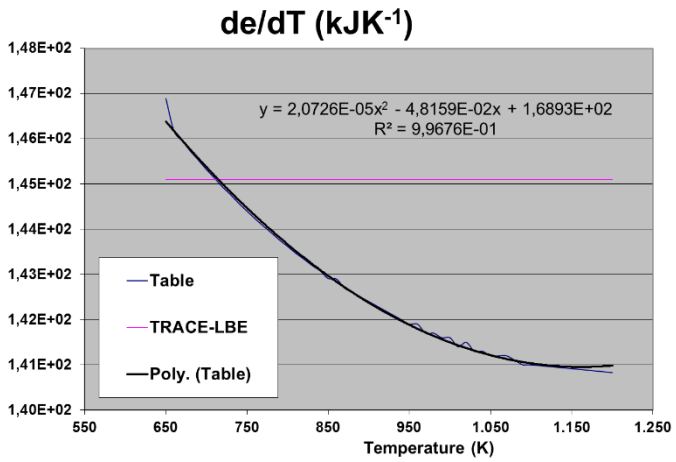

Figure 14: Lead internal energy derivative over time

the specific heat as a function of temperature (Figure 15),

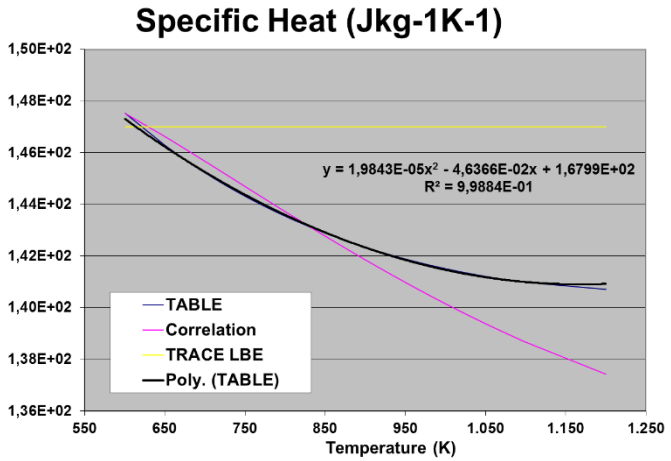

Figure 15: Lead specific heat

the density (Figure 16)

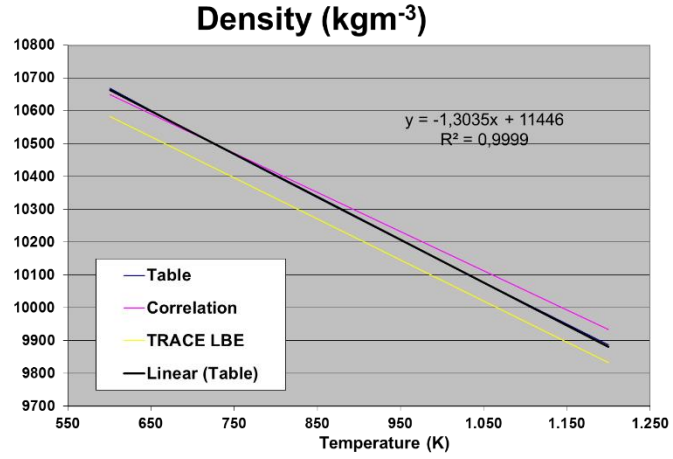

Figure 16: Lead density

and its derivative over temperature as a function of temperature (Figure 17).

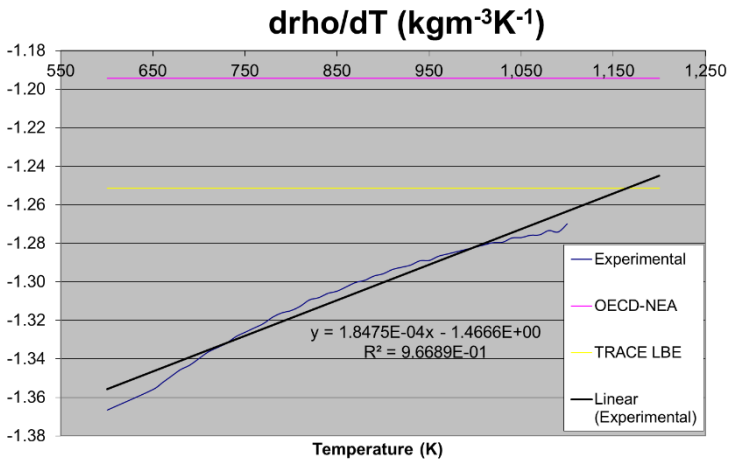

Figure 17: Lead density derivative over temperature

Since there is no experimental data available for the thermal conductivity, a comparison was made between the correlations available in literature. Finally, the original correlation embedded in TRACE code was substituted by the Takamichi correlation [Takamichi et al, 1988] to be consistent with other partners of the LEADER project. Figure 18 shows the comparison between the different correlations together with the relative difference between them.

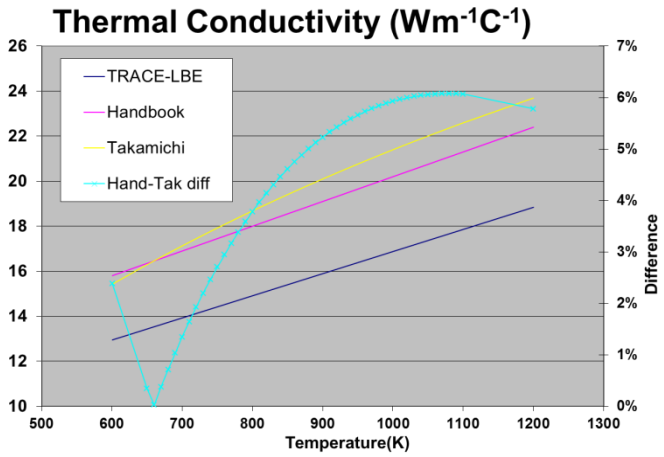

Figure 18: Lead thermal conductivity - Difference

2.3.2 RELAP5

The RELAP5 [RELAP, 1995] code used for the transient analysis of the ESFR reactor is a modified version of the RELAP5/MOD3.3 code, developed by INEL for the U. S. NRC, currently used world-wide for thermal-hydraulic transient analysis in light water reactors. The features and properties of sodium available in the ATHENA code have been implemented in the modified RELAP5 code. The basic properties for sodium are calculated from optional thermodynamic tables that tabulate saturation and single-phase properties as a function of pressure and temperatures. These tables are based on Young's soft sphere model formulation.

2.3.3 PARCS

PARCS [PARCS, 2010] is a three-dimensional (3D) reactor core simulator which solves the steady-state and time-dependent, multi-group neutron diffusion and low order transport equations in orthogonal and non-orthogonal geometries. PARCS is coupled directly to the thermal-hydraulics system code TRACE which provides the temperature and flow field information to PARCS during the transient calculations via the few group cross sections. The cross section set has been generated by the Monte Carlo techniques based code SERPERNT [Fridman et al, 2011].

PARCS code has been also modified to take into account the specific LMFBR phenomena. In particular it has been modified Doppler effect correlations. PARCS uses a square root correlation of the mean fuel temperature to calculate the Doppler effect feedback as it is common practice in LWR technology. Due to higher enrichment of the LMFBR fuel, and consequently, lower concentrations of U238 along with the presence of minor actinides, the dependence of the reactivity with the fuel temperature is slightly different, and it has been demonstrated that reactivity decreases logarithmically with fuel temperature. Consequently, PARCS source was modified to substitute its original correlation by a logarithmic dependent one. With this modification PARCS calculates the total macroscopic cross-section as follows:

$$\Sigma(T_f, T_c, Z) = \Sigma_0 + \left[\frac{\partial \Sigma}{\partial \ln(T_f)}\right](\ln(T_f) - \ln(T_{f0})) + \left[\frac{\partial \Sigma}{\partial T_c}\right](T_c - T_{c0}) + \left[\frac{\partial \Sigma}{\partial \mathrm{Z}}\right](Z - Z_0)$$

(4)

Where Σ is the total macroscopic cross-section, Σ_0 is the cross-section calculated at the reference conditions (T_{f0}, T_{c0}, Z_0) T_f is the fuel temperature, T_c is the temperature of the coolant and Z the control rod position.

PARCS code was also adapted to include a control rod movement control system. The code was adjusted to receive from TRACE the on-time positions of the controlled control rod banks. TRACE makes a calculation of the control rod position based on the thermal expansion effects created by the modification of the coolant and structure components following the specifications outlined in the next chapter.

3. Tools and methods

This chapter describes the details of the sequence of models developed for the two LMFBR concepts. First, it is described the one-dimensional thermal-hydraulic models of the SFR and LFR designs and afterwards the extension of the SFR design into a three-dimensional thermal-hydraulics model for the system code TRACE.

The chapter also includes the spatial kinetic neutronic core model developed and its coupling with the thermal-hydraulic models described.

3.1 The one-dimensional modelling

This section presents the one-dimensional thermal hydraulic model and the point kinetic model for TRACE of a SFR-kind and a LFR-kind plant designs. As introduced in Chapter 2, the SFR design selected was the European Sodium Fast Reactor (ESFR) design and the LFR design has been the ALFRED demonstrator design.

3.1.1 The ESFR model

The TRACE thermal-hydraulic system code has been used to model and analyse the thermal-hydraulic behaviour of the ESFR plant. In this first approach, the primary circuit (main vessel) is modelled with a set of one-dimensional components representing the different volumes that the coolant faces along the primary system, with special attention to the core modelling since there is a special need of detail in this zone. The secondary systems is lumped in an equivalent loop thermally linked with the primary circuit model via a representation of the Intermediate Heat Exchanger (IHX). This secondary system was also linked with an equivalent loop representing the combined effect of the 36 modular steam generators. The following sections describe in more detail each of these model components.

3.1.1.1 Primary System

Core Model

Based on the analysis of the power distribution at the Beginning of Life (BOL) (Figure 19), a core model with seven parallel channels is proposed to be used in the transient calculations. The seven simulated regions correspond to:

- One channel for the hot fuel assembly.
- One channel for the whole inner zone representing 225 fuel subassemblies.
- Two channels representing the core outer zones, with 119 and 108 fuel subassemblies.
- One channel for the central dummy and control assemblies.
- One channel for the reflector.
- One channel for the inter-assemblies by-pass.

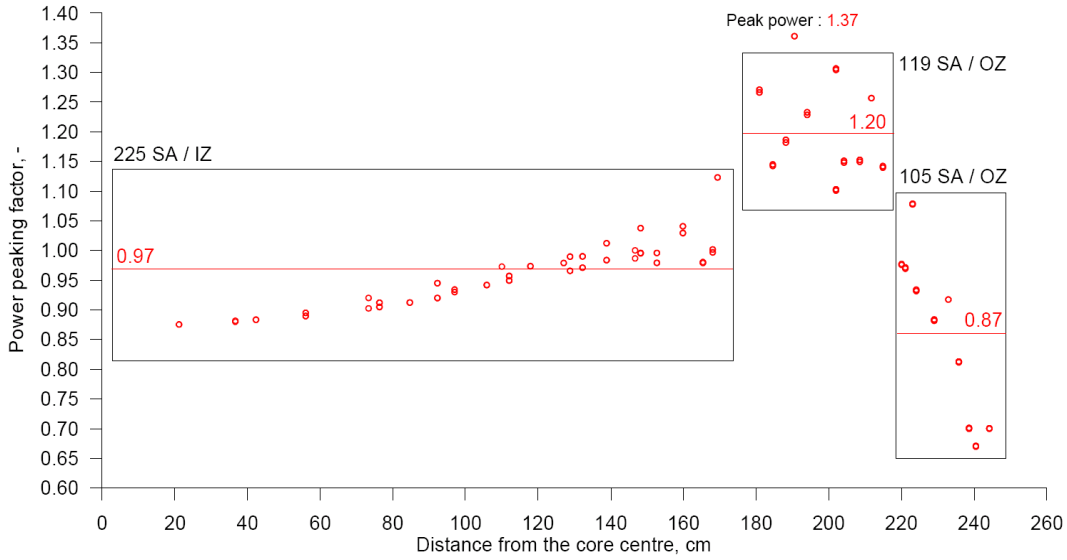

Figure 19: Fuel assembly-wise power distribution at BOL [Mikityuk, 2010]

These seven core regions are modelled by a PIPE component, and only six (by-pass excluded) are attached to a heat structure (HTSTR component) to simulate the heat transfer to the coolant. These core components are connected both, to the hot (upper) and cold (lower) plena of the plant.

The fuel thermal conductivity was evaluated according to the Phillipponneau model [Phillipponneau, 1992]. The axial power distribution used in the analysis is shown in Figure 20.

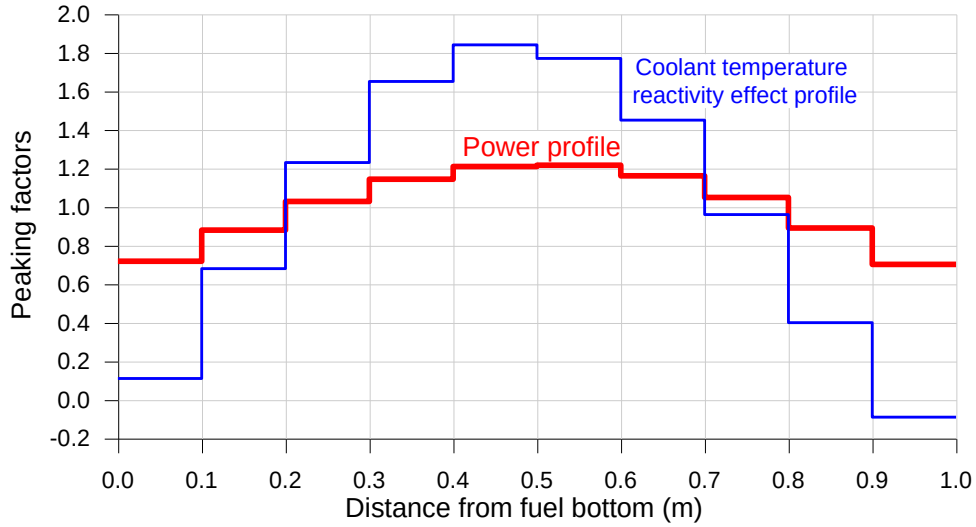

Figure 20: Axial profiles of power and coolant temperature reactivity effect [Mikityuk, 2010]

Point Kinetics Model

Since most of the system codes are only able to simulate the neutronic response of the system using a point kinetics model, the reactivity coefficients and other kinetics parameters were specified for the transient analysis in addition to the radial and axial power distribution described in the previous section. The use of point kinetics model as a first approach limits the analyses with neutronic response to symmetric scenarios, while asymmetrical transients require necessarily the coupling with 3D neutron kinetics codes as it is proposed at the end on the Chapter.

The neutronic response has been modelled considering the following six reactivity effects as proposed in [Mikityuk, 2010]:

1. **Doppler effect**: Represent the effect of the fuel temperature in its neutronic behaviour. This effect has been calculated using the following expression:

$$\Delta\rho_D = K_D \cdot \ln(T_{fuel} / T_{fuel0}) \qquad (5)$$

where K_D is the Doppler constant and T_{fuel} and T_{fuel0} are the transient and nominal core-average fuel temperatures (K).

2. Coolant temperature effect: This effect has been calculated using the following expression:

$$\Delta\rho_{cool} = \sum_i \chi^i \cdot c_T \cdot (T^i{}_{cool} - T^i{}_{cool0}) \quad (6)$$

where c_T is the coolant temperature reactivity coefficient χ^i is the axial contribution of the node, and T_{cool} and T_{cool0} are the transient and nominal coolant temperatures. The axial profile of the coolant temperature reactivity effect is shown in Figure 20, due to the leakage component of the effect, the profile steeply reduces towards axial reflector and even becomes negative close to the upper reflector.

3. Fuel expansion effect: The increase of the fuel height of the SFR core in average due to thermal expansion reduces the total reactivity due to the reduction of the fuel density and the increase of the neutron leakage. The fuel column is assumed no to be bonded by the cladding and expanding freely driven by the average fuel temperature. This effect has been modelled as follows:

$$\Delta\rho_{f.\exp} = c_{f.\exp} \cdot (T_{fuel} - T_{fuel0}) \quad (7)$$

where $c_{f.exp}$ is the fuel expansion reactivity coefficient, while T_{fuel} and T_{fuel0} are the transient and nominal core-averaged fuel temperatures.

4. Cladding expansion effect: The cladding expansion causes an increase in the total reactivity due to the reduction of the parasitic absorption by the stainless steel due to the axial expansion and the reduction of the sodium volume fraction due to the radial expansion. This effect has been modelled as follows:

$$\Delta\rho_{c.\exp} = c_{c.\exp} \cdot (T_{clad} - T_{clad0}) \quad (8)$$

where $c_{c.exp}$ is the cladding expansion reactivity coefficient, while T_{clad} and T_{clad0} are the transient and nominal core-average clad temperatures.

5. Diagrid expansion effect: The diagrid thermal expansion effect increases the radius of the core reducing the smeared fuel density and increasing the neutronic leakage. This effect has been modelled using the expression that follows,

$$\Delta\rho_{diagrid} = c_{diagrid} \cdot (T_{diag} - T_{diag0}) \quad (9)$$

where $c_{diagrid}$ is the diagrid expansion reactivity coefficient and T_{diag} and Td_{iag0} are the transient and nominal diagrid temperatures.

6. Differential core/control rods expansion: During a loss of flow transient in a fast reactor, one of the most important feedbacks is due to the relative axial displacement of the core and control rods. A simplified simulation of the reactivity feedback caused by a thermal expansion of the control rod driveline (CRD) mechanisms combined with the thermal expansion of the core support structures (CSS) following Superphenix experimental results [Mikityuk, 2010].

The axial insertion of the control rods Δz_1 due to the CRD thermal expansion corresponding to the CRD temperature increase ΔT_1 is given by

$$\Delta z_1 = \alpha_1 \Delta T_1 \qquad (10)$$

where α_1 is the thermal expansion coefficient of the CRD material (the recommended value is 0.15 mm/ºC).

The axial upward shift of the core Δz_1 due to the axial thermal expansion of the CSS corresponding to the CSS temperature increase ΔT_2 resulting in the control rods insertion is given by

$$\Delta z_2 = \alpha_2 \Delta T_2 \qquad (11)$$

where α_2 is the CSS thermal expansion coefficient (the recommended value is 0.11 mm/ºC).

The resulting reactivity effect is;

$$\Delta\rho = K(\Delta z_1 + \Delta z_2) \qquad (12)$$

where K is the corresponding reactivity coefficient (the recommended value is –8.5 pcm/mm).

The different values for the reactivity coefficients for the reference and optimised core were shown in Table 3.

The primary system nodalisation

Figure 21 shows the primary one-dimensional nodalisation. As introduced earlier, the core components are connected both, to the hot (upper) and cold (lower) plena (see Core model description above).

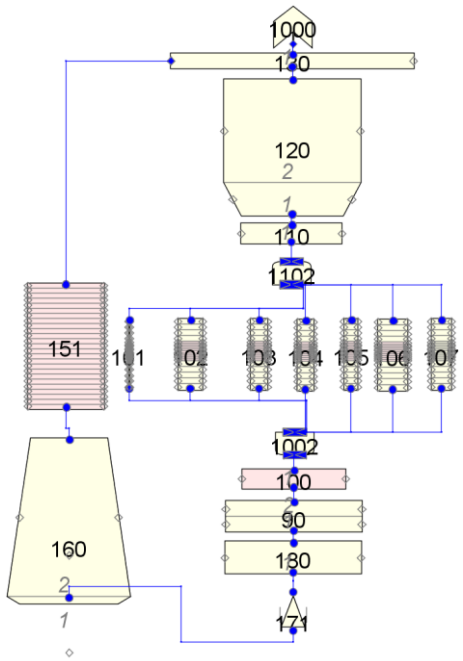

Figure 21: Primary one-dimensional model nodalisation - ESFR

The hot (upper) plenum is divided in 3 PIPE components (Components 100, 120 and 130) that convey the hot coolant towards the Intermediate Heat Exchanger (IHX) (Component 151) where the heat is transferred to the secondary loop.

After the heat is exchanged to the secondary loop, the coolant reaches the cold (lower) plenum, which is modelled by four different PIPE components (Components 160, 180, 90, 100) that convey the coolant to the core inlet (Component 1002).

The primary pump is simulated using a time dependent junction (Component 171) where the boundary conditions of the transients' massflows can be easily defined.

A BREAK component (Component 1000) acts as a pressure control to keep the primary system at atmospheric pressure.

Table 5 show the primary systems components numbers along with its related volume and lengths.

Component	Volume (m^3)	Length (m)
Break 1000	0.0	0.0
Pipe 90	123.5	2.0
Pipe 100	45.9	1.3
Pipe 101 (cor1)	0.1	4.2
Pipe 102 (cor2)	12.7	4.2
Pipe 103 (cor3)	6.7	4.2
Pipe 104 (cor4)	5.9	4.2
Pipe 105 (cor5)	3.1	4.2
Pipe 106 (cor6)	18.8	4.2
Pipe 107 (cor7)	5.6	4.2
Pipe 110	44.0	1.3
Pipe 120	1132.6	8.9
Pipe 130	196.0	1.0
Pipe 151 (ihxpri)	100.8	7.6
Pipe 160	955.7	11.2
Pipe 180	130.3	2.1
Plenum 1002	1.0	0.0
Plenum 1102	1.0	0.0
TDJ 171 (prim pump)	0.0	0.0

Table 5: Primary one-dimensional model components list - ESFR

3.1.1.2 Secondary System

The secondary system is simplified into two main PIPE components that simulate the secondary side of the IHX and SG and two PIPE components that close the circuit. This loop is the thermal equivalent of the different 6 Intermediate loops that the system comprises. Since the secondary circuit is linked with the primary circuit and this is one dimensional, there is no added value in reproducing the six circuits individually, since all of them would reproduce the same phenomena.

Their geometrical characteristics have been adjusted to provide the adequate sodium inventory in the secondary system that plays and important role in the transient behaviour of the plant. The secondary system nodalisation can be seen in Figure 22.

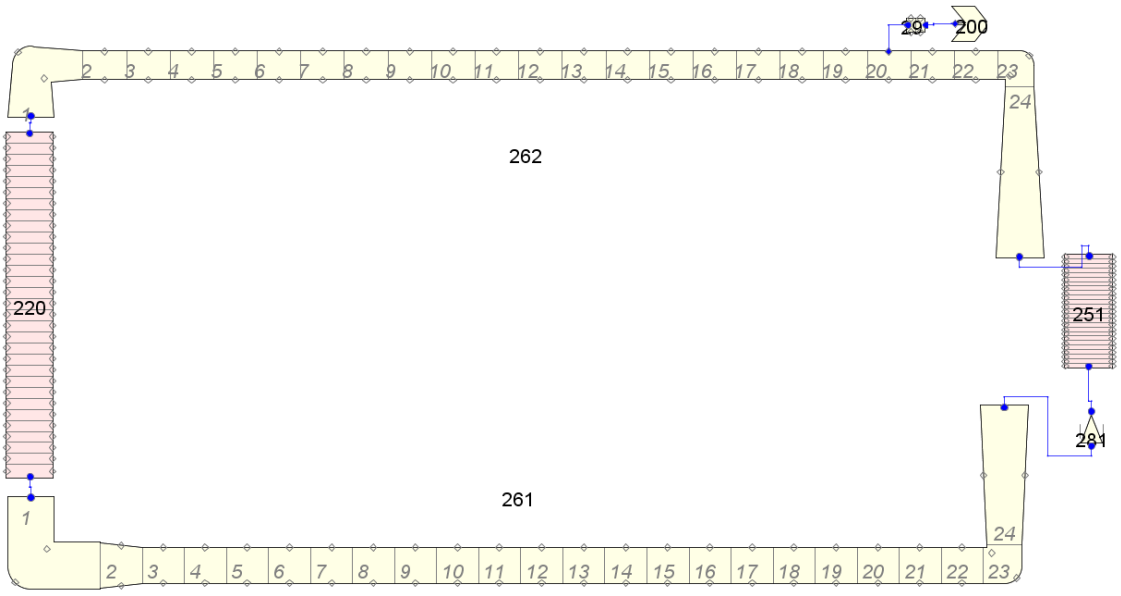

Figure 22: Secondary one-dimensional model nodalisation - ESFR

The heat is received from the primary loop in the pipe 251 (secondary side of the intermediate heat exchanger) and it is conveyed to the tertiary circuit through Pipe 220 (secondary side of the steam generators). Pipe 261 and 262 adjust the secondary cold and hot piping respectively.

As in the primary system, the secondary pump is simulated using a time dependent junction (Component 281) where the boundary conditions of the transients can be easily defined.

A BREAK component (Component 200) acts as a pressure control to keep the secondary system at reference pressure.

Table 6 show the primary systems components numbers along with its related volume and lengths.

Component	Volume (m^3)	Length (m)
Break 200	0.0	0.0
Pipe 220 (nasg)	215.2	24.2
Pipe 251 (ihxsec)	71.2	7.6
Pipe 261	339.4	86.2
Pipe 262	339.4	88.5
Pipe 291	1.0	1.3
TDJ 281 (sec pump)	0.0	0.0

Table 6: Secondary one-dimensional model components list - ESFR

3.1.1.3 Tertiary System

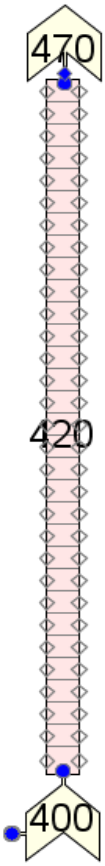

The tertiary has been modelled lumping the 36 steam generators composing the system into one equivalent steam generator model. A Pipe component with its heat structure connected to the secondary system (Pipe 220) simulates the tube bundle. A FILL component (Component 400) represents the lower plenum and determines the inlet water mass flow while a BREAK component (Component 470) is the upper plenum where the design pressure is defined. The FILL and BREAK components impose the boundary conditions of the tertiary system. The tertiary system nodalisation can be seen in Figure 23.

Table 7 shows the primary systems components numbers along with its related volume and lengths.

Figure 23: Tertiary one-dimensional modelisation – ESFR

Component	Volume (m^3)	Length (m)
Break 470 (h2oout)	0.0	0.0
Fill 400	0.0	0.0
Pipe 420 (sgtube)	25.4	24.2

Table 7: Tertiary one-dimensional model components list - ESFR

3.1.1.4 Heat structures

The heat produced in the core is transferred first to the primary coolant, which conveys it to the secondary circuit coolant in the intermediate heat exchanger and this one to the tertiary coolant, the water, in the steam generators. These three heat exchangers are modelled by HEAT STRUCTURE components.

The core heat transfer is modelled by 6 HEAT STRUCTURE components (Components 1011, 1021, 1031, 1041, 1051, 1061) representing the different core regions (Hot Fuel Assembly, Inner Core region, Outer Core region, control assemblies and reflector). The intermediate heat exchanger

is represented by the component 2511 and the steam generator structure is represented by the component 4201. Component 1001 represents the Diagrid structure, which is important to measure the geometry variations of the core due to thermal expansion (Eq. (12)).

Table 8 shows the different HEAT STRUCTURE components characteristics. The table also shows the inner and outer exchange areas of the fuel pins for core heat structures and tube bundles for the IHXs´ and SGs´ structures. The total volume of the material structure is also shown.

These structures are modelled according to the core description [Blanchet et al, 2009].

Component	Inner area (m^2)	Outer area (m^2)	Volume (m^3)
Heat Structure 1001 - Diagrid structure	223.0	223.0	11.2
Heat Structure 1011 - Hot fuel assembly	0.0	9.1	0.0
Heat Structure 1021 - Inner core	0.0	2055.4	5.5
Heat Structure 1031 - Outer core I	0.0	1087.1	2.9
Heat Structure 1041 - Outer core II	0.0	959.2	2.6
Heat Structure 1051 - Control assemblies	0.0	310.6	0.8
Heat Structure 1061 - Reflector	0.0	3042.0	8.2
Heat Structure 2511 - IHX (6)	16176.0	17846.0	13.6
Heat Structure 4201 - SGs (36)	12894.0	18976.0	39.8

Table 8: Heat structure components characteristics - ESFR

The core structures are cylindrical geometries with a radial nodalisation consisting in 3 radial nodes covering 1 mm representing the fuel pellet, 10 radial nodes covering 3,79 mm representing the fuel material, 3 radial nodes covering 0,075 mm representing the gas contained in the gap between the fuel and the cladding, and finally 3 radial nodes 0,5 mm representing the cladding material. The IHXs, and SGs heat structures are also cylindrical structures nodalised by 5 radial nodes representing the cladding material between the inner and outer surfaces of the structures. The Diagrid is represented by a flat slab structure with 5 radial nodes.

The different peaking factors affecting the core heat structures are shown in Table 9. These peaking factors are extracted from the core regions distribution that was shown in Figure 19. These peaking factors keep constant all along the transient, which is a limitation of the point kinetic neutronic feedback approach since the power distribution may be different according specific phenomena taking place in the simulated transients.

Powered Components	Axial Levels	Radial nodes	Power Fraction
Heat Structure 1011 - Hot fuel assembly	10	19	1.370000
Heat Structure 1021 - Inner core	10	19	0.969950
Heat Structure 1031 - Outer core I	10	19	1.204780
Heat Structure 1041 - Outer core II	10	19	0.865750
Heat Structure 1051 - Control assemblies	10	19	0.027485
Heat Structure 1061 - Reflector	10	19	0.006829

Table 9: Heat structure peaking factors profile - ESFR

These structures take into consideration the heat transfer coefficient correlations specific of liquid metal coolants implemented in the source as described in section 2.3.1.2.

3.1.2 The one-dimensional model of a LFR

An equivalent one-dimensional model was developed for the ALFRED design in the framework of the Collaborative Project LEADER [LEADER, 2012]. As justified in the previous chapter, this design includes the steam generators inside the primary vessel, so the secondary circuit is water cooled and there is no tertiary system. The primary and secondary system nodalisation is shown in Figure 24.

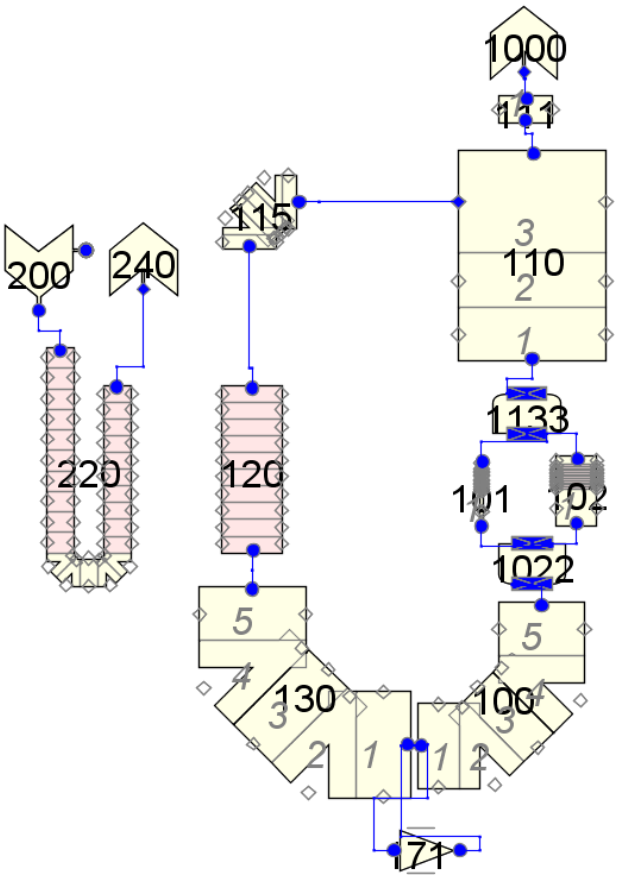

Figure 24: Primary and secondary one-dimensional model nodalisation – ALFRED

3.1.2.1 Primary system

The core model

The ALFRED core model is composed by two Pipe components (Components 101 and 102) with attached Heat Structures representing the hot fuel assembly and average power assemblies respectively, according to the ALFRED core description.

The point kinetic feedback model followed in this approach is equivalent to the one implemented in the ESFR model described in the previous section. Since, the neutronic phenomena expected in both reactors types is very similar, both models use the same reactivity feedback affected by the particular reactivity coefficients of each design.

There are small differences in two reactivity components. There is a different approach to model the fuel and diagrid expansion coefficients. The modelling guidelines [LEADER, 2012] establish a different approach if the fuel is linked or not with the cladding. This linking caused by the thermal expansion affects the expansion mechanism, and consequently two coefficients have been defined for each component. The transitions between one mechanism and the other is settled when the coolant outlet temperature is over Tc, defining Tc as:

$$Tc = 480 + 0.6552 * (Tinlet - 400) \quad (13)$$

The differential insertion of control rods due to thermal expansion is also modelled following a different approach since, in this case there is no experimental data to refer. There were identified two coefficients related with the core outlet temperature measuring the short and long term effect of the control rod differential insertion.

Table 10 shows the different values for the reactivity coefficient in two core condition, Beginning Of Cycle (BOC) and End Of Cycle (EOC).

Reactivity Coefficients	BOC	EOC
Doppler constant KD (pcm)	-555	-566
Lead expansion (pcm/K)	-0.271	-0.268
Fuel expansion (pcm/K) Free / linked	-0.148/-0.232	-0.155/-0.242
Cladding expansion (pcm/K)	0.037	0.039
Diagrid expansion (pcm/K) Free / linked	-0.519/-0.147	-0.43 /-0.152
Control rod expansion coefficient (pcm/K) Prompt/delayed	-0.455/-0.897	-0.218/-0.429

Table 10: Reactivity coefficients in BOC and EOC – ALFRED

The primary systems nodalisation

Two components (Components 110 and 115) are representing the upper vessel parts (plena) and the structure that carries lead flow towards the heat exchanger.

The eight heat exchanges are modelled by a single Pipe component (Component 120) where the heat is removed from the primary system towards the steam generators, so it is thermally linked with the secondary circuit.

The lower vessel plena (cold pool) is modelled with two Pipe components (Components 100 and 130) adjusting the primary coolant and geometric characteristics of the design.

The eight primary pumps are modelled by a Time-dependent junction component (Component 171), imposing the expected massflow.

The main primary thermal-hydraulic components can be seen in Table 11.

Component	Volume (m^3)	Length (m)
Break 1000	0.0000	0.0
Pipe 100	68.3400	8.5
Pipe 101 HFA	0.0367	2.3
Pipe 102 AFA	4.1344	2.3
Pipe 110	186.1200	7.8
Pipe 111	3.1416	1.0
Pipe 115	8.7965	2.8
Pipe 120	23.5730	6.0
Pipe 130	125.0000	10.0
Plenum 1022	1.0000	0.0
Plenum 1133	1.0000	0.0
TDJ 171 (prim pump)	0.0000	0.0

Table 11: Primary one-dimensional model components list – ALFRED

3.1.2.2 Secondary system

The steam generators are represented by lumped Pipe component (Component 220) with the design boundary conditions (i.e., water flow rate, inlet temperature, and pressure) imposed by a Fill and a Break component (Components 200 and 240).

It should be highlighted the particular shape of Pipe 220 is justified by the particular steam generator design selected. The steam generators selected in ALFRED design are bayonet type. In this configuration the steam generator is instated in the hot lead pool and is surrounded by the coolant. In the inner part of the steam generator the fluid enters downwards through an internal pipe that later evolves into an external ring wrapping the inner pipe with the coolant flowing upwards.

This configuration is shown in Figure 25. The configuration justifies the U-shape that the hydraulic component 220 shows and the need to use two heat structures. One to model the heat transfer between the hot coolant and the outer ring, and another one to model the heat transfer between the outer ring and the inner pipe.

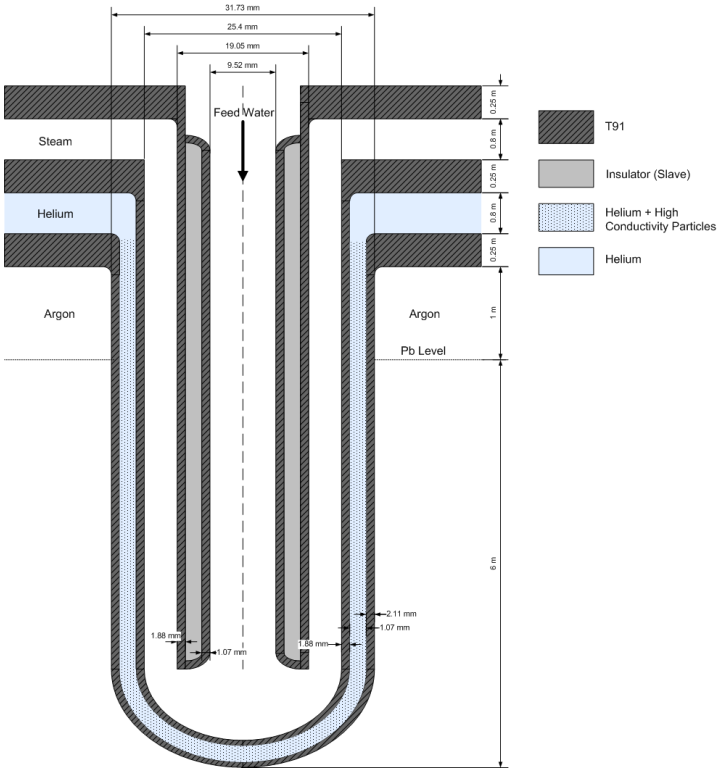

Figure 25: Steam generators bayonet-type configuration - ALFRED

The geometric characteristics of the steam generators components are shown in Table 12.

Component	Volume (m^3)	Length (m)
Break 240 (h2oout)	0.0000	0.0
Fill 200	0.0000	0.0
Pipe 220	13.8790	16.4

Table 12: Secondary one-dimensional model components list - ALFRED

3.1.2.3 Heat Structures

The heat produced in the core is transferred into the primary coolant using 24 Heat Structure components, (Components 1101 to 1112 and 1201 to 1212), 12 structures for the hot fuel assembly pipe and 12 structures for the averaged fuel assembly pipe. This detailed approach is justified by the need to take into account the different gap sizes along the fuel assembly height. For that reason, each fuel assembly was coupled with 12 heat structure components each of them with a different gap size according to the design gap size profile that is considered to be constant along the transient. This approach allows to take into account different gap sizes along the fuel assembly, but a more detailed dynamic fuel-pin-mechanics models should be implemented in the code in order to actualise the gap size profile along the transient, taking into consideration also possible fuel-cladding interaction phenomena.

Table 13 shows the gap distance (m) considered for 10 axial nodes of the active core region extracted form detailed fuel-pins-mechanic calculations provided in the project documentation [Bandini et al, 2013].

	BOC		EOC	
Height	HFA	MFA	HFA	MFA
0.03	2.18E-05	3.05E-05	6.86E-06	1.54E-05
0.09	1.32E-05	2.23E-05	5.03E-06	9.01E-06
0.15	6.36E-06	1.56E-05	5.03E-06	5.04E-06
0.21	5.05E-06	1.25E-05	5.03E-06	5.04E-06
0.27	5.05E-06	9.17E-06	5.03E-06	5.04E-06
0.33	5.06E-06	7.14E-06	5.03E-06	5.04E-06
0.39	5.06E-06	6.80E-06	5.03E-06	5.04E-06
0.45	5.06E-06	7.57E-06	5.03E-06	5.04E-06
0.51	5.06E-06	1.02E-05	5.04E-06	5.04E-06
0.57	5.06E-06	1.32E-05	5.04E-06	5.04E-06

Table 13: Gap distance (m) axial profile in different core configurations

Table 14 shows the main geometrical values of the modelled heat structures in the core and in the steam generators. Each core heat structure has 16 radial nodes corresponding, 2 for the fuel pellet, 11 for the fuel material, 1 for the gap and 2 for the cladding material. Heat structures 4201 and 4202 have 4 radial nodes, 2 for the cladding material and one for the isolation/high conductivity layer (Figure 25) respectively.

Component	Inner area (m^2)	Outer area (m^2)	Volume (m^3)
Heat Structure 1101 to 1112	0.000	0.249	0.001
Heat Structure 1201 to 1212	0.000	42.392	0.132
Heat Structure 4201	1896.800	2783.800	11.842
Heat Structure 4202	902.980	1806.900	6.456

Table 14: Heat structure components characteristics – ALFRED

Table 15 shows the different core power peaking factors related with each heat structure. This value are extracted from the neutronic analysis of the core and are assumed to remain constant along the transients. The power fraction represents the relative power that is allocated to the heat structure per fuel assembly. The hot fuel assembly represent 1 fuel assembly and the mean fuel assembly represents the rest, 170 fuel assemblies with averaged values. Each fuel assembly contains 127 fuel pins, geometrically modelled by the heat structure.

Powered Component	Power Fraction	Powered Component	Power Fraction
Heat Structure 1101	0.7470648	Heat Structure 1201	0.6167628
Heat Structure 1102	0.8795385	Heat Structure 1202	0.7079742
Heat Structure 1103	1.0359009	Heat Structure 1203	0.8122158
Heat Structure 1104	1.194435	Heat Structure 1204	0.912114
Heat Structure 1105	1.3095351	Heat Structure 1205	0.9794367
Heat Structure 1106	1.4268069	Heat Structure 1206	1.042416
Heat Structure 1107	1.4941296	Heat Structure 1207	1.0771632
Heat Structure 1108	1.5180183	Heat Structure 1208	1.0793349
Heat Structure 1109	1.5006447	Heat Structure 1209	1.064133
Heat Structure 1110	1.4463522	Heat Structure 1210	1.0141839
Heat Structure 1111	1.3659993	Heat Structure 1211	0.9533763
Heat Structure 1112	1.2899898	Heat Structure 1212	0.9164574

Table 15: Heat structure peaking factors profile – ALFRED

3.2 The three-dimensional modelling

In order to have a complete representation of the phenomena that may occur during an asymmetrical accidental transient scenario in a power plant a 3D-modelisation is mandatory. Indeed, hypothetical transients that potentially threat the reactor safety may have an asymmetrical component which a one-dimensional nodalisation with a point kinetics scheme cannot reproduce.

The approach followed to upgrade the thermal-hydraulic model with three-dimensional capabilities was to substitute the one-dimensional components of the primary loop by a set of components able to reproduce radial and azimuthal flows. In particular, three azimuthal sectors were considered taking into account the components layout of the vessel internals (three pumps with six IHX groups uniformly distributed).

Indeed, the one-dimensional components 90, 100, 102, 103, 104, 105, 106, 107, 110, 120, 160, 280, 1002 and 1102 described in the previous section were replaced with one single TRACE Vessel component with three-dimensional capabilities.

The hot fuel assembly (Pipe 101) kept the one-dimensional nodalisation as better approach to simulate the behaviour of that particular fuel assembly.

The new primary nodalisation layout can be seen in Figure 26.

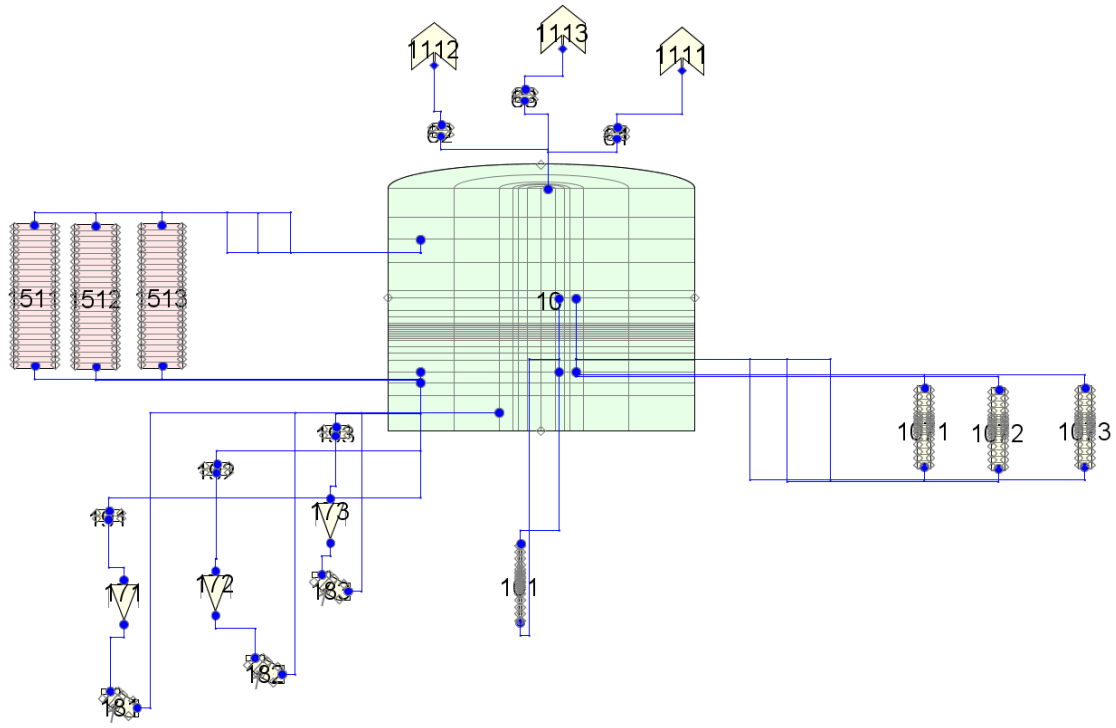

Figure 26: Primary three-dimensional nodalisation - ESFR

The core is represented by 14 axial levels and 4 radial sectors. These radial sectors are representing the inner fuel (1) outer fuel (2) and radial reflector (1) assemblies. 10 of these axial levels and 4 radial rings are representing the active core and axial reflector, so are coupled with 12 Heat Structure components (4 radial sectors x 3 azimuthal sectors) modelling the fuel and reflector assemblies. The by-pass is modelled with one-dimensional pipe components since the computational cost increase of an additional radial ring is no justified for the level of accuracy needed in this particular component.

The core rings are closed, so no radial or azimuthal flow is permitted between the different radial rings.

The Upper Vessel (hot zone) of the primary pool is represented by 6 axial levels and 6 radial rings taking into consideration the different cross sections that the flow faces in this area due to the influence of the Above Core Structure.

The lower vessel is composed by 5 axial levels and 6 radial sectors. The pumps are taking the flow from the external rings and pump it into the strongbow area under the diagrid. The previous one dimensional Time-dependent junction is replaced by three time-dependent junctions with equivalent characteristics.

The primary side of the intermediate heat exchanger is simulated by three equivalent one-dimensional pipes (Components 1511, 1512, 1513). The one-dimensional approach is more convenient to model the intermediate heat exchangers since they have tubular geometry. Each

of this pipes is linked to one group of two lumped secondary loops, keeping the azimuthal consistency.

The main geometrical characteristic of the new primary system thermal-hydraulic nodalisation is shown in Table 16.

Component	Volume (m^3)	Length (m)
Break 1111	0.0000	0.0
Break 1112	0.0000	0.0
Break 1113	0.0000	0.0
Pipe 61	0.6283	0.8
Pipe 62	0.6283	0.8
Pipe 63	0.6283	0.8
Pipe 101 (HFA)	0.0563	4.2
Pipe 181	1.6630	2.1
Pipe 182	1.6630	2.1
Pipe 183	1.6630	2.1
Pipe 191	1.1440	0.7
Pipe 192	1.1440	0.7
Pipe 193	1.1440	0.7
Pipe 1071 (reflector)	1.8592	4.2
Pipe 1072 (reflector)	1.8592	4.2
Pipe 1073 (reflector)	1.8592	4.2
Pipe 1511 (ihxpri)	33.5980	7.6
Pipe 1512 (ihxpri)	33.5980	7.6
Pipe 1513 (ihxpri)	33.5980	7.6
TDJ 171 (prim pump)	0.0000	0.0
TDJ 172 (prim pump)	0.0000	0.0
TDJ 173 (prim pump)	0.0000	0.0
Vessel 10	3313.7000	651.0

Table 16: Primary three-dimensional model components list – ESFR

The secondary loop shown in Figure 22 is divided into three equivalent one-dimensional loops thermally coupled with each of the primary sides of the intermediate heat exchangers described in the previous paragraph. The secondary side of the intermediate heat exchanger the components 2521, 2522 and 2523. The secondary side of the steam generators are components 2521, 2522 and 2523. Components 2611 to 2613 and 2621 to 2623 are Pipe components that link the intermediate heat exchangers con the steam generators volumes adjusting the secondary circuit sodium inventory.

The secondary pumps are modelled by three Time-dependent junction components (Components 2811, 2812 and 2813).

The main geometrical characteristic of the new secondary systems thermal-hydraulic nodalisation is shown in Table 17.

Component	Volume (m^3)	Length (m)
Break 2000	0.0000	0.0
Break 2001	0.0000	0.0
Break 2010	0.0000	0.0
Pipe 291	1.0210	1.3
Pipe 292	1.0210	1.3
Pipe 301	1.0210	1.3
Pipe 2201 (nasg)	106.4800	24.2
Pipe 2202 (nasg)	106.4800	24.2
Pipe 2203 (nasg)	106.4800	24.2
Pipe 2521 (ihxsec)	72.4800	7.6
Pipe 2522 (ihxsec)	72.4800	7.6
Pipe 2523 (ihxsec)	72.4800	7.6
Pipe 2611	114.2300	86.2
Pipe 2612	114.2300	86.2
Pipe 2613	114.2300	86.2
Pipe 2621	114.4000	88.5
Pipe 2622	114.4000	88.5
Pipe 2623	114.4000	88.5
TDJ 2811 (sec pump)	0.0000	0.0
TDJ 2812 (sec pump)	0.0000	0.0
TDJ 2813 (sec pump)	0.0000	0.0

Table 17: Secondary three-dimensional model components list – ESFR

In the same line, the one-dimensional tertiary loop with boundary conditions shown in Figure 23 is now divided into three equivalent ones thermally coupled with the secondary equivalent loops described. The new components are listed in Table 18.

Component	Volume (m^3)	Length (m)
Break 471 (h2oout)	0.0000	0.0
Break 472 (h2oout)	0.0000	0.0
Break 473 (h2oout)	0.0000	0.0
Fill 401	0.0000	0.0
Fill 402	0.0000	0.0
Fill 403	0.0000	0.0
Pipe 421 (sgtube)	8.4199	24.2
Pipe 422 (sgtube)	8.4199	24.2
Pipe 423 (sgtube)	8.4199	24.2

Table 18: Tertiary three-dimensional model components list – ESFR

The different Heat Structure components have been adapted to the new nodalisation. The heat structure modelling the core power have been divided into three equivalent ones and coupled

with the related cells of the Vessel component. Each Heat Structure component has been coupled with one azimuthal sector and one radial ring. The number of heat structures modelling the generated power is 13, one representing the hot fuel assembly (111) coupled with Pipe 101, three representing the inner core area (121, 122, 123) coupled with radial level number 1, six representing the outer core area (131, 132, 133, 141, 142, 143) linked with radial rings 2 and 3 and three representing the reflector zone (161, 162 and 163) linked with radial ring number 4.

The heat structure modelling the diagrid structure has been also divided in three equivalent structures (Components 1001 to 1003).

The heat structures representing the heat transfer in the intermediate heat exchanger in the steam generators were adapted to the new nodalisation dividing them into three equivalents coupled with the new thermal-hydraulic components (Components 2511 to 2513 and 4201 to 4203).

Table 19 shows the details of the three-dimensional modelling heat structure components.

Component	Inner area (m^2)	Outer area (m^2)	Volume (m^3)	Power Fraction
Heat Structure 111	0.0000	3.1	0.0	1.370000
Heat Structure 121	0.0000	685.1	1.8	0.969950
Heat Structure 122	0.0000	685.1	1.8	0.969950
Heat Structure 123	0.0000	685.1	1.8	0.969950
Heat Structure 131	0.0000	362.4	1.0	1.204780
Heat Structure 132	0.0000	362.4	1.0	1.204780
Heat Structure 133	0.0000	362.4	1.0	1.204780
Heat Structure 141	0.0000	319.7	0.9	0.865750
Heat Structure 142	0.0000	319.7	0.9	0.865750
Heat Structure 143	0.0000	319.7	0.9	0.865750
Heat Structure 161	0.0000	1014.0	2.7	0.006829
Heat Structure 162	0.0000	1014.0	2.7	0.006829
Heat Structure 163	0.0000	1014.0	2.7	0.006829
Heat Structure 1001	223.0000	223.0	11.2	
Heat Structure 1002	223.0000	223.0	11.2	
Heat Structure 1003	223.0000	223.0	11.2	
Heat Structure 2511	3676.4000	4056.0	3.1	
Heat Structure 2512	3676.4000	4056.0	3.1	
Heat Structure 2513	3676.4000	4056.0	3.1	
Heat Structure 4201	3360.2000	4958.4	10.4	
Heat Structure 4202	3760.2000	5533.9	11.6	
Heat Structure 4203	3760.2000	5533.9	11.6	

Table 19: Heat structure components in 3D model characteristics – ESFR

3.3 The coupling scheme

The three-dimensional thermal-hydraulic model described in the previous section is able to simulate thermodynamic asymmetric phenomena that may take place in the main systems of the design. But, in order to be a consistent calculation, the neutronic behaviour of the core must be also able to take into account spatial differences. Since the point kinetic neutronic feedback approach uses averaged values of the different zones it may overlook important localised effects. For that reason, a spatial detailed neutronic response is required to be developed and integrated in the thermal-hydraulic model.

The spatial neutronic code selected for such a purpose is PARCS (Purdue Advanced Reactor Core Simulator) code. PARCS solves the time-dependent two-group neutron diffusion equation in three-dimensional Cartesian geometry using nodal methods to obtain the transient neutron flux distribution. It is prepared to perform dynamic calculations of the core response of light water reactors and it is prepared for such a purpose to be coupled with the system code TRACE.

3.3.1 The neutronic model

The neutronic model comprises the core geometry description along with the neutronic characteristics of its materials. The core geometry is composed by the different subassemblies distributed as specified in the core design [Genot, 2009 and Blanchet, 2009].

The core geometry and its compositions should be translated into a geometrical model with a related cross section set that will be processed by PARCS to supply the thermal-hydraulic model with an on-line spatial neutronic calculations.

3.3.1.1 The cross-section set

The first step towards the development of a spatial neutronic response code is the generation of a cross section set that defines the nuclear behaviour of the core materials. This cross section set depends on the composition of the materials that are allocated in the core and the distribution of these different materials along it. For that purpose, it is needed to use an external code able to generate the cross section set from the design details using a nuclear data source. In this case it is used the Monte-Carlo based code SERPENT [Fridman et al, 2011] and the nuclear data evaluated library JEFF - 3.1.

A cross section set is required for each energy group in which the neutron energy spectrum is divided. The common approach for light water reactor technology is to divide the energy spectrum into two/three groups. Fast reactor technology requires a more detailed energy spectrum division in order to have a better approximation to the cross section value in the high energy zone since the neutronic energy distribution is wider. For this case, a seven group configuration is selected as recommended in the related bibliography [Fridman et al, 2013].

A sensitivity study to find the compromise solution between accuracy (number of groups) and computing time economy is needed.

The different cut-off energies used to generate the cross section set are shown in Table 20. They are based in ECCO structure collapsed in 7 groups.

Group	Upper energy limit (MeV)
1	19.64033
2	0.82085
3	0.1831564
4	0.04086771
5	0.00911882
6	0.002034684
7	0.000304325

Table 20: Upper energy limits for the 7 energy groups

Furthermore, the cross section set for each energy group is generated for in specific thermal conditions, in particular, the reference cross section set is defined for 1500K of fuel temperature and 900 K coolant. In addition to this reference set, two more sets are calculated, one for a higher and another for a lower temperature respectively in order to generate cross section derivatives, and thus, being able to calculate cross section values along the temperature interval considered for each one of the seven energy groups.

Each cross section set includes the following values:

- Transport cross section
- Absorption cross section
- Nu-fission cross section
- Kappa fission cross section
- Down scattering cross section (n-1 groups)

3.3.1.2 Core Model

A core model input is required in both, SERPENT and PARCS codes, representing the different sub-assemblies allocated in the core. These are the active fuel assemblies, control assemblies and reflector assemblies.

Figure 27 shows a snapshot of the core layout distribution. Components 1 and 2 represent inner and outer core fuel assemblies, components 3, 4 and 5 represent control rod assemblies, component 6 represents a coolant assembly placed in the core centre and component 7 represent the reflector assemblies.

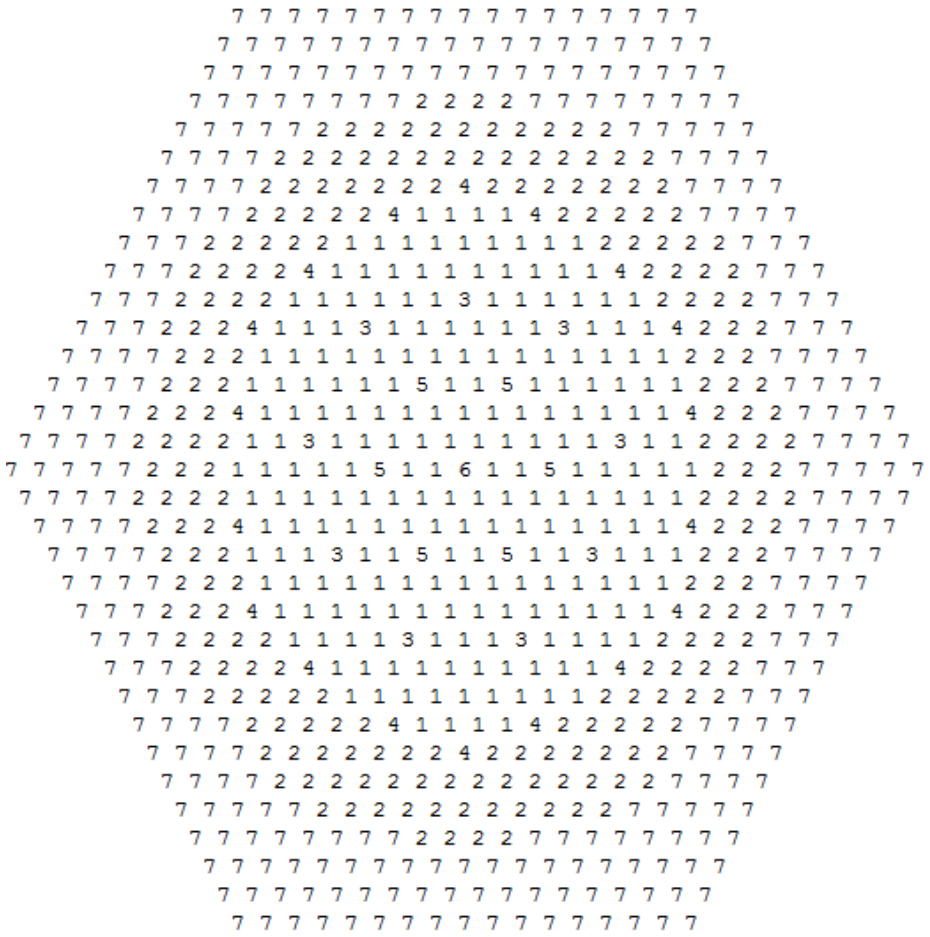

Figure 27: Core three-dimensional model radial layout – ESFR

Each assembly is divided into 15 axial levels according to the specific configuration of each type. Figure 28 shows the axial nodalisation of the three kinds of fuel assemblies.

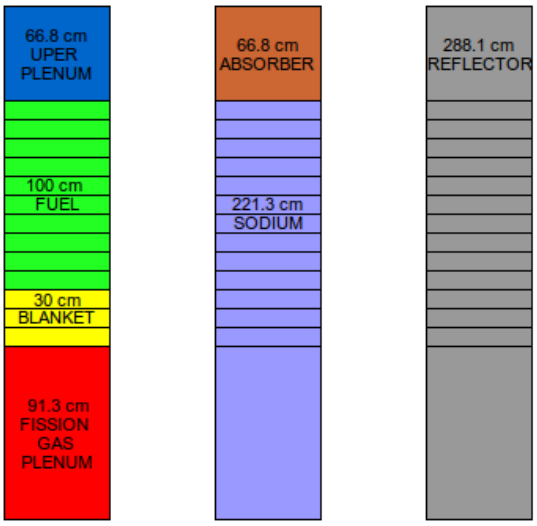

Figure 28: Core three-dimensional model axial nodalisation – ESFR

The number of axial fuel assemblies depend on the level of definition expected in the different areas (active core area requires higher definition that reflector), numeric stabilities (the power gradients are higher in the active core fuel regions) and computational cost considerations. Fifteen nodes are a compromise solution between the detail level needed and the computational cost associated.

3.3.1.3 Stand-alone calculations

With the core model implemented in SERPENT code it is possible to perform a static calculations with the objective to obtain the cross section sets and steady-state power profile distributions.

Then, the cross section set together with its derivatives and core model as described in the previous section are implemented in PARCS, which is able also to perform static core calculations. Therefore, the first step to check the consistency of the calculations is the benchmarking of the results between SERPENT and PARCS codes, in particular, the power profile obtained.

Figure 29 shows the relative differences between the two codes for the radial power profile in a sector of the core with the highest differences. The difference is limited to 1.5 %.

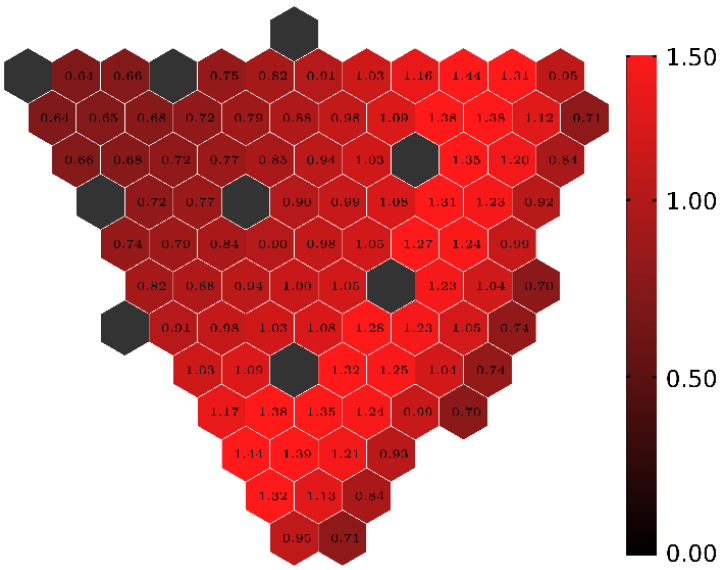

Figure 29: Radial steady-state power profile relative differences (%) SERPENT – PARCS

Figure 30 shows the relative difference in the axial power profile between the two codes.

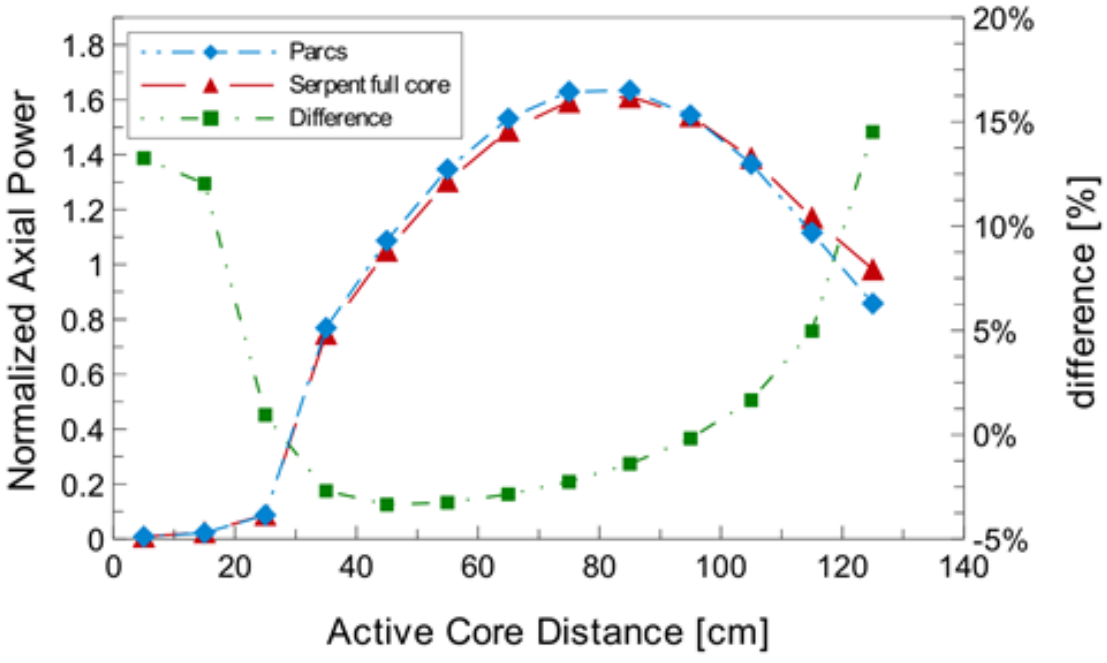

Figure 30: Axial steady-state power profile difference between SERPENT – PARCS

As Figure 29 and Figure 30 show, both code present very similar results. The higher discrepancies appear in the lower and upper regions of the axial profile and not in the fissile areas, where the differences are lower than 5%.

The consistency of the results supported the adequacy of the cross-section set and models generated in order to be integrated with the thermal-hydraulic three-dimensional model.

3.3.1.4 TRACE-PARCS coupling scheme

The last step consists of coupling neutronic and thermal-hydraulic models (codes) with the objective to perform dynamic calculations taking into account the thermal feedback. TRACE code contains PARCS code embedded in its source, but, some adaptations have to be done when applying it to fast reactor designs.

PARCS code can only take into account the three main components of the neutronic reactivity effects that take place in a fast reactor. These are the Doppler effect, the coolant expansion (void) effect and the differential insertion of the control rods as shown in Equation (4). Unfortunately, PARCS cannot take into account geometry variations during the transients, so the fuel, cladding and diagrid expansion effects are neglected. Previous studies have confirmed [Lázaro A. et al-I, 2014] that the combined effect of these three contributions is negative and one order of magnitude lower than the others, so the cancellation of these effects is a conservative assumption.

The coupling scheme between TRACE and PARCS is settled in such a way that TRACE sends to PARCS the main thermodynamic data needed to calculate the corresponding power profile, and PARCS feedbacks TRACE with this calculated power profile used to derive the thermodynamic variables of the next time step. The variables sent from TRACE to PARCS to perform the power calculation are fuel temperature, coolant temperature and void fraction. PARCS sends back the power value of each of the powered Heat Structure components axial nodes. Figure 31 shows the data exchange scheme.

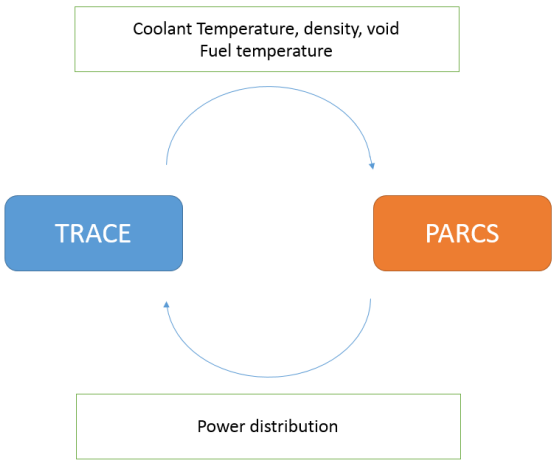

Figure 31: TRACE-PARCS data exchange flowchart

As explained in the model description, the three-dimensional thermal hydraulic model devotes 10 axial levels, 4 radial rings and 3 azimuthal sectors for the active core and reflector. This means that TRACE code calculates the behaviour of 120 thermal-hydraulic nodes, ten axial levels of 12 nodes each numbered as shows.

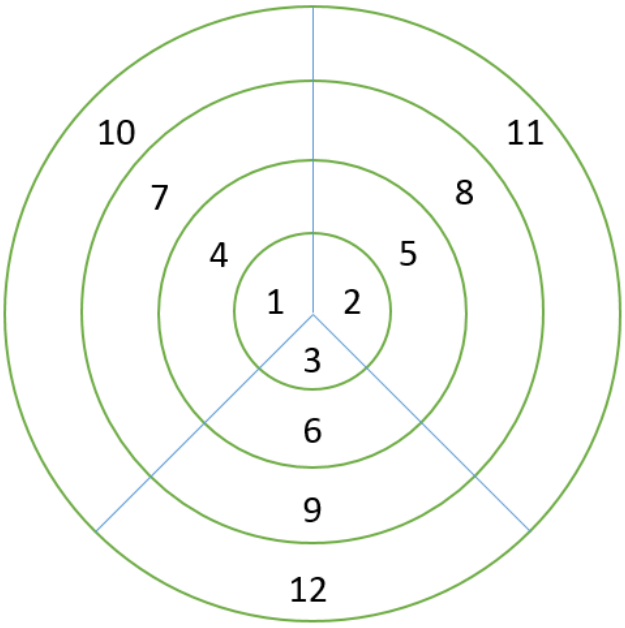

Figure 32: Vessel thermal-hydraulic nodes numbering

For each axial level the numbering scheme is repeated, so it should be specified to which axial level belongs each node.

There are 12 heat structures calculating the thermal behaviour of the fuel assemblies and each heat structure has 10 axial levels, thus these are also 120 nodes too, which are in direct coupling with the hydraulic ones in the TRACE model as was explained in section 3.2. There is no specific numbering for the heat structure nodes, they are identified by the heat structure number and the axial level they represent.

The neutronic model has 817 assemblies and each one of them has 15 axial levels as explained in the neutronic model description in section 3.3.1. This means that the neutronic model has 12255 nodes. Each of these nodes require values of the coolant thermal conditions (temperature, density, void) and structure (fuel) temperatures, therefore each one of these neutronic nodes has to be mapped with a thermal-hydraulic node and a heat structure node.

In order to be coupled with TRACE code, PARCS requires the input of a mapping file in which each of the PARCS nodes are linked with the corresponding TRACE nodes. PARCS nodes are numbered by the code according to the scheme shown in Figure 33. These nodes correspond to the first (lower) axial level of the fuel assemblies. The subsequent (upper) levels are numbered keeping the same structure differing ((n-1)*817), with n the axial level.

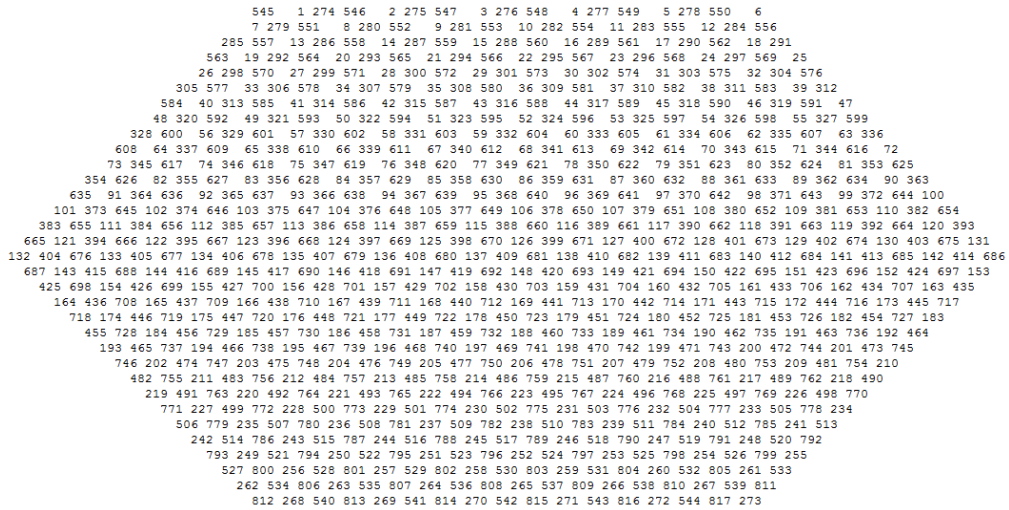

Figure 33: PARCS node numbering

The mapping file that links the 12255 PARCS nodes with the 240 TRACE nodes (120 TH nodes + 120 HS nodes) has to suit to a specific pattern required by PARCS code. This file is generated using an ad hoc MATLAB script developed for this purpose. Figure 34 shows the first lines of the mapping between the thermal hydraulic (TABLE1) and heat structures (TABLE2) nodes and the neutronic nodes.

```
%TABLE1                                                    %TABLE2
10      10      6       545     1.0000          161     1       1       545     1.0000
10      10      6       1       1.0000          161     1       1       1       1.0000
10      10      6       274     1.0000          161     1       1       274     1.0000
10      10      6       546     1.0000          161     1       1       546     1.0000
10      10      6       2       1.0000          161     1       1       2       1.0000
10      10      6       275     1.0000          161     1       1       275     1.0000
10      10      6       547     1.0000          161     1       1       547     1.0000
10      10      6       3       1.0000          161     1       1       3       1.0000
10      10      6       276     1.0000          161     1       1       276     1.0000
10      10      6       548     1.0000          161     1       1       548     1.0000
10      10      6       4       1.0000          161     1       1       4       1.0000
10      10      6       277     1.0000          161     1       1       277     1.0000
10      10      6       549     1.0000          161     1       1       549     1.0000
10      10      6       5       1.0000          161     1       1       5       1.0000
                                                161     1       1       278     1.0000
```

Figure 34: TRACE-PARCS nodes mapping

For the thermal hydraulic nodes, the first number of each row represents the vessel component number (10), the second one the number of the radial sector involved (see Figure 29) the third one represents the axial level, the forth one represents the neutronic node and the fifth the weight of the neutronic node in the hydraulic one. This number is used in case the neutronic node is placed in between two or more thermal-hydraulic nodes, then this coefficient weights the contributions of the hydraulic node into the neutronic one. The sum of the coefficients related to each neutronic node should be one. But in this case, the models were done in such a way that every neutronic node was falling under one single thermal-hydraulic node. That is the reason why all the coefficients are strictly 1.0000.

Regarding the heat structure nodes mapping (TABLE2), the first numbers represents the number of the structure mapped, the second number the rod group number, the third number represents the axial level of this heat structure and the fourth the weighting factor similarly as in TABLE 1.

4. Results – 1D modelling

This chapter describes the results provided by the one-dimensional models described in Chapter 3. The one dimensional models have been benchmarked with their equivalents developed by partner organisations in the framework of international research projects for both ESFR and ALFRED designs. Afterwards, in Chapter 5, the one-dimensional models results are used as a reference to compare the three-dimensional model results for symmetrical cases.

4.1 The one dimensional SFR model

In the framework of the Collaborative Project on the European Sodium Fast Reactor [Vasile et al, 2011], a dedicated working group was devoted to the development and assessment of computational tools and models to evaluate the behaviour of the design to withstand a number of postulated transients defined in the safety assessment of the design.

The partners of this working group are research institutes, with renowned experience in fast reactor safety assessments. The results of the models from CEA using CATHARE code (France), KIT using SIM-SFR and SAS4 (Germany), PSI (Switzerland) using FAST code, ENEA (Italy) using RELAP and CATHARE code, NRG (Netherlands) using SPECTRA, EdF (France) using MAT4DYN and JRC-IET (European Commission) using RELAP5 and TRACE, which is the one detailed in 3.1 and referred as JRC-TRACE in the upcoming plots, are considered in this Chapter.

The methodology followed within the working group to achieve an acceptable consistency in the calculations started with the settlement of a benchmarking case consisting in a fictitious transient. The organisations compared their results for this scenario and adjusted specific features of each code to reach common modelling practices [Lázaro A. et al-I, 2014].

4.1.1 Steady-state calculations

Before simulating the selected transients, a steady state calculation was performed and compared both with the reference design data and with other partners' calculations to test the capability of the models to calculate the nominal conditions. These results are show in Table 21.

PARAMETER	ESFR - Nominal	TRACE	RELAP5
Primary mass flow rate (kg/s)	19535	20692 (5.92%)	20860 (6.78%)
Secondary mass flow rate (kg/s)	15330	16444 (7.27%)	16907 (10.29%)
Core Inlet Temperature (˚C)	395	391(1%)	395
Core Outlet Temperature (˚C)	545	545	545
IHX Inlet Temperature (˚C)	340	335 (1.5%)	332 (2.35%)
IHX Outlet Temperature (˚C)	525	522 (0.5%)	517 (1.52%)
SG outlet Temperature (˚C)	490	493 (0.3%)	487 (0.6%)
SG pressure (bar)	185	185	185
SG mass flow rate (kg/s)	1650	1650	1650

Table 21: ESFR 1D model steady-state calculations

The results show a fair level of agreement between the reference design ones, the ones predicted by the thermal-hydraulic TRACE model detailed in this thesis and the ones predicted by an equivalent model developed by a partner organisation (ENEA) using the code RELAP5 [Dufour et al, 2011].

The major discrepancies appear in the primary and secondary mass flow rates. The discrepancy is due to the fact that each of the codes used by the designers and the two codes employed in this comparison use different thermo dynamic data tables for liquid sodium since there is not available a unified standardised thermal data table for sodium as there is for water. A unified data source will contribute to reduce this uncertainty.

4.1.2 Selected transients

4.1.2.1 Benchmarking exercise

As mentioned before, an artificial transient was defined by the participants to compare the results achieved by the various organisations using different system codes and models. This comparison exercise was recommended to harmonize the different approaches and methods employed in the different code systems.

This transient was defined as a “limited unprotected flow coast-down” event, which is characterized by the following simultaneous perturbations:

• The reduction in the primary mass flow-rate up to 40% nominal value following the equation:

$$\frac{Q}{Q_0}(t) = \frac{1}{1+{}^{t}/_{10}} \quad (14)$$

• The reduction in the secondary mass flow-rate up to 40% nominal value following the equation:

$$\frac{Q}{Q_0}(t) = \frac{1}{1+{}^{t}/_{10}} \quad (15)$$

• Reduction of the feedwater mass flow-rate in the water side of the steam generators, decreasing from its nominal value to 50% in 6 seconds.

• The reactor is unprotected (does not trip).

The mass flow-rates (primary, secondary, tertiary) were assumed to remain constant after reaching their asymptotic states.

Figure 35 to Figure 48 show the time evolution of the main safety related variables of the ESFR plant during the first 700 seconds of the limited ULOF transient. These variables are namely,

- Core inlet and outlet temperatures,
- Steam Generator outlet steam temperature,
- Peak fuel and cladding temperatures,
- Total reactivity and its different components (Doppler, coolant temperature, fuel and cladding expansion, diagrid expansion and differential core/control rods expansion).
- Reactor, Intermediate Heat Exchanger and Steam Generators powers

Coolant temperatures

Figure 35 shows the temperature evolution of the sodium coolant at the hot fuel assembly outlet and in Figure 36 the evolution of the core inlet temperature is displayed. The abrupt increase in outlet temperature as a consequence of the massflow reduction triggering the transient can be observed. All the calculations performed by the different partners predict quite similar coolant maximum outlet temperatures taking into account that most of the codes use somewhat different sodium specific heat correlations and core inlet temperatures (Figure 35). After the maximum coolant temperature is reached all the codes predict a similar behaviour as the results are gathered in a relatively narrow band. The outlet temperature evolves to a new equilibrium state at a higher value for this particular transient. SAS-SFR shows a steeper increase of the temperature over time as the sodium temperature at the core outlet is evaluated by averaging the coolant temperatures at sub-assembly outlet of the individual fissile channels. The results from the model described in this thesis (JRC-TRACE) are in line with the general trend defined by the partners' calculations.

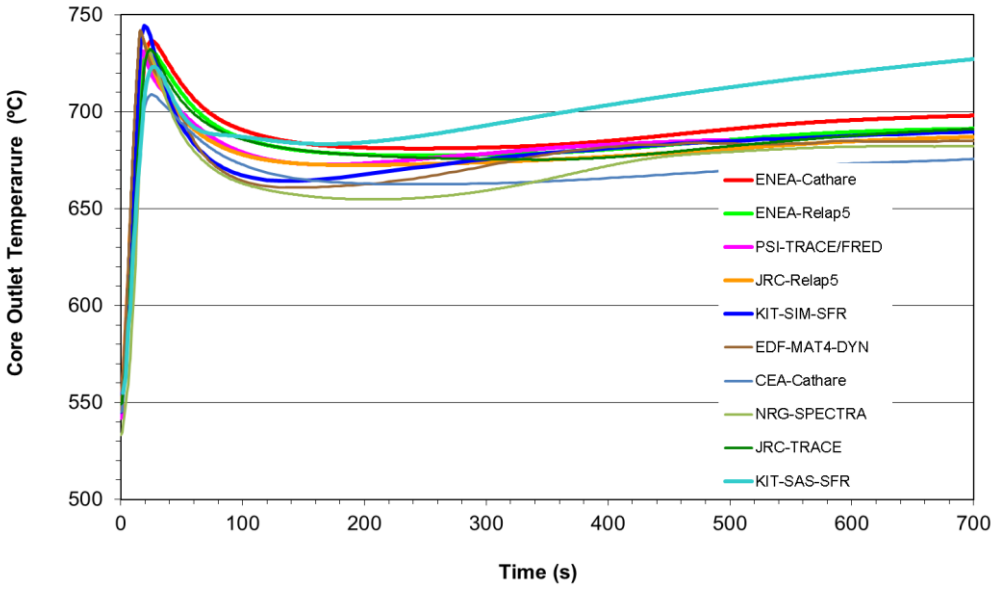

Figure 35: Core outlet temperature – Benchmarking

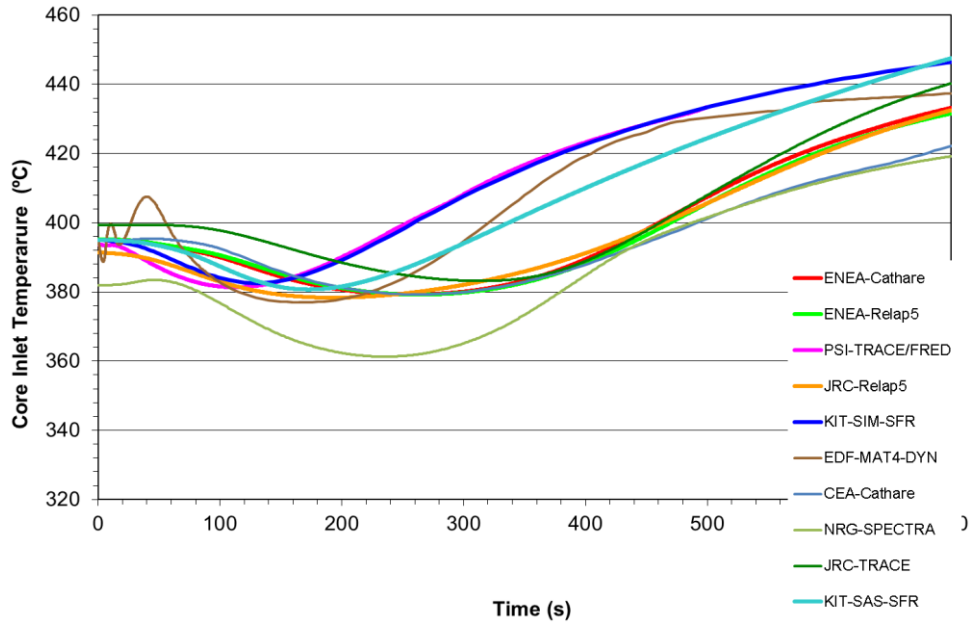

Figure 36: Core inlet temperature – Benchmarking

The steam temperature at the Steam Generator outlet (Figure 37) presents a much wider range of predicted values by the different partners' calculations. Even though they predict that the temperature stabilises at a value between 650°C and 680°C, its evolutions during the first seconds of the transient display notable differences. The reasons behind these deviations among the partners are possibly ascribable to the different modelling of the sodium/water thermal interface of the SG and the differences in the assumed thermal inertia of the secondary systems due to uncertainties in the ESFR BOP design. The difference in modelling of the dynamics of the water interface in the SG (highly superheated steam conditions) could be another reason for the observed deviations.

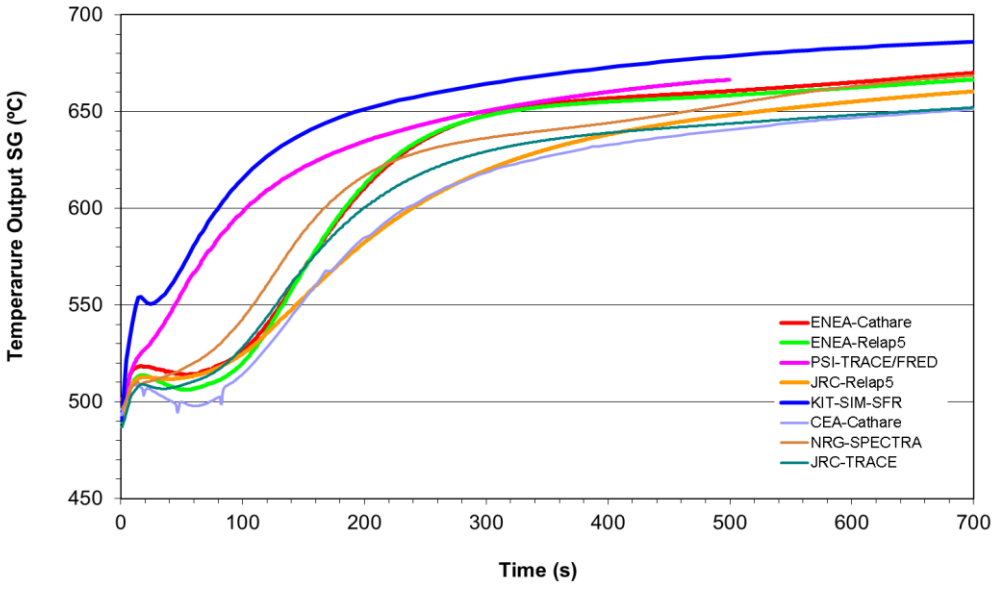

Figure 37: Steam generator outlet temperature (steam) - Benchmarking

Fuel and cladding temperatures

Figure 38 and Figure 39 show the evolution of the fuel and cladding peak temperatures respectively. These temperatures are taken from the highest loaded node from the fuel and cladding models respectively of the hot fuel assembly (peak power pin).

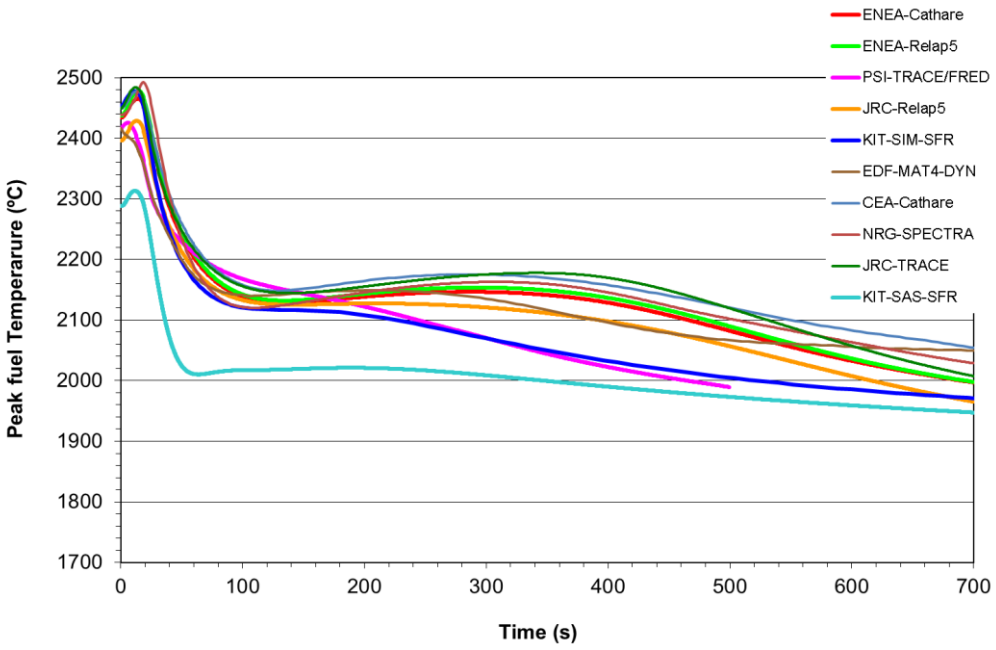

Figure 38: Peak fuel temperature - Benchmarking

Figure 38 shows that the peak fuel temperature at steady state presents values ranging from 2420°C to 2500 °C. This value is strongly influenced by the degree of detail in modelling the fuel rod mechanical behaviour. Some of the codes have models that evaluate the fuel-cladding gap dynamically. Other codes keep a constant gap size that underestimates fuel temperatures. A sensitivity analysis was performed between equivalent models developed by ENEA for CATHARE (dynamic model) and for RELAP5 (static model) showing that the difference is however limited for this particular transient. The results obtained by JRC-TRACE model follow the trend of the other partners' calculations.

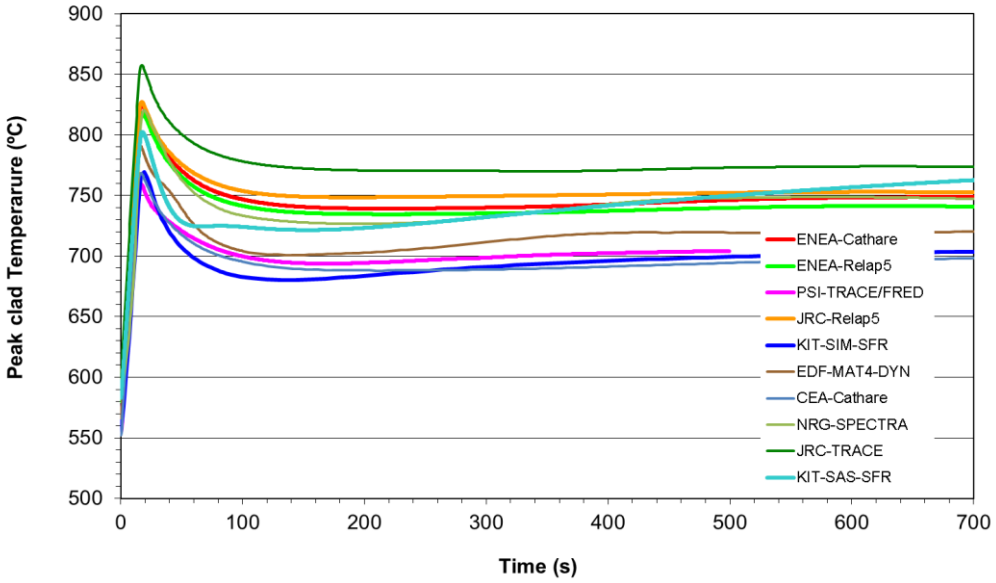

Figure 39: Peak cladding temperature - Benchmarking

Figure 39 shows the evolution of the peak cladding temperature. It displays a maximum value in the range between 740°C and 860 °C. This value is influenced by the massflow distribution in the different flow channels modelled differently by the different partners since the gagging specification is not clearly stated in the project documentation. This accounts for the relatively large band in calculated maximum clad temperatures. The cladding temperatures stabilise between 700°C and 760°C. The results obtained by JRC-TRACE model are close to other partners' calculations.

Reactivity feedback

Figure 40 shows the evolution of the Doppler reactivity feedback effect calculated by the different partners. It is related with the fuel temperature evolution as shown in Figure 38. During the first seconds of the transient the fuel temperature increases abruptly, this creates a negative reactivity that contributes to lower the reactor power. The results obtained by JRC-TRACE model are in line with the other partners' calculations.

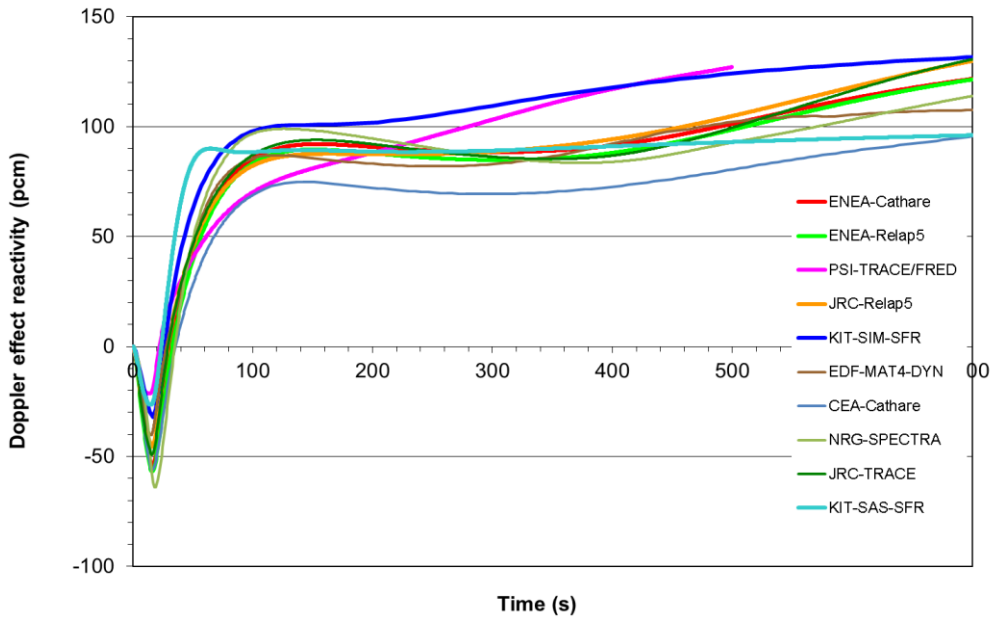

Figure 40: Doppler effect reactivity - Benchmarking

Figure 41 shows the evolution of the coolant expansion reactivity feedback. As this reactivity feedback is governed by a positive reactivity feedback coefficient, the increase in the coolant temperature creates a positive reactivity contribution which has to be limited by design measures in order to prevent this reactivity component to become excessively positive (as it may occur when the centre of the core should become voided). This effect must then be counterbalanced by other negative reactivity feedbacks in order to prevent power excursions. In this particular transient (flow-coast down to 40%), core voiding was not reached as the coolant outlet temperatures remained significantly below (~ 200 °C) the boiling point of the sodium coolant (~ 935 °C) as can be seen in Figure 35.

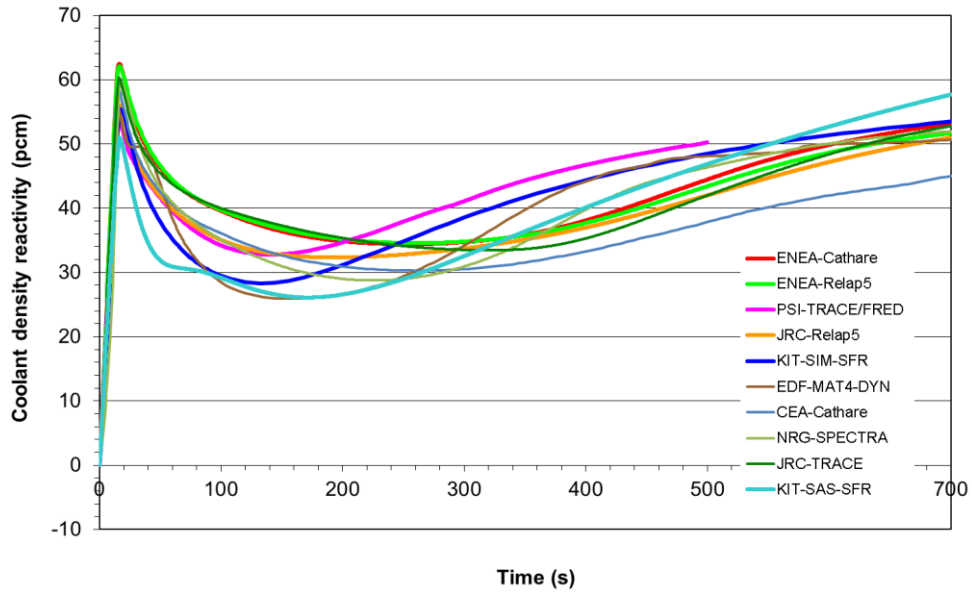

Figure 41: Coolant expansion reactivity - Benchmarking

Figure 42 shows the evolution of the axial expansion reactivity effect. This effect is the combination of the fuel axial expansion effect (Eqn. (7)) and the cladding expansion effect (Eqn. (8)). As it is related with the fuel temperature it has a similar but a lower reactivity response than the Doppler effect. So, it also contributes to decrease the reactor power when the fuel becomes overheated.

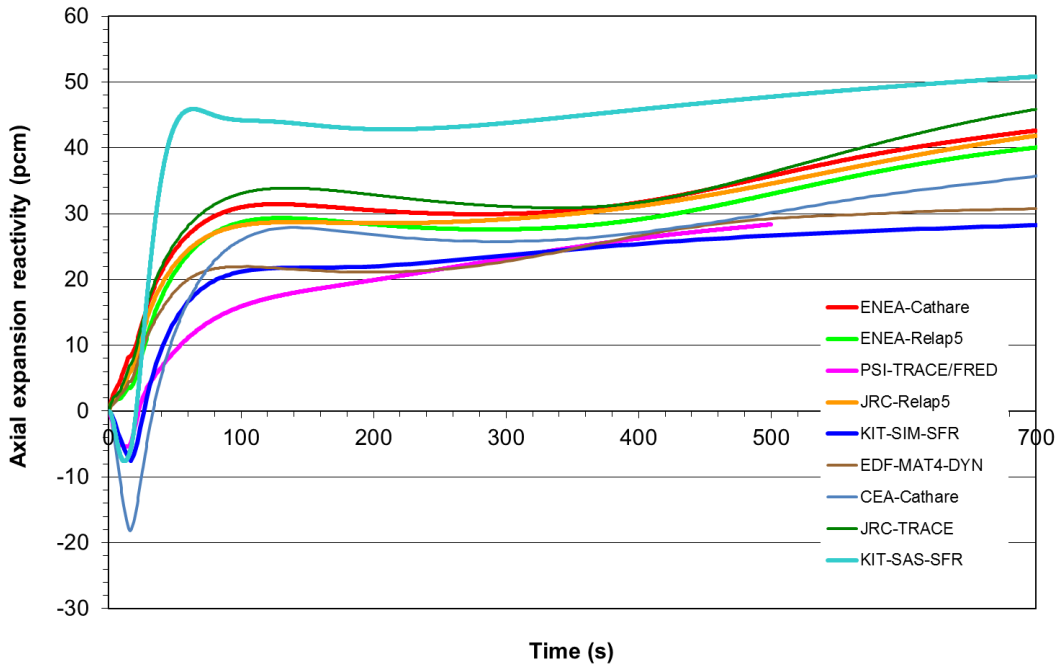

Figure 42: Axial expansion reactivity - Benchmarking

Figure 43 shows the effect of the radial expansion of the diagrid due to thermal effects. There is a significant deviation between the different partner's results. The main cause of this spread is the uncertainty about the thermal inertia of the diagrid structure and the evolution of the outlet temperature of the intermediate heat exchanger, as reflected in the evolution of the core inlet temperature (Figure 36), which leads consequently to correspondingly different reactivity feedback responses. It should be noted that this reactivity component is smaller than most of the other reactivity components, so its contribution to the total reactivity evolution is rather limited. Besides, models for this feedback coefficient have not yet been validated by corresponding operational plant data. The results obtained by JRC-TRACE model are in line with the other partners' calculations.

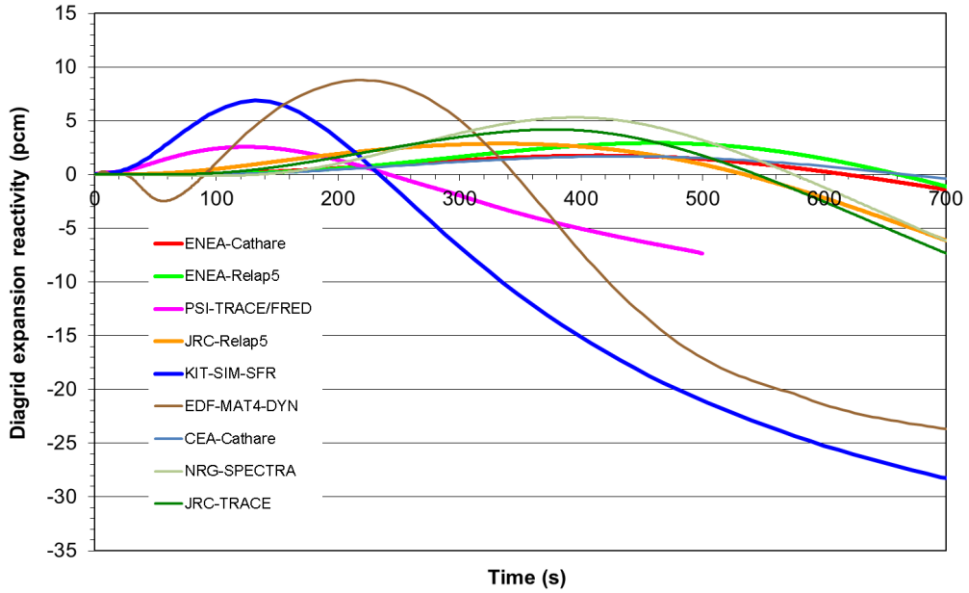

Figure 43: Radial expansion reactivity - Benchmarking

Figure 44 represents the reactivity feedback evolution caused by the partial insertion of the control rods due to the differential core / control rod thermal expansion. As it can be observed by the reactivity feedback scale it is a very strong negative reactivity feedback component causing the reactor power to decrease substantially during this transient. This effect is the most important feedback component in ESFR under BOL conditions assuring the reduction of reactor power in case of the overheating of the core coolant and structures. The deviations among the partners' calculations, though limited, are caused by the combined influence of the differences of core inlet, core outlet and upper plenum coolant temperatures. The results obtained by JRC-TRACE model follow general trend of the other partners' calculations.

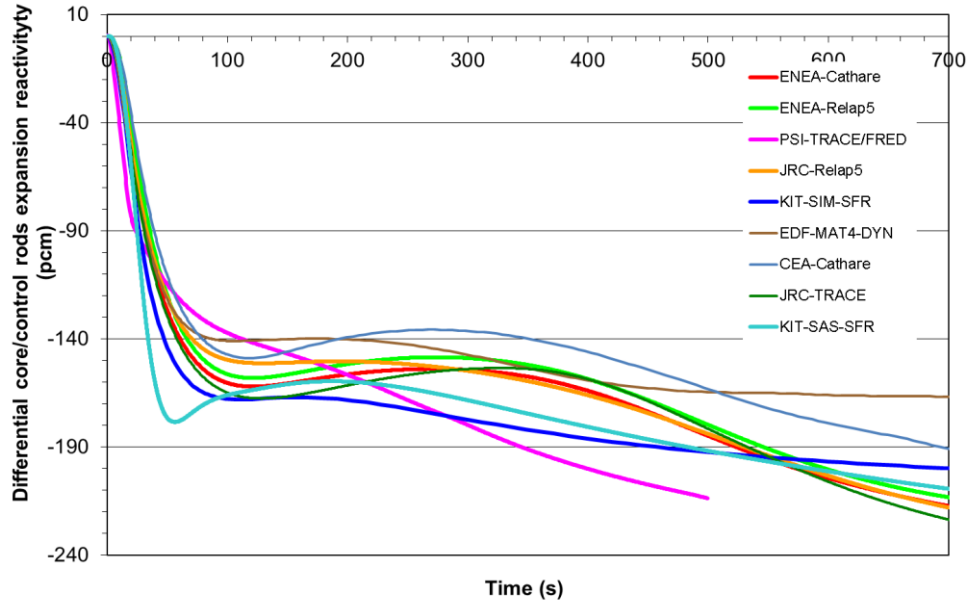

Figure 44: Differential control rod expansion reactivity - Benchmarking

Figure 45 shows the total reactivity feedback evolution of this transient. It is composed of the various contributions of the above mentioned individual reactivity feedback effects. It is important to highlight that during the first seconds of this particular transient the reactor power increases slightly (initially to ~ 103 % nominal value) due to the positive reactivity created by the coolant expansion effect. This effect is then counterbalanced by the various other reactivity feedback components such as the Doppler effect, and in particular the thermal expansion of the control rods effectively decreasing reactor power thereafter.

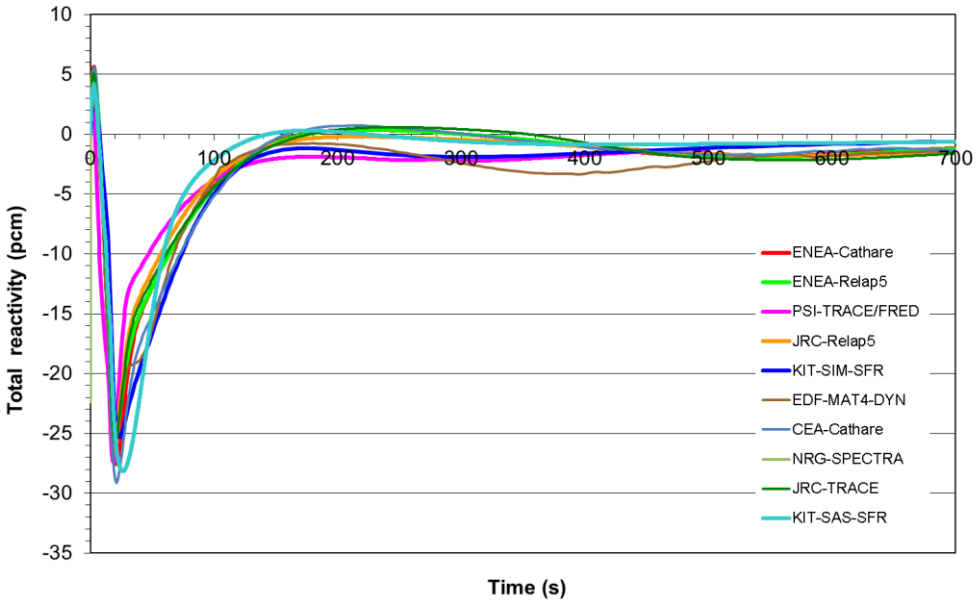

Figure 45: Total reactivity - Benchmarking

There is a satisfactory level of agreement between the different partners' results to this "limited" ULOF event (40% primary flow reduction). This agreement is of particular importance as the total reactivity determines the reactor power behaviour, which in turn is of importance for the safety assessment of the entire system.

Powers

The total reactivity feedback leads to the power evolution as shown in Figure 46. During the earlier seconds of the transient the reactor slightly increases in power. Thereafter, the negative reactivity created by the Doppler effect and the differential core/control rod expansion effect reduces the reactor power. The different partners calculated the peak power at around 103% nominal, with a power reduction to 70% to 63% during the time interval considered (700 s).

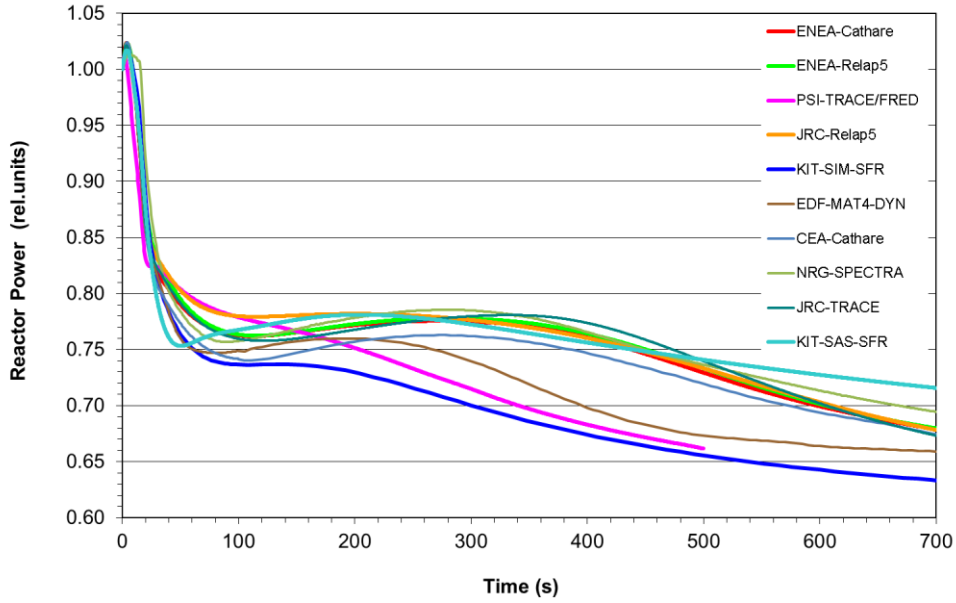

Figure 46: Core power evolution - Benchmarking

The evolution of the powers exchanged in the IHXs and SGs are shown in Figure 47 and Figure 48 respectively. Due to the reduction of the sodium mass flow on the primary side the power exchanged from the primary to secondary and tertiary systems is significantly reduced. After the initial power undershoot to below 50% in the IHX (Figure 47) and below 55% in the SG (Figure 48) the power increases again as the primary coolant temperature increases. The observed deviations between the participants in these figures are caused by the different modelling assumptions of the secondary loops (uncertainty about coolant inventory). The asymptotic value of ~60% of nominal power is predicted quite consistently by all codes.

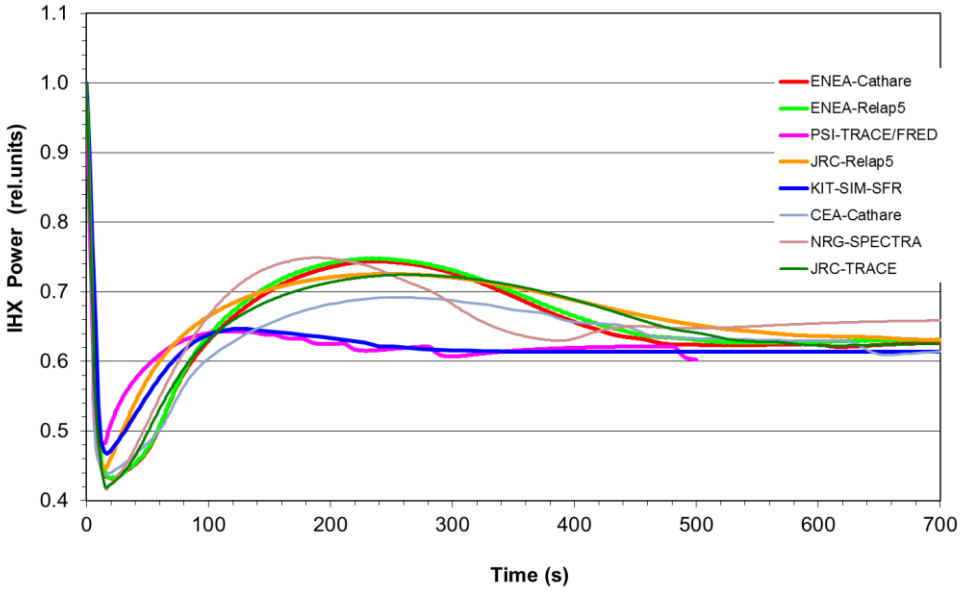

Figure 47: IHX power evolution - Benchmarking

The heat exchanged in the SGs between the secondary and tertiary circuits follows the trend imposed by the power exchanged between the primary and secondary circuits in the IHX. It is also influenced by the different secondary inventory assumed by the different partners. The final value after 700 seconds transient time is again quite close to ~60% nominal value.

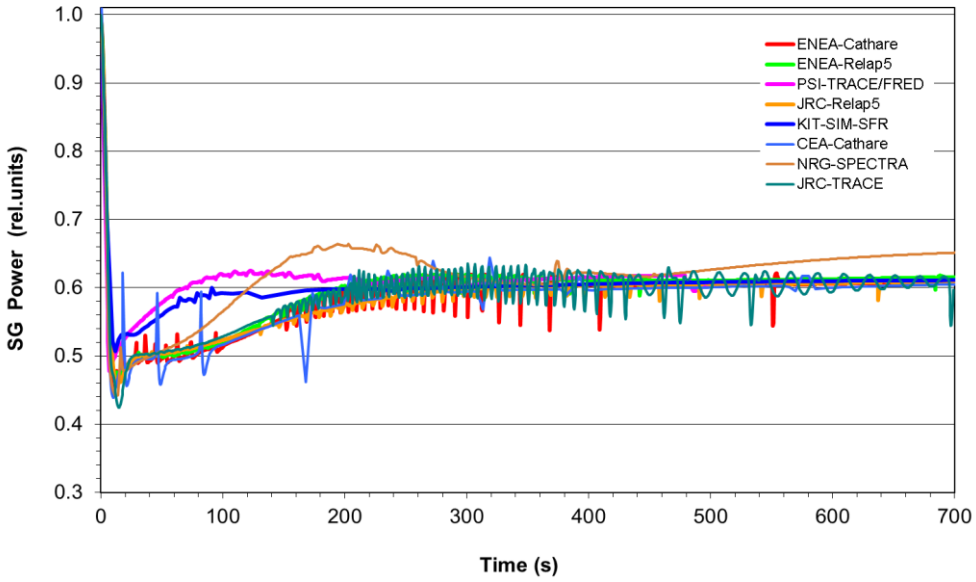

Figure 48: SG power evolution - Benchmarking

As it can be observed from Figure 35 to Figure 48, the results calculated by the one-dimensional model developed is able to calculate the main system variables according to its equivalent state-of-the-art models.

4.1.2.2 Representative transients

Once the models had a fair level of consistency as shown in the results gathered in the benchmarking case, each of the partners used the models and codes to calculate the system behaviour against certain postulated initiating events defined in the safety assessment of the design.

Among these postulated transients, the unprotected loss of primary pump, ascribed as an Unprotected Loss of Flow (ULOF) transient, consists in the simultaneous coast-down of all primary pumps reducing the primary mass flow abruptly. It stands out for its potentially harmful consequences to the system. It can be considered as a Design Basis Accident (DBA) level 4 or even as a Design Extension Conditions (DEC) accident, since its probability of occurrence is extremely low (below 10^{-5}).

The following sections describe the system behaviour of the plant after the initiating event happens, for two core configurations; first the reference core design as established in the plant documentation and, afterwards, with an optimized core in order to see the effect of the void effect reduction.

4.1.2.2.1 Reference Core

The ULOF transient is initiated by the trip of all primary pumps, causing a strong reduction in the primary coolant mass flow rate (Figure 49). The primary mass flow rate is assumed to decrease according to the characteristics of the primary pumps (10 seconds half-time as stated in the design specification). The decrease in the mass flow rate would continue until the natural convection process takes over at some point into the transient if boiling of sodium at the core outlet would not precede this event. The remaining mass flow rate under natural circulation conditions depends on buoyancy forces and friction losses closely associated with the inner-vessel coolant flow paths, so it is directly related to the particular primary system design configuration.

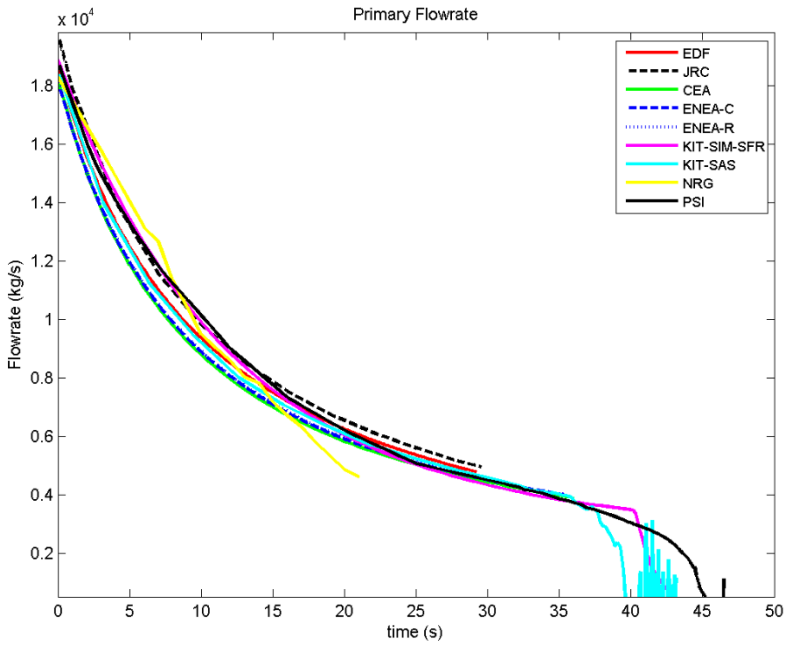

Figure 49: ULOF – Primary massflow rate

The decrease in the in-core mass flow rate will lead to a marked mismatch between the power generated and the convective power extraction from the active core region, leading subsequently to an increase in the maximum temperatures of the core structures (cladding, wrapper, etc.) and the sodium coolant, in particular the sodium coolant temperatures at the active core outlet region. At some point into the ULOF transient, sodium boiling temperatures at the active core outlet region are reached (934°C at 1.6 bar).

Most of the system codes terminated their calculations once sodium boiling temperatures were reached at the active core outlet. The codes (SAS-SFR, SIM-SFR, TRACE-FRED) that were able to continue the calculation beyond sodium boiling onset predict a sharp drop in the mass flow rate several seconds after the core coolant reaches the boiling point, resulting in a rapid rise in local peak cladding temperatures (beyond the boiling temperature of sodium) due to the sharp decrease in the heat-transfer coefficient between clad surface and the bulk coolant vapour after the boiling crisis (dryout).

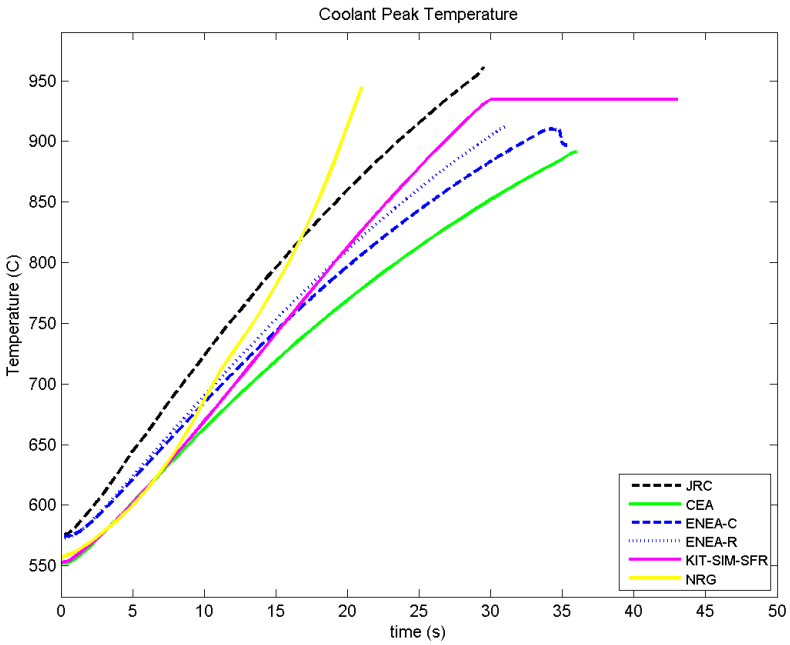

Figure 50: Coolant peak temperature

As shown in Figure 50, all codes predict that sodium reaches boiling conditions at the active core outlet after ~ 30 seconds into the ULOF transient. This should be considered as an upper limit value of the grace time for the reactor protection system to become activated and initiate reactor shut-down within a few hundred milliseconds time period.

Figure 51 and Figure 52 show the evolution of peak fuel temperature and peak cladding temperature respectively. The cladding temperature increases all along the transient quite consistently with the coolant temperature. All the codes predict a slight increase in the fuel temperature during the initial seconds of the transient followed by a decrease caused by the reduction in core power. The results of the model developed are close to the other partners´ calculations and is among the highest predictions, consistently with the maximum fuel temperature predicted in the benchmarking case Figure 38.

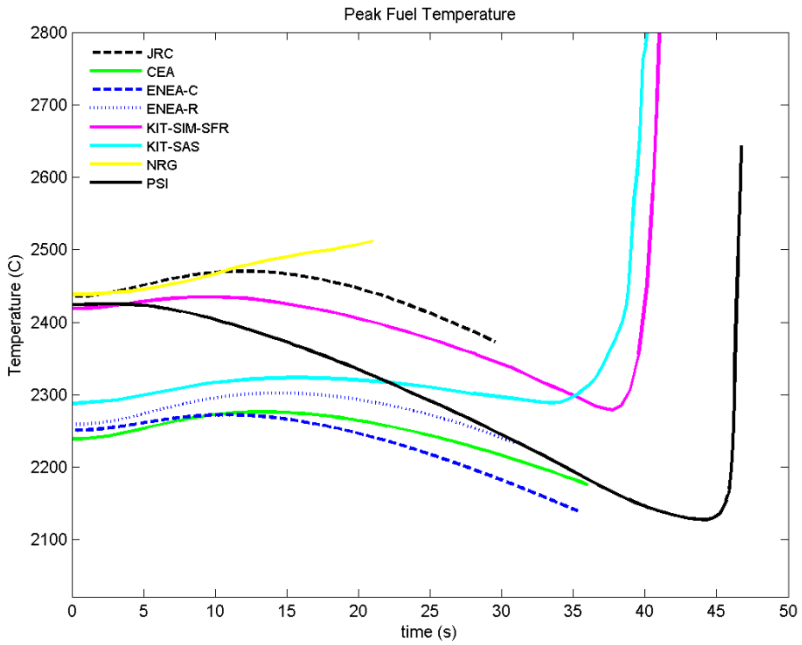

Figure 51: ULOF – Peak fuel temperature

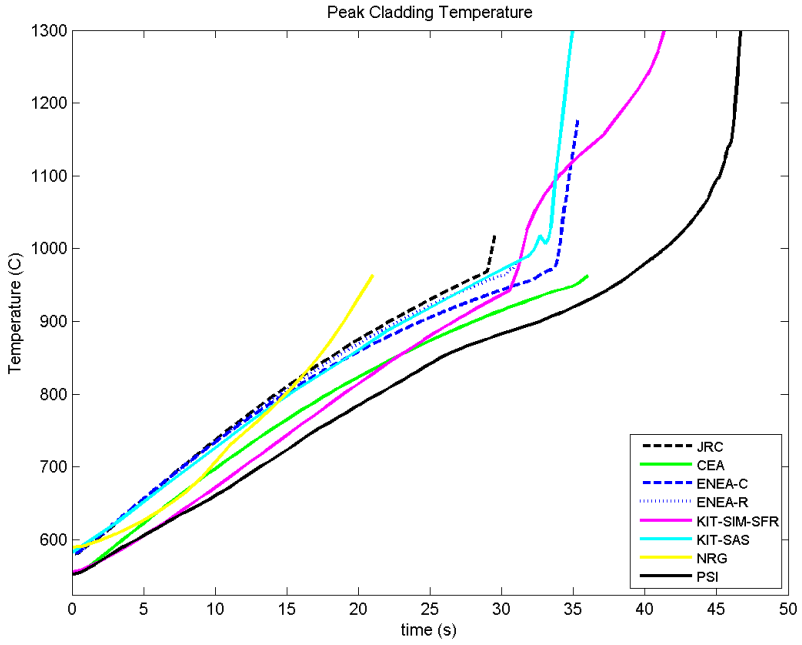

Figure 52: ULOF - Peak cladding temperature

The total reactivity evolution is shown in Figure 53. The total reactivity is the result of the contributions of the different reactivity components, which are plotted in the subsequent figures. The behaviour of the system is similar to the behaviour shown in the benchmarking exercise, due to the positive coolant expansion reactivity feedback the reactivity increases during the early seconds of the transient. Nevertheless, it is spontaneously compensated by the negative reactivity feedbacks (such as Doppler or differential control rod insertion effects) which

reduces the system reactivity, until boiling conditions are reached (˜ 30 s). The results of the model developed are in line with other partners' results.

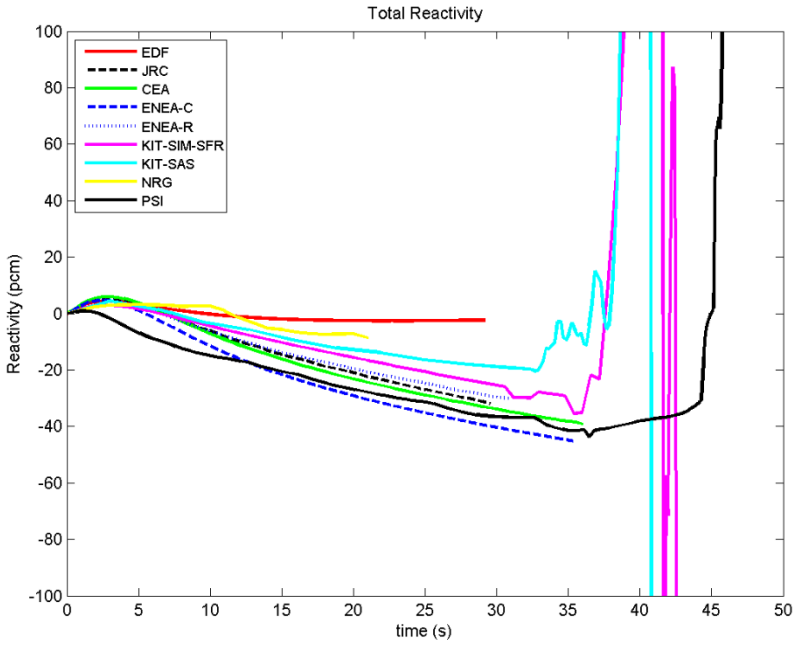

Figure 53: ULOF – Total reactivity

It can be observed that the codes able to go beyond boiling conditions predict a sharp increase in reactor power at 38 - 45 seconds into the ULOF transient due to the positive reactivity inserted by the coolant voiding (Figure 54).

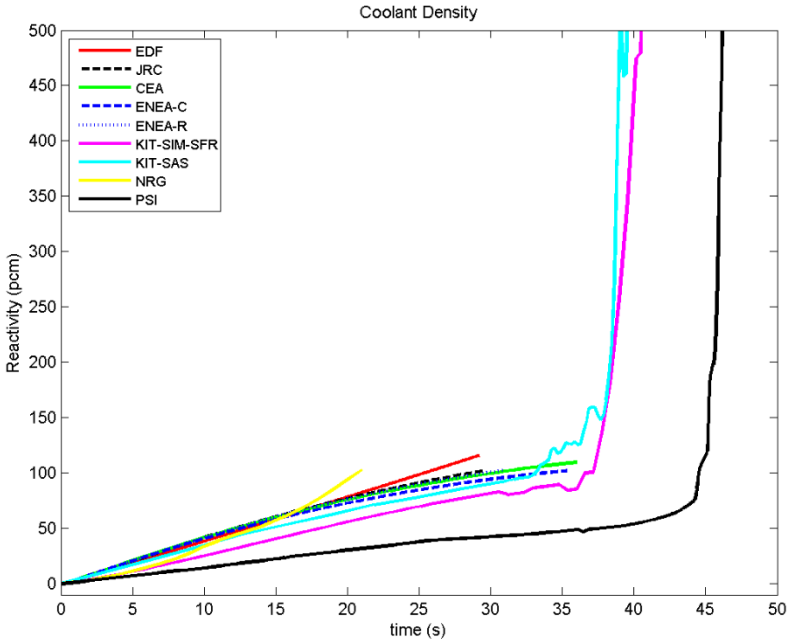

Figure 54: ULOF - Coolant density effect

After that, reactor power may drop as major negative reactivity effects such as the partial insertion of the control rod bank (Figure 55) or Doppler effect (Figure 56) take place.

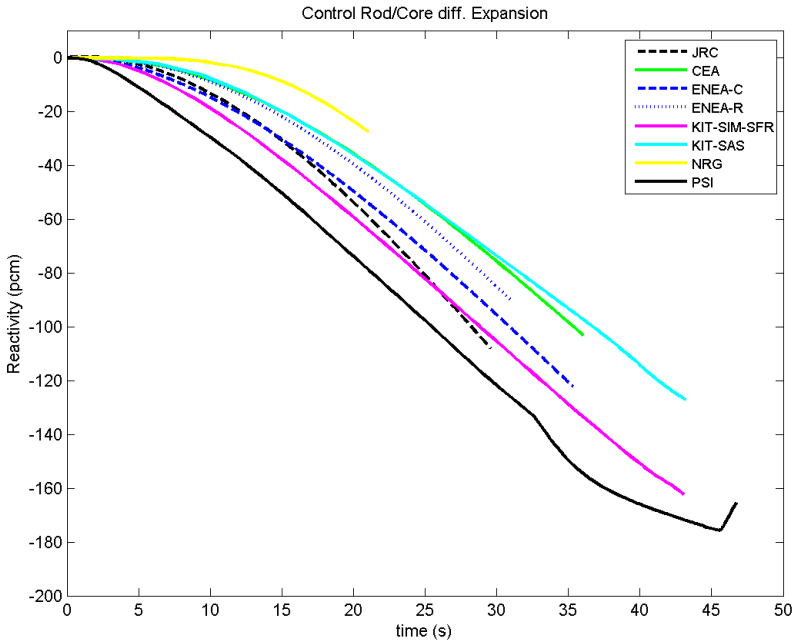

Figure 55: ULOF - Control rod/core differential expansion effect

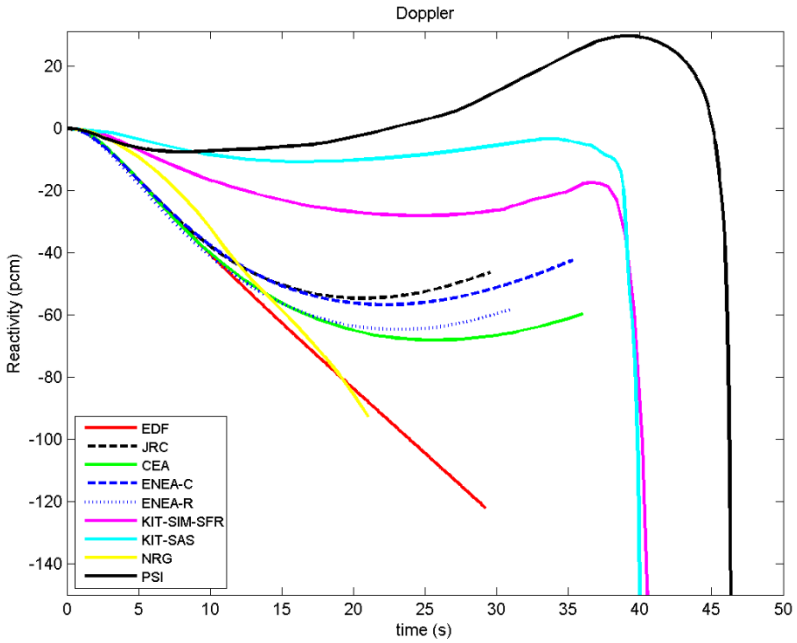

Figure 56: ULOF - Doppler effect

Figure 57 shows the power evolution of the core during the transient. After the small increase in the early seconds of the ULOF transient the following power decrease is governed by the negative control rod insertion reactivity effect (Figure 55). When boiling conditions are reached at the core outlet the reactor is predicted to become unstable due to the large positive reactivity insertion caused by sodium voiding of the central core region.

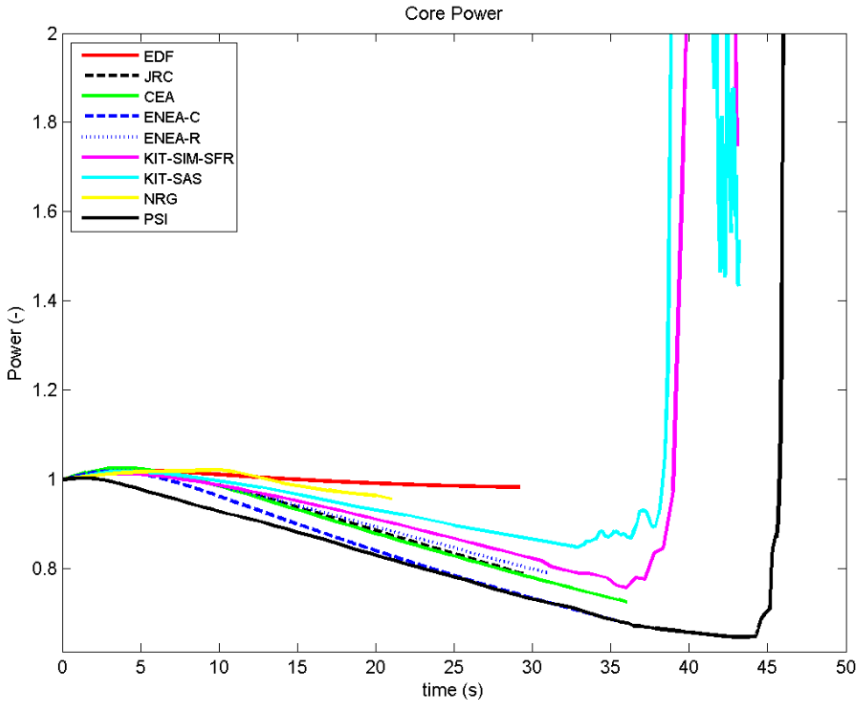

Figure 57: ULOF – Core power

The response of the above described SFR core to the ULOF transient indicates that this unprotected transient must be either avoided under all circumstances. Alternatively, the design of the core/primary system configuration may be adapted in such a manner that boiling of the primary sodium coolant is prevented by appropriate design measures (e.g. optimized core design introduced in Chapter 3) in order to exclude a power excursion resulting in core destruction.

4.1.2.2.2 Optimised Core

The major impact of the core optimisation effort can be noticed in the unprotected loss of flow transient, since it is a transient driven by a strong and abrupt decrease of the coolant density, and consequently, the void effect plays an important role.

Figure 58 displays the decreasing core mass flow rate during the ULOF-OO event and Figure 59 shows the corresponding sodium temperature at active core outlet of the average subassembly.

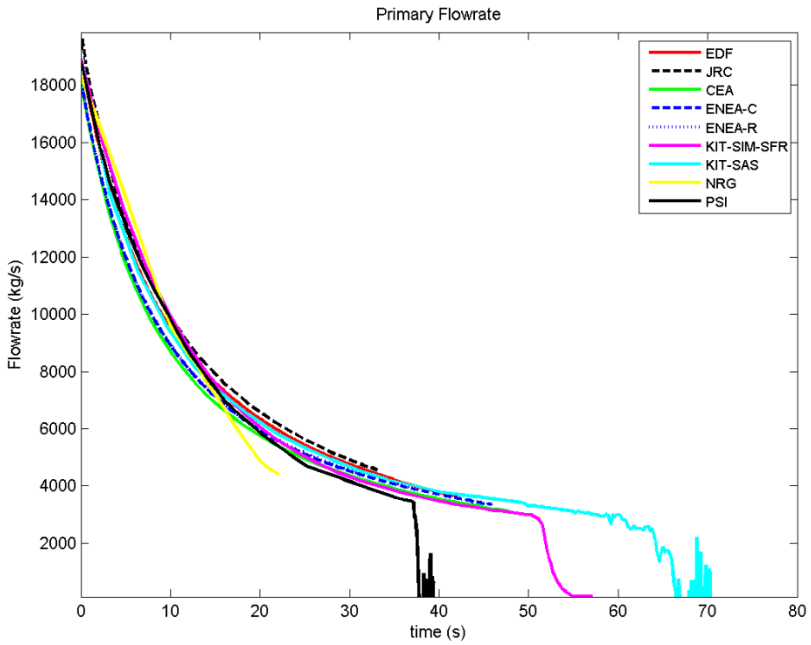

Figure 58: ULOF-OO – Primary massflow rate

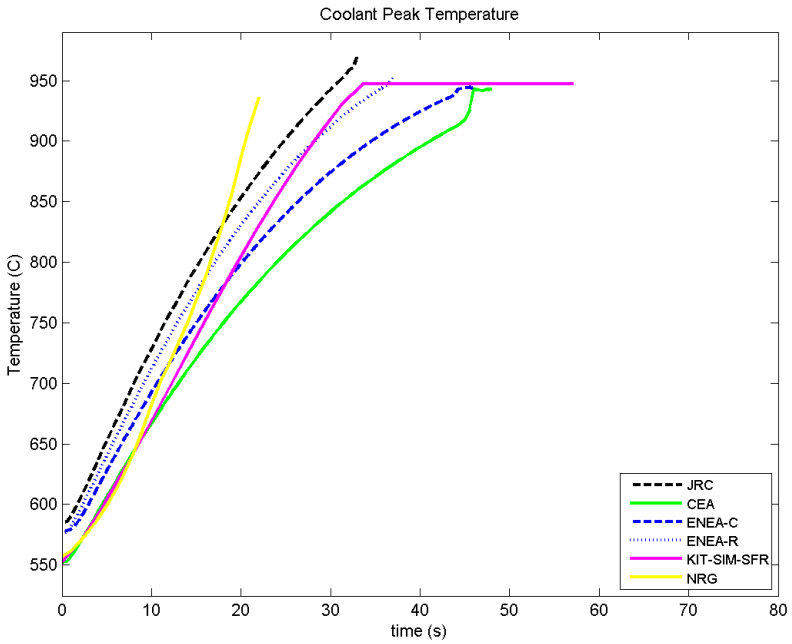

Figure 59: ULOF – OO: Coolant peak temperature

As can be observed in Figure 59, boiling of the coolant at the active core outlet of the average subassembly begins ~ 40 seconds into the ULOF-OO transient, implying that boiling of the hottest subassembly begins a few seconds (~ 3-4 sec) beforehand. Boiling of the coolant leads to a chocking axial flow pattern under the established power to flow ratio at the time of boiling onset. This in turn results then in an almost complete stagnation of mass flow in this affected subassembly, affecting the total core coolant flow. Sodium vapour will first expand axially by penetrating the upper sodium plenum region. Voiding of the plenum region results in a local, limited negative reactivity insertion (about –1.5 pcm/SA for the average-power assembly and about –9 pcm/SA for the peak-power assembly), resulting in a small decrease in reactor power, as removing liquid sodium of the upper sodium plenum region has been demonstrated to lead to negative reactivity insertions in this core design due to enlarged neutron leakage. A few seconds after voiding the plenum, the sodium voiding front however will proceed axially downward into the central core region due to the nearly stagnating flow in the flow channel, releasing then locally a large, positive reactivity (about + 3 pcm/SA for average-power assembly and about +17 pcm/SA for the peak-power assembly) due to neutron spectrum hardening. The net sum of reactivity insertion due to complete sodium vaporization will become positive again (about + 1.5 pcm/SA), even though it was briefly negative initially. Under the transiently established power to flow ratios at this time into the transient voiding of the sodium plenum leads to voiding of the central core region due to the still high reactor power of 0.6 nominal (see Figure 57). This time-wise cyclic characteristic in the sodium reactivity component can be clearly observed in Figure 60. Initially, only the hottest subassembly will be voided. The voiding front will however continue to expand in radial direction by progressively involving an increasing number of lower powered subassemblies until the average powered subassemblies will also start voiding. At this time, the total positive reactivity inserted into the core will become sufficiently large and positive (Figure 63).

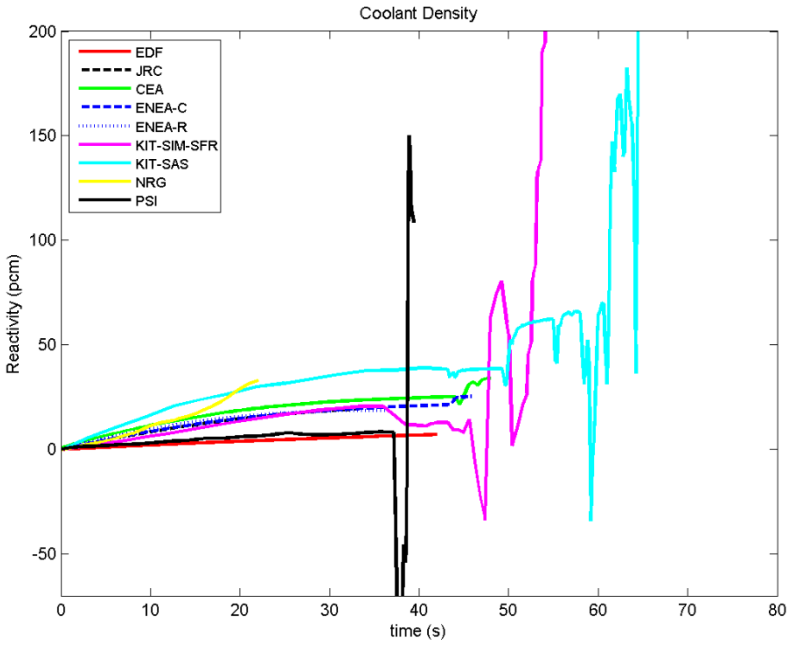

Figure 60: ULOF – OO – Coolant density effect

The progression of the radial voiding front can only be limited if either the power level becomes sufficiently suppressed by the voiding process of the hottest flow channels or by other triggered negative reactivity feedback effects (such as insertion of control rods or other active or passive safety devices), or the nature of the continuously decreasing flow rate (pump coast-down) can be mitigated (i.e., by large natural convection level, or pony motors), or even reversed (i.e., restart of pumps).

As the boiling process in the hottest subassemblies starts at relative mass flow rates in the range of ~ 23 to 33% (specifics depend on the exact power level and the core inlet temperature at this time in the ULOF-OO transient), the mass flow rate will continue to decrease according to the pump coast down characteristics until the natural convection level is attained. In the current ESFR primary system design, the mass flow rate in the natural convection mode will be less than 10%, implying that the decreasing nature of the mass flow rate at the time boiling in the hottest subassemblies commences (~ 23 to 33% mass flow rate) is far away from the natural convection level (< 10%). An early stabilization of the mass flow rate after initiation of sodium boiling thus cannot be expected under current ESFR plant design characteristics. The issue of the continuously decreasing mass flow rate alone will drive the continued radial expansion of the sodium boiling front enveloping more and more lower-powered subassemblies.

As the basic nature of a continuously decreasing mass flow rate cannot be influenced during the coast-down process of the primary pumps, the only other mechanism terminating the radial expansion of the sodium boiling process is to significantly depress the power level by providing a sufficiently large negative reactivity insertion at the time boiling in the hottest subassemblies is initiated. As this cannot be demonstrated under current ESFR conditions (even for the optimized core), further ESFR primary system design optimisation efforts are needed in order to conclusively demonstrate that the resulting core design will be able to accommodate a ULOF.

Figure 61 displays the time evolution of the peak cladding temperature with the concurrent evolution of the peak fuel temperature in Figure 62.

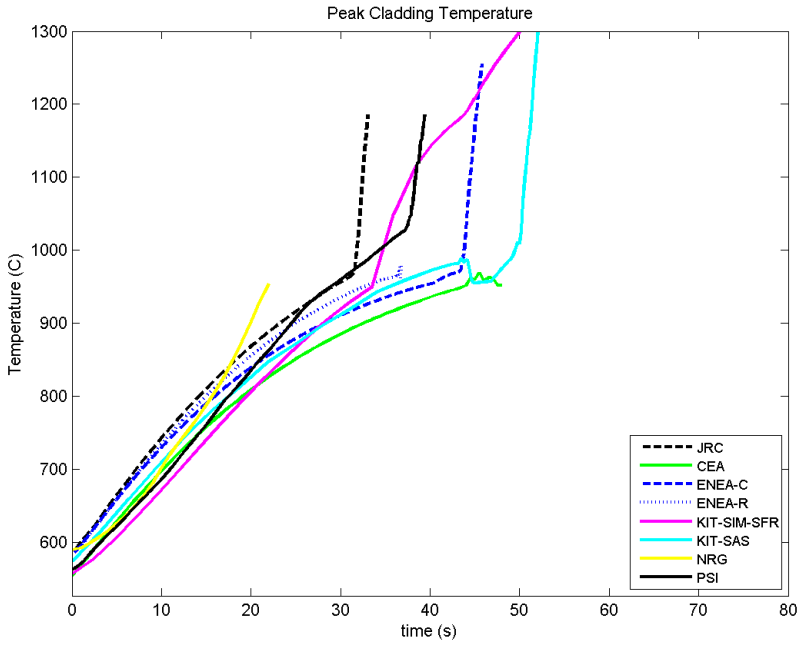

Figure 61: ULOF – OO- Peak cladding temperature

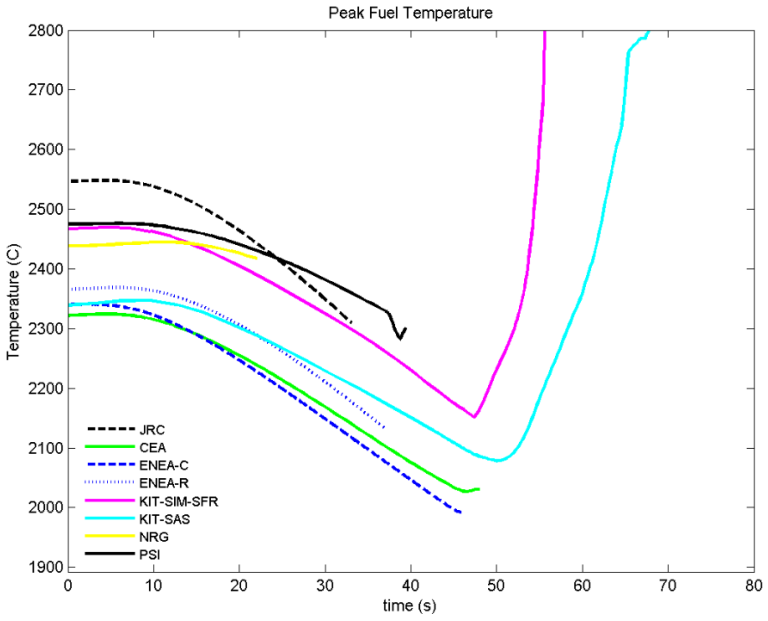

Figure 62: ULOF –OO – Peak fuel temperature

Due to sodium vapour generation on a relatively high power level, clad melting temperatures (~ 1340°C) are quickly reached as the heat transfer coefficient between clad surface and bulk coolant after the boiling crisis (dryout) becomes substantially reduced (~ factor 10). Once melting of the cladding material commences, clad material becomes axially expelled from the active core region (due to the chugging channel flow characteristics), resulting in an additional, and significant positive reactivity insertion. This positive clad reactivity insertion in conjunction with the net positive sodium voiding reactivity from above will add sufficient total positive reactivity (as displayed in Figure 63) into the core resulting in a power excursion, see Figure 64, shortly after 40 seconds into the ULOF-OO transient.

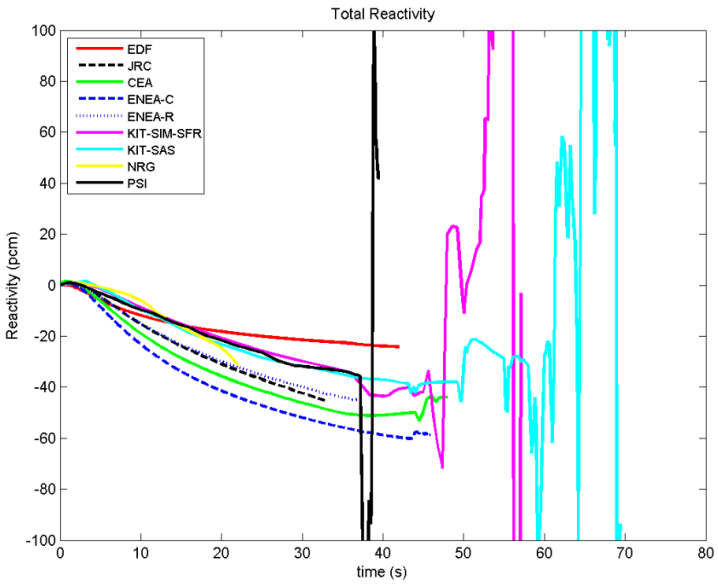

Figure 63: ULOF-OO – Total reactivity

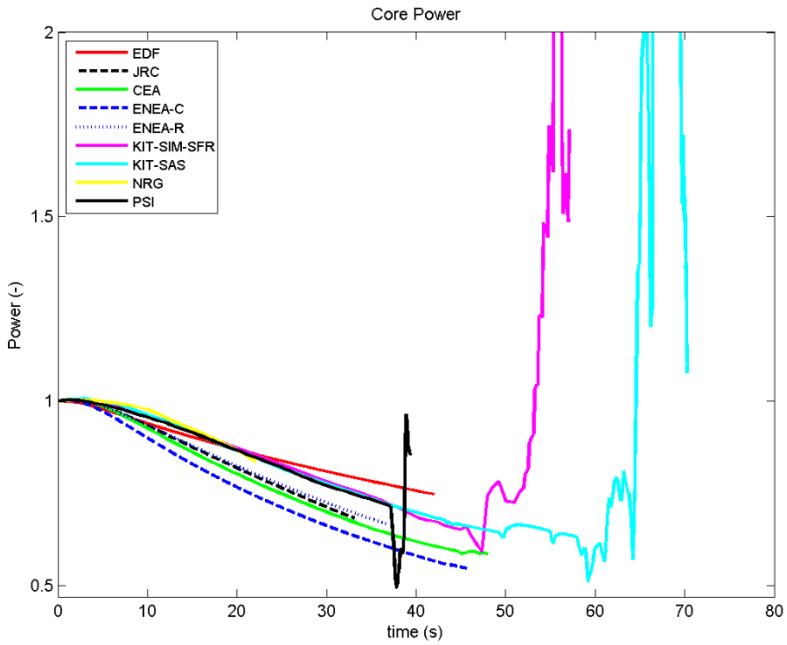

Figure 64: ULOF –OO – Core power

The observed differences in timing of the above described events between the three code system (SAS-SFR, TRACE-FRED, and SIM-SFR) that allow calculations to proceed into and through the core boiling phase are model-dependent and not really decisive for an answer to the question whether design optimisation performed for the CP-ESFR OO core design are sufficient to prevent the transient entering into core destruction as consequences of a ULOF. However, differences are interesting and important for better understanding of the sodium boiling physics and consequences of the differences in the modelling approaches.

4.2 The one dimensional LFR model

The methodology followed to develop one-dimensional models of the ALFRED design within the LEADER project was equivalent to the one detailed in the previous section for the ESFR Project.

In this case, a dedicated task was devoted to develop thermal-hydraulic models of the ALFRED design and apply them to analyse the response of the system to Design Extended Conditions transients [Bandini et al, 2013].

Each of the organisation participating in the project (KIT (Germany), PSI (Switzerland), NRG (Netherlands), KTH (Sweden), ENEA (Italy), CIRTEN (Italy) and JRC-IET (European Commission)) developed its own model of the design and performed a number of simulations of the following selected transients:

- Unprotected loss of flow (ULOF)
- Unprotected transient over power (UTOP)
- Unprotected loss of heat sink (ULOHS)

The following subsections show the results obtained by using the model developed in the framework of this PhD thesis and reported in the previous chapters for steady state calculations and the simulation of UTOP and ULOF transients.

For a complete description of the benchmarking exercise performed between the different partners of the task refer to the project deliverable [LEADER, 2013] or the dedicated publications [Bandini et al, 2013].

4.2.1. Steady state calculations

Before starting with assessments of selected postulated transients, a benchmarking exercise was performed among the different LEADER project partners to compare results of steady state analyses at nominal power. This was done with the objective to verify the consistency of the different codes and models used by individual partners.

The model developed using TRACE code does not contain a state-of-the-art fuel pin mechanics model, the pellet-clad gap distances and conductivities in the different axial levels of the individual modelled fuel assemblies were adopted based on evaluations performed by other partners. Fuel assemblies corresponding to hot fuel (peak value of power profile), inner as well as outer assemblies (with two different power values) were modelled.

Two core conditions were considered in the analysis, Beginning-of-Life conditions (BOL) and End-of -Cycle conditions (EOC). Table 22 shows the main plant parameters in the nominal steady state conditions for the two core configurations as predicted by the TRACE code. These values are in good agreement with results obtained by other partners [LEADER, 2013].

Parameter	BOC	EOC
Reactor power (MWth)	300 (0.0%)	300 (0.0%)
Flow rate (kg/s)	25598 (0.0%)	25598 (0.0%)
Core outlet temperature (°C)	491.85 (2.5%)	493.85 (2.9%)
Max fuel temperature (°C)	2139 (6.9%)	2088 (4.4%)
Max cladding temperature (°C)	513 (6.7%)	513 (6.7%)
ΔP core (bar)	0.78 (22.0%)	0.775 (22.5%)

Table 22: ALFRED steady-state calculations

Table 22 also shows the differences (in brackets) between these calculations and the values defined in the design specification. The highest discrepancy appears in the pressure gap throughout the core. This difference is justified by the different pressure correlations used by the designers and the ones used by TRACE code that are meant to be used in light water reactors. An upgrade of the TRACE source using specific liquid metal correlations is pending to reduce this uncertainty.

4.2.2. Representative transients

Following the steady-state analysis, two initiating events in the Design Extension Condition domain were further analysed: the unprotected reactivity insertion transient (UTOP) and the unprotected loss of flow (ULOF). The results of the different partners 'calculations can be consulted and compared in the project task deliverable [LEADER, 2013].

These transients were initiated at steady state, nominal power and under EOC conditions.

Consistently with the current capabilities of the code, the values of the gap distance and conductivities as defined at steady state were kept constant during the transient calculations, which might somewhat impact our predictions of fuel temperatures during transients.

4.2.2.1. UTOP

The UTOP transient is initiated by the reactivity insertion of 250 pcm during 10 seconds (Figure 65). This leads to net positive reactivity in the initial phase of the transient, resulting in an increase of the core power and correspondingly also coolant and structure temperatures. The resulting positive reactivity is thereafter counterbalanced mainly by negative reactivity feedbacks due to fuel expansion and Doppler effects, together with negative feedbacks due to the radial core expansion and the control rod driveline expansions, the contribution of the latter being however relatively small.

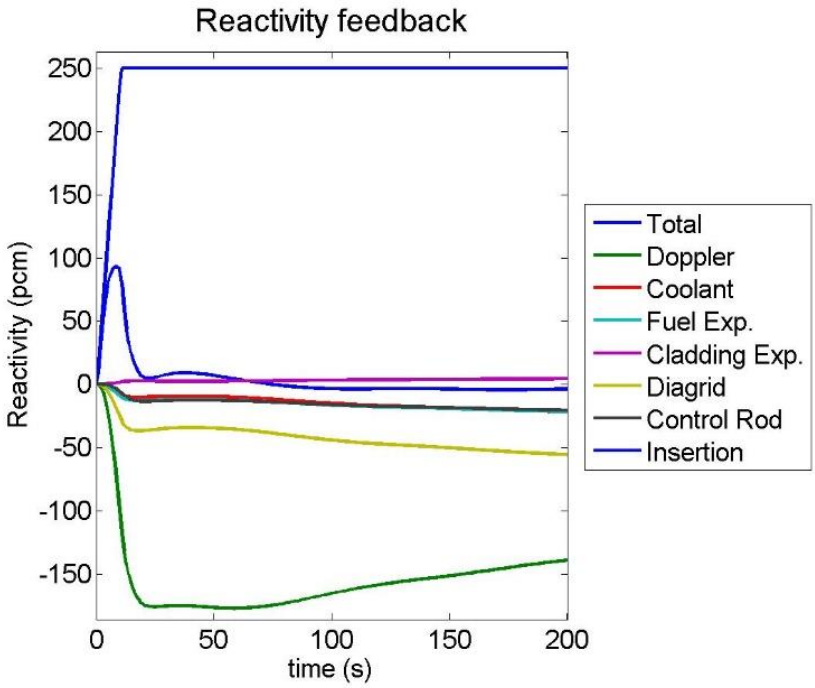

Figure 65: ALFRED – UTOP – Reactivity Evolution

The reactivity insertion initiates a power excursion up to a value of 640 MWth (213% nominal power). This transient is unprotected; however, the system evolves to a new equilibrium state at higher power (Figure 66).

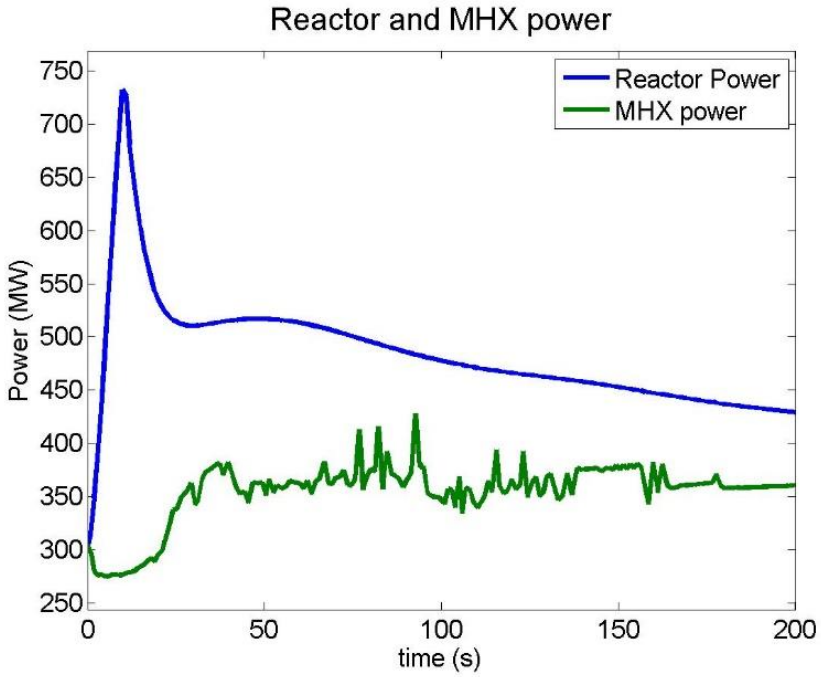

Figure 66: ALFRED – UTOP – Power evolution

Figure 67 shows that the increase in the temperature of the primary lead is limited as the heat transfer to the secondary side in the MHX also increases in a constant rate all along the transient.

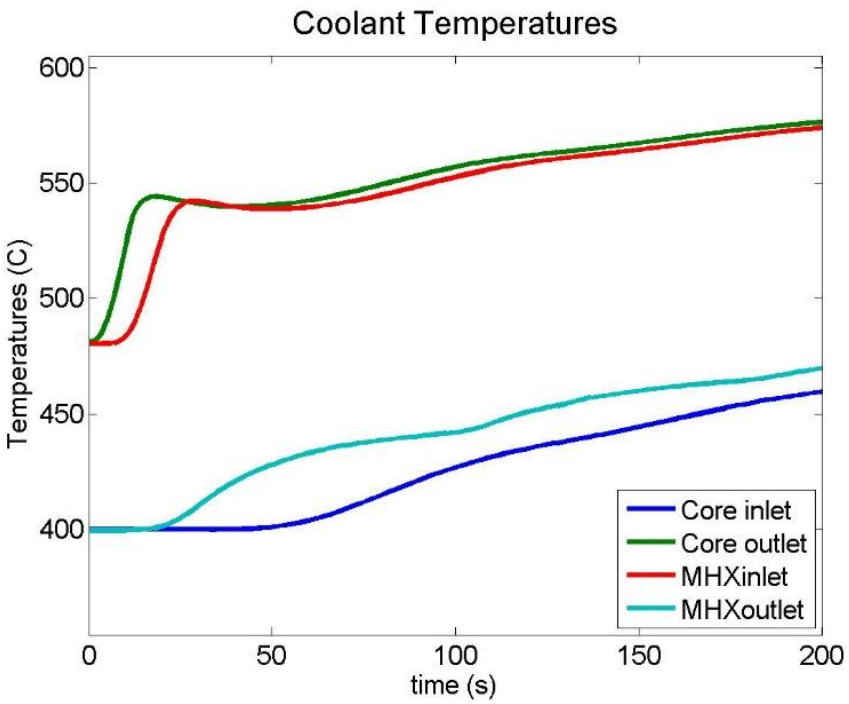

Figure 67: ALFRED – UTOP – Coolant temperatures

Figure 68 shows the peak fuel temperature. A maximum fuel temperature slightly over 3000°C is predicted in the hot fuel assembly, which is already above the melting temperature of the mixed-oxide fuel. Consequently, fuel melting in the centre of the fuel pellet is expected. The maximum cladding temperature is of 625°C.

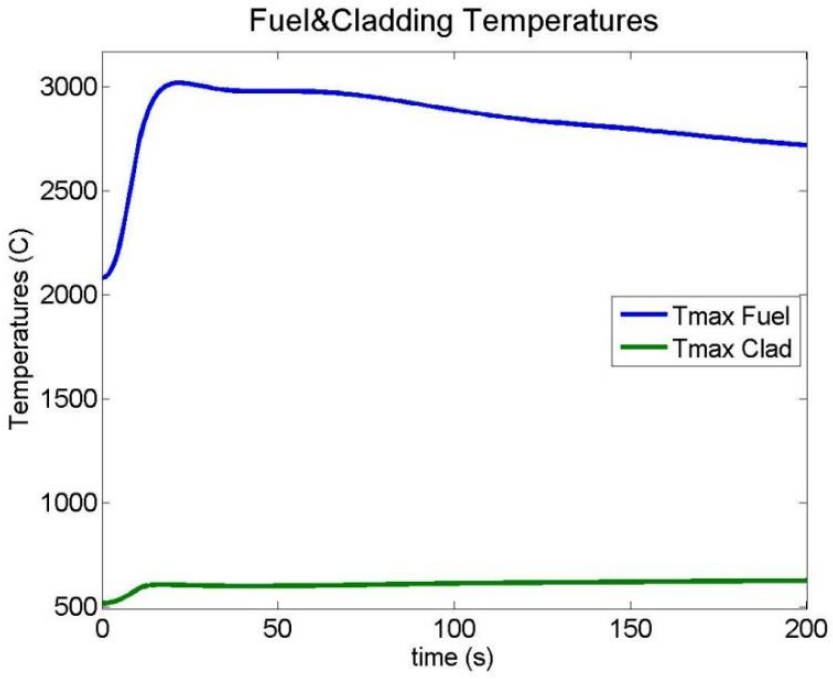

Figure 68: ALFRED – UTOP – Peak fuel temperature

4.2.2.2. ULOF

The ULOF transient is initiated by the coast-down of all primary pumps. Consequently, the system gradually evolves in a continuous decrease of primary coolant massflow until the natural convection process takes over (around 20% of the nominal flow rate).

As it can be seen in Figure 69 the transient is characterized by an abrupt increase of the primary coolant temperatures as a consequence of the reduced mass flow across the core. The core outlet temperature increases abruptly during the first seconds of the transient, increasing the IHX inlet temperature. Nevertheless, this increase is quite limited and remarkably lower than the lead boiling point. This is a very positive safety feature.

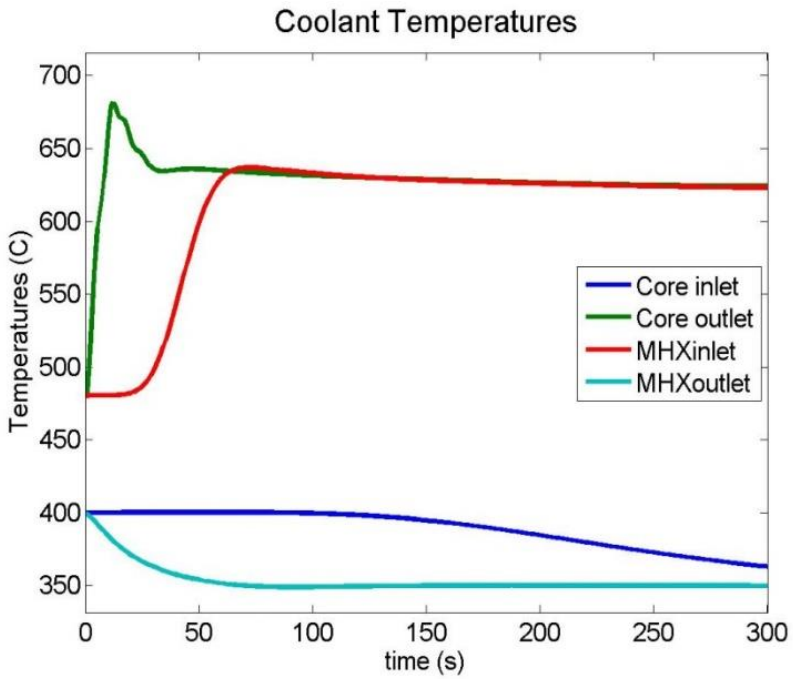

Figure 69: ALFRED – ULOF – Coolant temperature

This increase in temperatures of coolant and structures implies the insertion of reactivity feedbacks (Figure 70), out of which dominating is the negative feedback due to the diagrid (radial) expansion. The control rod (due to the driveline expansion) and the coolant expansion effects also introduce negative reactivity, which leads to further decrease of the net reactivity. In the longer term, however, as a consequence of decreased fuel temperatures, the positive reactivity insertion is observed due to the Doppler and cladding expansion reactivity feedbacks.

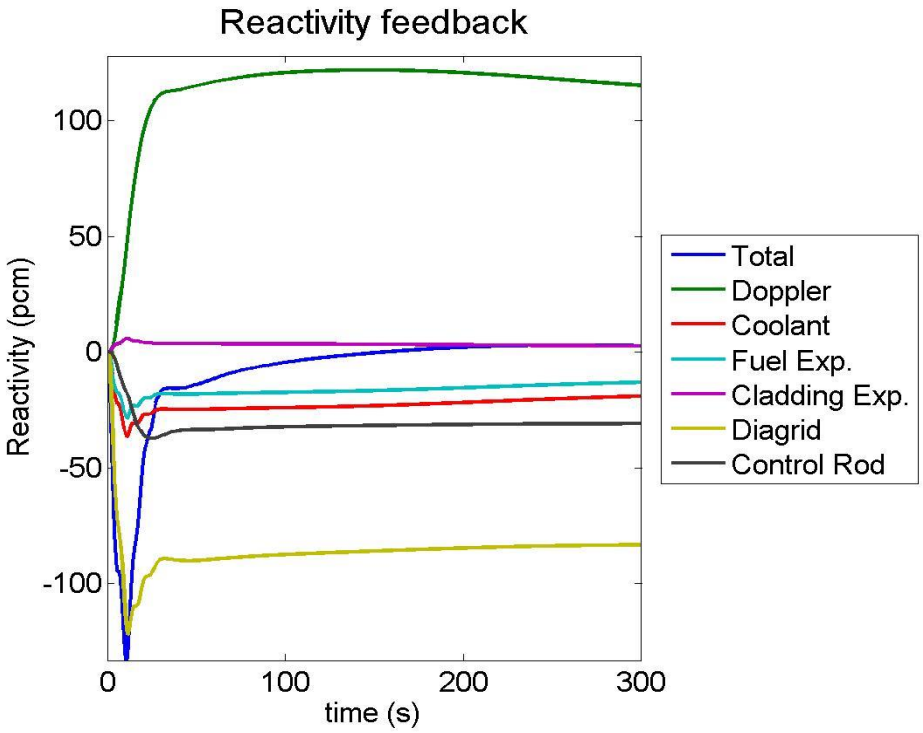

Figure 70: ALFRED – ULOF – Reactivity

Figure 70 shows that the core becomes subcritical during the first seconds of the transient, with a remarkable decrease in power, after which the core power slowly attains a new equilibrium state at about 180 MWth (60% nominal power) as it can be observed in Figure 71 .

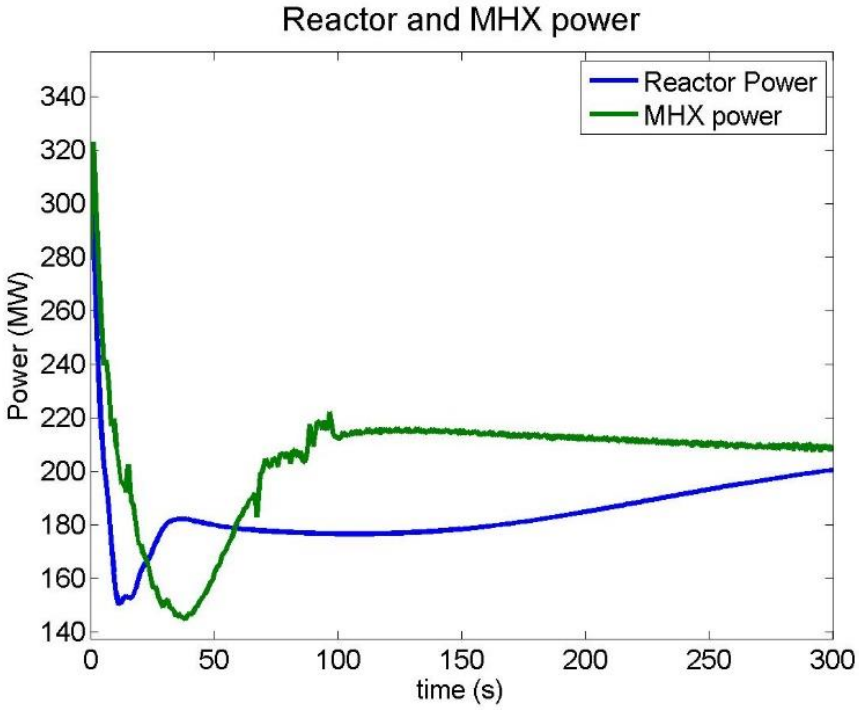

Figure 71: ALFRED – ULOF – Power evolution

Even though the reduced coolant mass flow results in an abrupt increase in the cladding temperature (Figure 72), the safety margins can be maintained during the transient and no deterministic clad ruptures are to be expected (Tmax 782°C). Equally, safety margins can be kept with respect to fuel melting or coolant boiling. Thus, the analyses show that the ALFRED design is robust with respect to a ULOF transient providing sufficient grace times for corrective actions to be taken to terminate the transient.

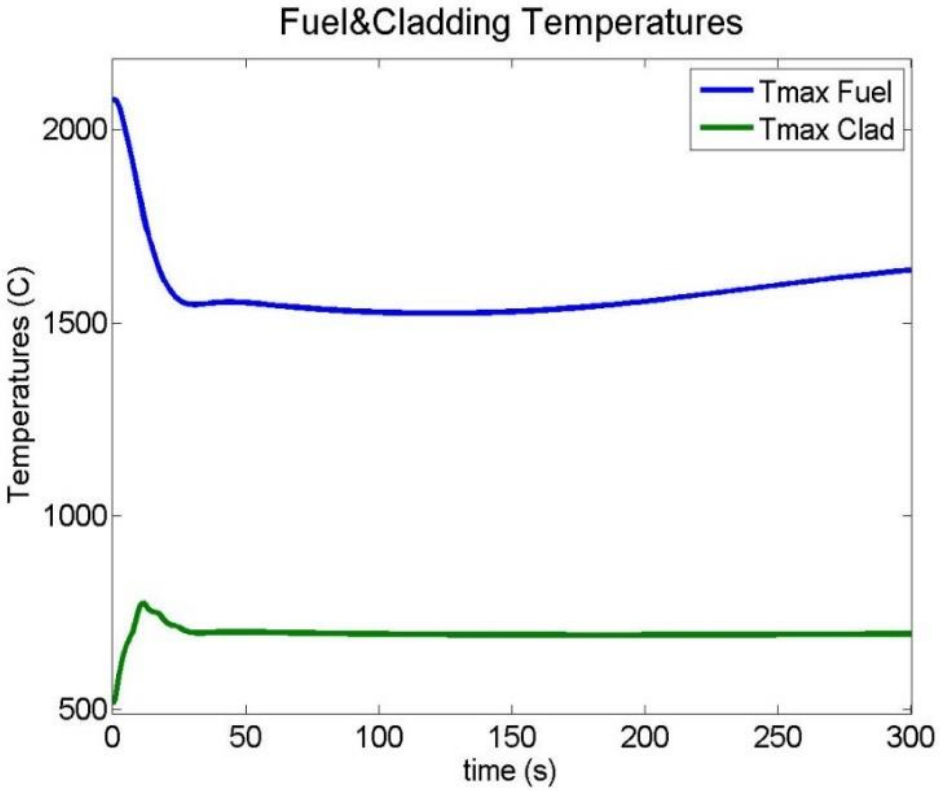

Figure 72: ALFRED – ULOF – Peak fuel and cladding temperature

5. Results – 3D modelling

Due to the nature of one-dimensional models, their use in the safety assessment is essentially limited to symmetric transients. When asymmetric scenarios are considered a more detailed three-dimensional neutronic and thermal-hydraulic multi-physics system is therefore necessary to take into account the asymmetric neutronic and thermal-hydraulic behaviour of the system.

The methodology followed to develop such a multi-physics approach started with the transformation of the one-dimensional thermal-hydraulic model into a three-dimensional equivalent one while keeping the point kinetic neutronic response. Afterwards, a neutronic model was developed for the spatial neutron kinetic code PARCS. The final step was then to couple these two models, to obtain a multi-physics scheme.

The final model and the intermediate step should be equally able to perform symmetric calculations as the one-dimensional model. The consistency in the comparison of the three models on the symmetric simulations should represent a first validation step for the reliability of the three-dimensional multi-physics scheme.

5.1. Benchmarking of the 3D thermal-hydraulic + 1D neutronic model

A three-dimensional thermal-hydraulic model will have the ability to calculate transients triggered by an asymmetric initiating event such as:

- Failure of one single primary pump
- Failure of one single secondary pump
- Leak in an intermediate heat exchanger
- Asymmetric sub-assembly blockage
- Asymmetric withdraw of control rod bank

In addition to this capability, the model can also take into account specific three-dimensional thermal-hydraulic phenomena such a coolant temperature stratification.

However, the model used in this section is the one that keeps the point kinetic neutronic feedback of the 1D model. In this respect, the reference temperatures are averaged azimuthally. This means that, even though the thermal hydraulic model is now three-dimensional, the power evolution keeps non-dimensional, and consequently the three-dimensional capabilities of the system are limited.

Table 23 shows the main thermal-hydraulic parameters of the ESFR design including the nominal data, and the 1D TH and 3D TH model results. The calculation of the steady-state parameters resulted in equivalent values regarding the one-dimensional model ones.

PARAMETER	ESFR - Nominal	TRACE 1D	TRACE 3D	1D-3D
Primary mass flow rate (kg/s)	19535	20692	20859	0.80%
Secondary mass flow rate (kg/s)	15330	16444	16907	2.74%
Core Inlet temperature (˚C)	395	391	387	1.03%
Core Outlet temperature (˚C)	545	545	541	0.74%
IHX Inlet temperature (˚C)	340	335	333	0.60%
IHX Outlet temperature (˚C)	525	522	517	0.97%
SG outlet temperature (˚C)	490	493	491	0.41%
SG pressure (bar)	185	185	185	0.00%
SG mass flow rate (kg/s)	1650	1650	1650	0.00%

Table 23: Nominal, 1D and 3D models working parameters comparison for the ESFR design

Once steady state was achieved, the model was configured to simulate the benchmarking transient and compare the results with the ones obtained and already shown of the one-dimensional model.

Figure 73 to Figure 76 show the evolution of the main neutronic and thermal-hydraulic parameters. In Figure 73 the evolution of the core inlet and outlet temperature, the IHX inlet and outlet temperature and the SG outlet temperature can be observed.

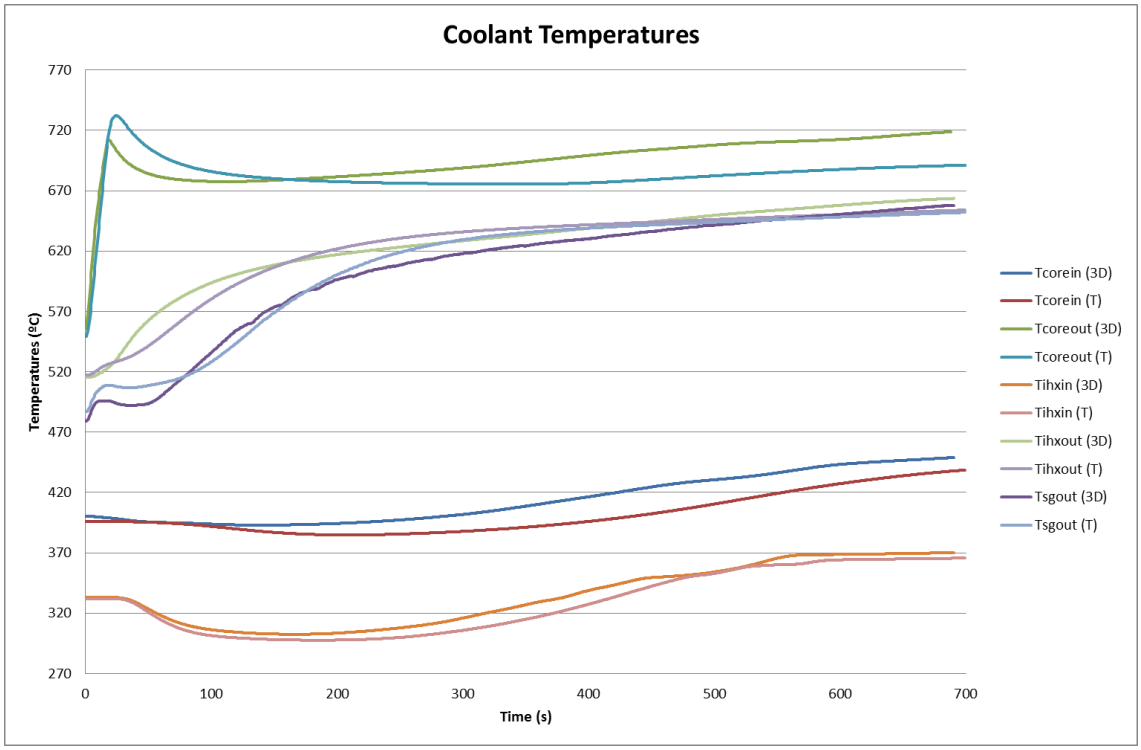

Figure 73: Coolant temperature comparison 1D-3D

As Figure 73 shows there is a fair level of agreement between the 1D and 3D models' predictions. The small discrepancies appearing are justified by the different volumes used in the two modelling techniques. The 1D model uses large averaged nodes, while the 3D model uses a more detailed nodalisation. In any case, the difference is lower than 10%.

This close behaviour is translated into a very similar neutronic behaviour along the transient. Figure 74 shows the different reactivity feedbacks, namely the Doppler effect, the coolant density effect feedback, the axial and radial expansion feedbacks and the differential control rod movement reactivity feedback. As it can be observed the results are very close between the one-dimensional and the three-dimensional nodalisations with differences bounded to 5 – 10%.

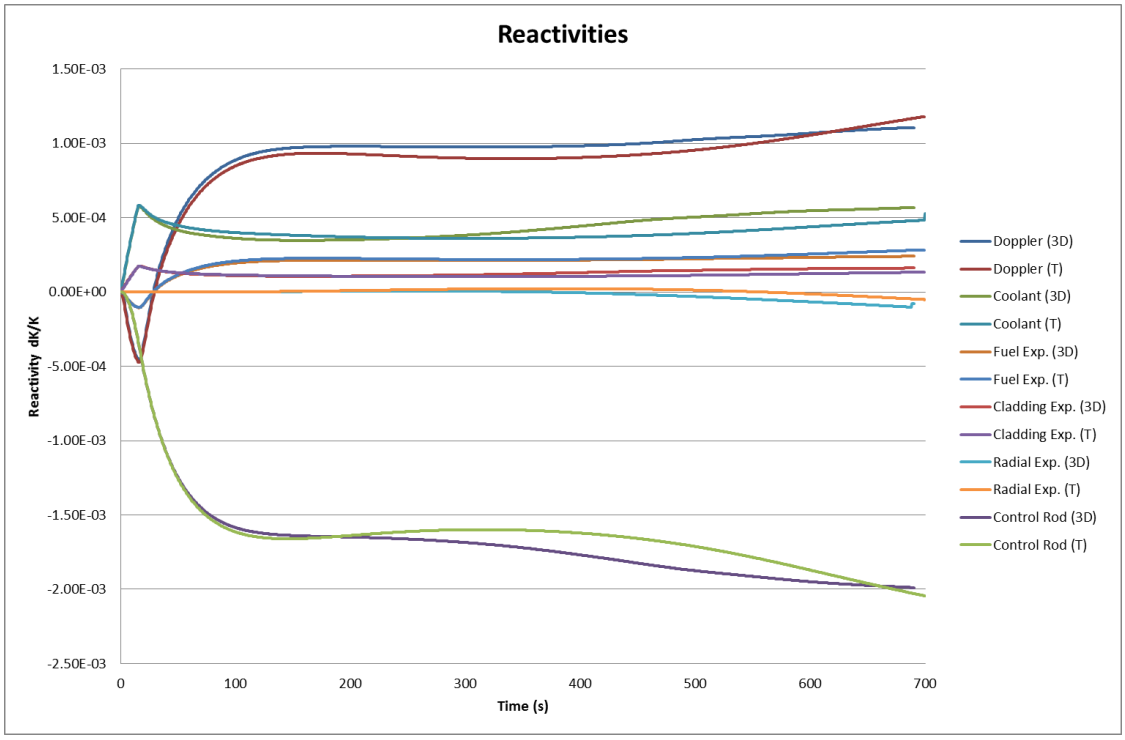

Figure 74: Reactivity feedbacks comparison 1D-3D

Figure 75 shows the evolution of the different core power profiles. Consistently with the reactivity feedbacks evolution, the comparison of generated power presents very similar results. Indeed, the differences between the 1D and the 3D models are lower than 5%.

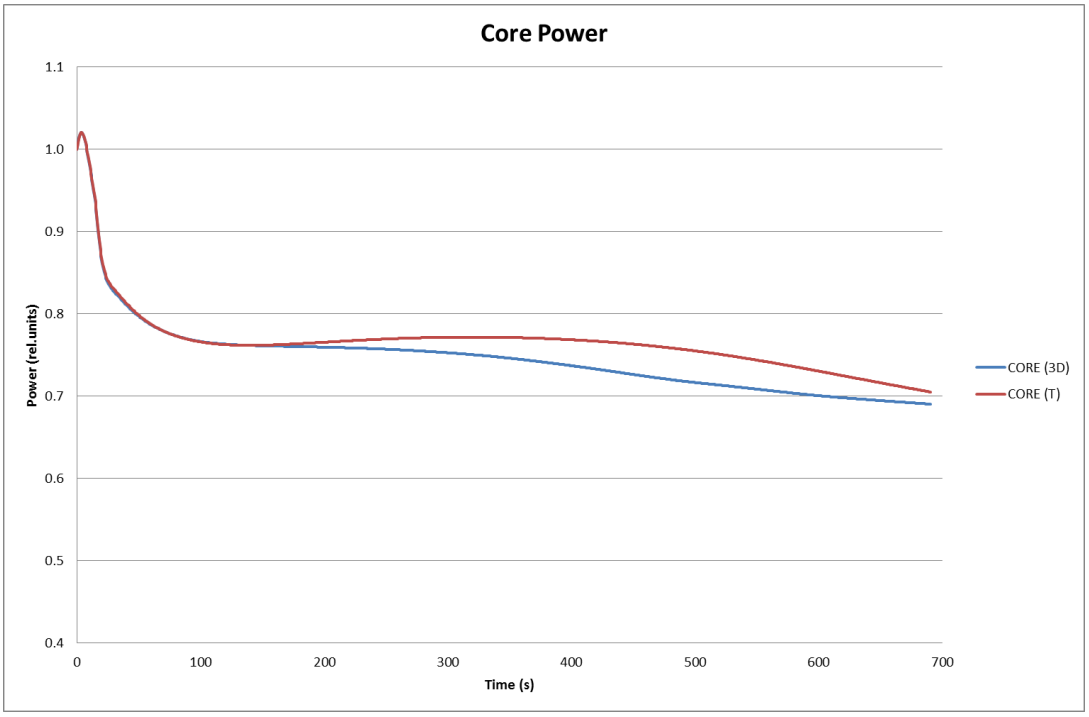

Figure 75: Core power evolution (relative units) comparison 1D-3D

The evolution of the power exchanged in 3 IHXs and 3 SGs can be observed in Figure 76 as compared with the lumped IHX and SG of the one dimensional model. Consistently with the other system parameters already analysed they present a very close behaviour.

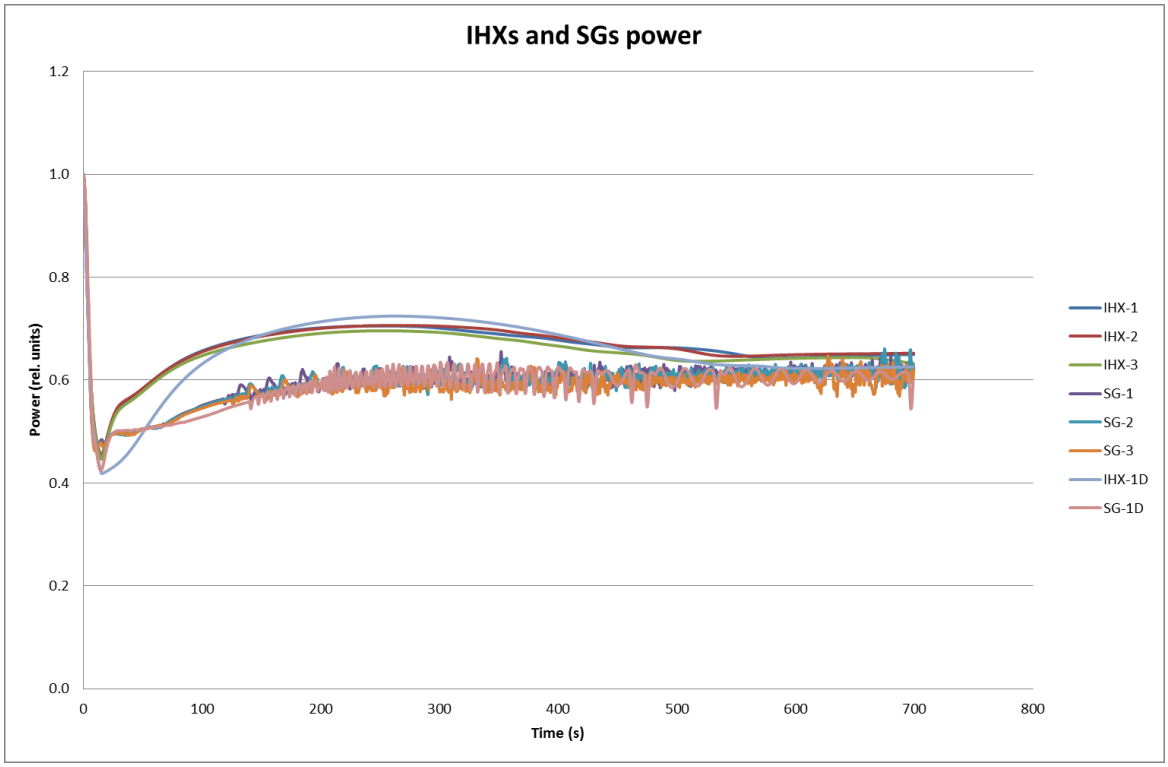

Figure 76: IHXs and SGs power evolution (relative units) 1D-3D comparison

The figures have shown a very high level of agreement between the one and the three-dimensional thermal-hydraulic models with point kinetic reactivity feedback. This intermediate step was necessary to develop the coupling scheme consistently.

It should be remarked that further research should be focused in modelling three-dimensional pressure losses in the system. The one dimensional models use a K-factor system to take into account generalised energy losses along the one-dimensional path considered. This approach has been kept for the three-dimensional model, but a more detailed three-dimensional friction factor scheme should be implemented to take into account the different losses that appear axially, radially and azimuthally.

5.2. Benchmarking of the 3D thermal-hydraulic + 3D neutronic model

Once the 3D thermal-hydraulic + 1D neutronic model has been benchmarked to test the ability to reproduce a symmetrical transient of reference, the next step towards the achievement of a tool ready to perform consistent asymmetrical studies is to benchmark this model coupled with a spatial kinetics neutronic model, i.e. the 3DTH + 3DN model, considering the same symmetrical transient of reference.

The 3DTH + 3DN model is developed using the deterministic code PARCS for the spatial kinetic neutronic model and code TRACE for the three dimensional thermal-hydraulic model, and the cross section set developed with the Monte Carlo based code SERPENT. A description of both models and of the methodology followed to couple them is detailed in Chapter 3.

The first step in using this 3DTH + 3DN model is settled in reaching consistent steady-state results. In the thermal-hydraulic model with point kinetic feedback the core power level (3.6 GWth) is hardcoded in the input. With the coupled models this core power should be achieved by the neutronic model design using PARCS code granted the steady-state thermal-hydraulics conditions given by TRACE code. The calculation gives a value of 3.557 GW, which is 1.21% under the nominal value. Table 24 shows the main parameters again comparing the nominal design values with the 3DTH-1DN model and the coupled 3DTH-3DN model calculations.

Once the 3DTH + 3DN coupled model demonstrates to simulate accurately the steady-state conditions of the plant, next step consist of testing the behaviour of its performance to simulate the behaviour of the system under transient conditions. The coupled code is used now to simulate the benchmarking transient of reference and then comparing the results with the ones obtained using the 3DTH + 1DN model.

It should be highlighted that originally PARCS is not fully prepared to implement the control rod bank insertion with temperature dependence. Indeed, the relative movement between the core and control rod bank creates a relative insertion of the control rods, and consequently, a strong reactivity reduction, which is a particular effect of LMFBRs. On the contrary, PARCS is only ready to simulate predefined control rods insertions with time dependence.

PARAMETER	ESFR - Nominal	TRACE 3D	TRACE-PARCS	3D-PARCS
Power (MW)	3600	3600	3557	1.21%
Primary Mass flow rate (kg/s)	19535	20859	20859	0.00%
Secondary Mass flow rate (kg/s)	15330	16907	16905	0.01%
Core Inlet temperature (˚C)	395	387	380	1.84%
Core Outlet temperature (˚C)	545	541	533	1.50%
IHX Inlet temperature (˚C)	340	333	325	2.46%
IHX Outlet temperature (˚C)	525	517	510	1.37%
SG outlet temperature (˚C)	490	491	491	0.00%
SG pressure (bar)	185	185	185	0.00%
SG mass flow rate (kg/s)	1650	1650	1650	0.00%

Table 24: Nominal, 3D-PK and 3D-PARCS models TH variables comparison for the ESFR

Since this movement is governed by the thermal expansion of the control rod banks and structures these temperatures should be considered by TRACE code. Indeed, a control system was implemented in the TRACE model to take into account the thermal expansion of the control rod banks and structures following the equations (10) and (11). The value of the differential movement is sent to PARCS code in every time-step and it is used to actualise on-time the vertical positions of the different control rod banks included in the model.

Figure 77: Core power evolution – 1D & 3D – PK vs 3D - PARCS - Benchmarking case shows the core power evolution in the benchmarking case using for models 1DTH+1DN, 3DTH+1DN and 3DTH+3DN. Two simulations are done with the 3DTH+3DN coupled model. First (in green), the control rod movement is imposed following the insertion curve extracted from the point kinetic model (named PARCS), while the second (purple line) shows the simulation imposing the time-dependent control rod bank position (labelled CRMOV) where PARCS code is able to perform the reactivity calculations taking into account the control rod bank position on time.

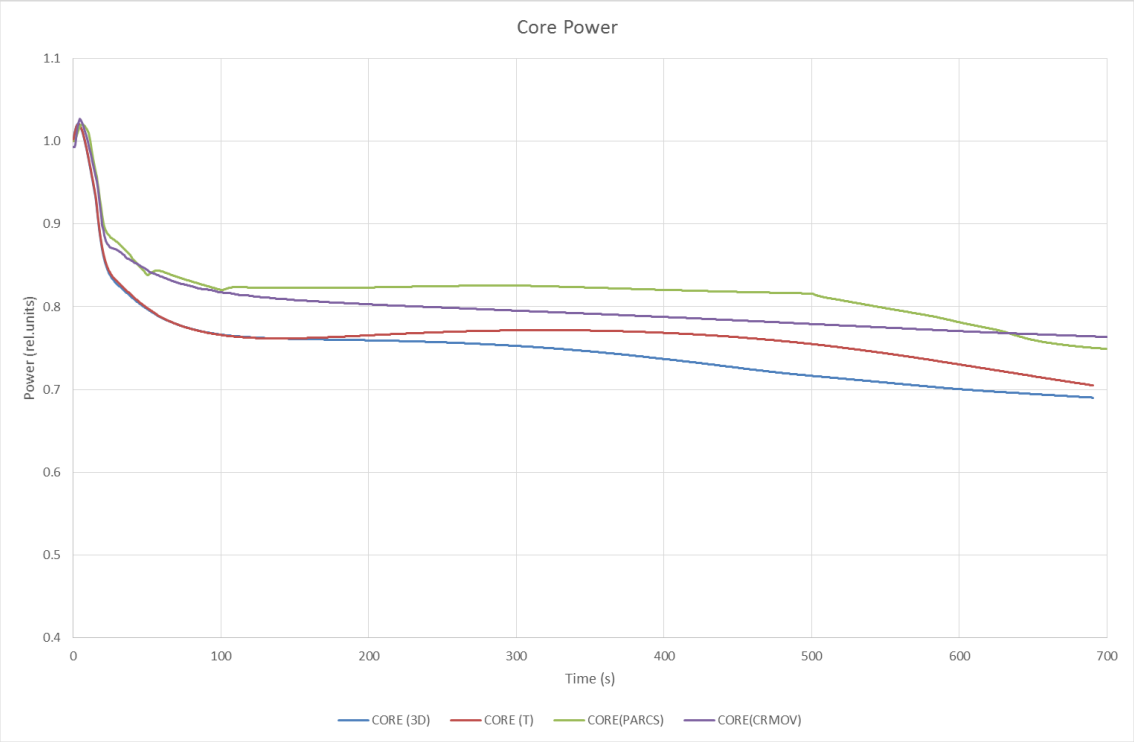

Figure 77: Core power evolution – 1D & 3D – PK vs 3D - PARCS - Benchmarking case

The above figure shows limited discrepancies between the different models. The highest differences appear between the models with point kinetic response and the models with spatial kinetic neutronic feedback. This discrepancy is justified by the assumptions that must be done in order to develop a very simplified approach to the point kinetic neutronic response for a complex spatial kinetic neutronic phenomenon. Furthermore, the point kinetic scheme uses averaged values of large volumes and it is affected by a single averaged coefficient. On the contrary, the spatial neutronic model uses 12255 nodes that contribute to the power profile and consequently the total generated power. In any case, the differences are bounded to around 10%.

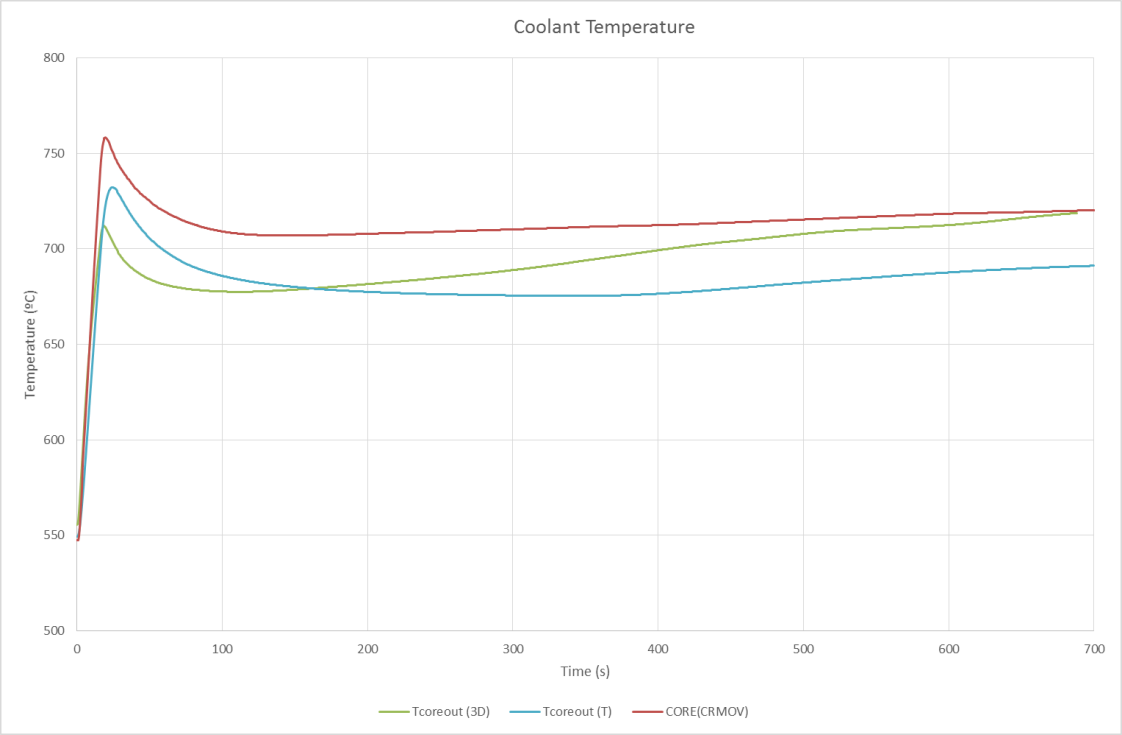

Figure 78: Coolant temperature comparison – 1D & 3D – PK vs 3D - PARCS - Benchmarking case

Figure 78 shows the maximum coolant temperature at the core outlet of each of the selected models. From now, only the CRMOV version for 3DTH+3DN model (TRACE-PARCS) is considered. The maximum difference appears at the peak value during the early seconds of the transient. The difference between the minimum predicted value (TRACE-3D) and the maximum value (coupled TRACE-PARCS) is around 50º C what is around 7%. The difference is justified by the fact that, even though the predicted powers by the three models are very similar, the point kinetic models are not able to take into account a power profile, just a single value affected by predefined constant peaking factors for the different core regions, which is an uncertainty approach to reality. On the contrary, the PARCS code calculation performs a detailed and realistic power profile along the core geometry in every time step. This feature may lead to have highest localised power values that justify the slightly higher peak maximum coolant temperature in the core.

Figure 79 shows the power profile as predicted by PARCS code in steady-state conditions. The highest power values appear in the core periphery.

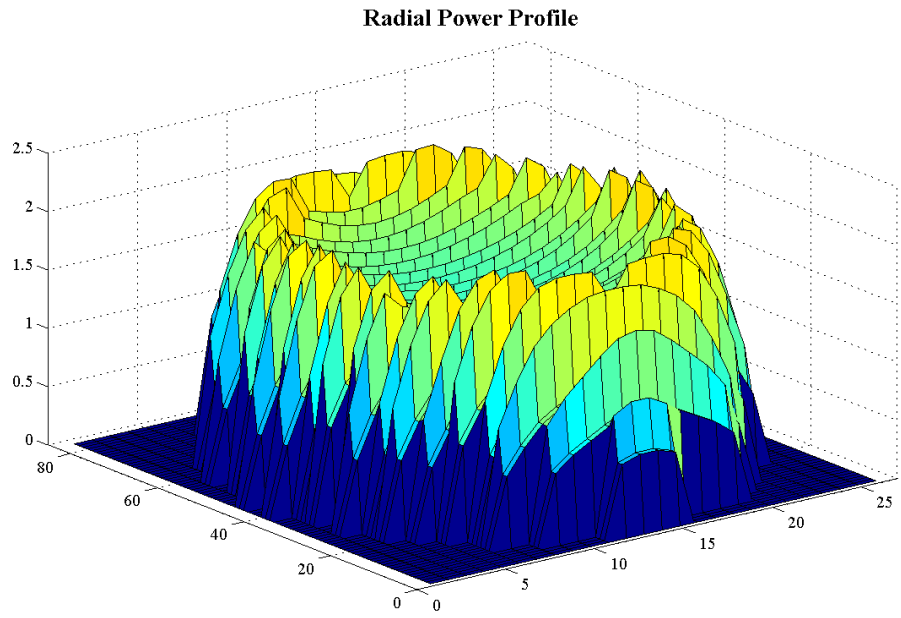

Figure 79: Radial core power profile in steady state

Furthermore, the coupled models are now able to simulate the radial power profile of a core element. Figure 80 shows the axial power profile of an inner and an outer fuel assembly in steady-state.

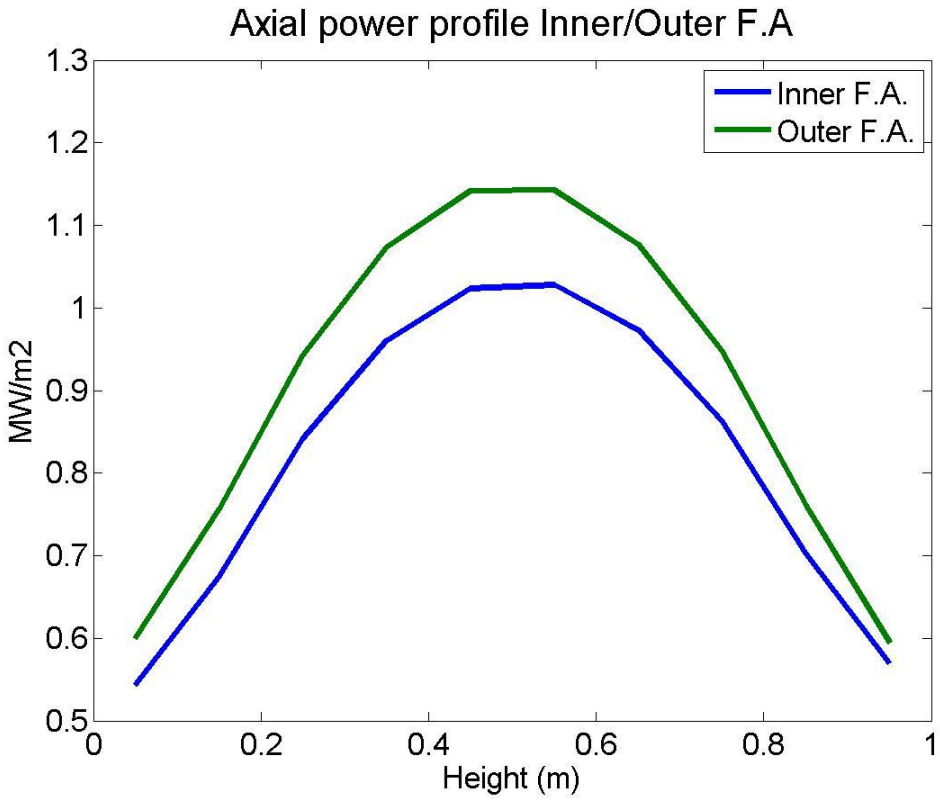

Figure 80: Axial power profile of an inner and an outer fuel assembly

This axial and radial power profiles are translated into the heat structures and hydraulic components of the thermal-hydraulic TRACE code. Figure 81 show the axial power distribution of the different regions of the vessel component of the thermal-hydraulic model in TRACE code.

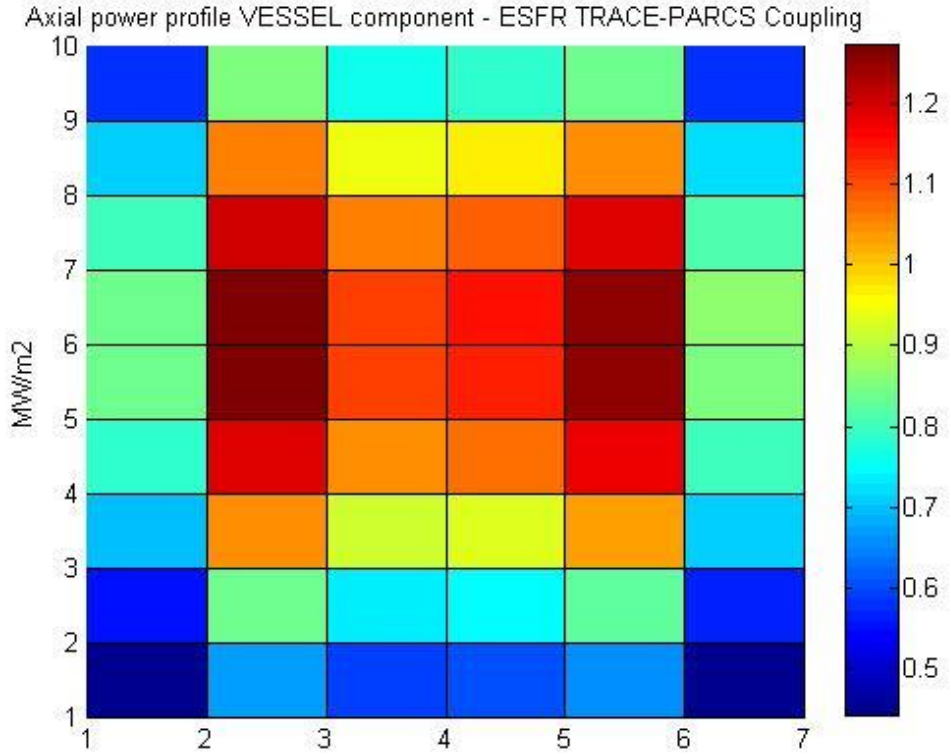

Figure 81: Axial power profile in the VESSEL component in steady state

This three-dimensional TRACE-PARCS coupled model gives not only a much more detailed view of the phenomena occurring in the core, but also a broad and intuitive notion of the thermal behaviour of the entire system.

Figure 82 shows a snapshot of an animation showing the different fluid conditions of the coolant all over the system. On the right side, it appears a cross section of the primary pool design, and overlapping the plot, a representation of the coolant temperature in the main pool volumes. It has been divided by its vertical axis into two sides representing the cross section of two azimuthal sectors.

The figure provides with a more intuitive picture of vertical stratification of the coolant temperatures. In asymmetrical transients this view will highlight differences in temperature between the two different azimuthal sectors. At the left side a representation of one single secondary and tertiary circuits is also included. The secondary circuit is represented by the coolant liquid temperature and the tertiary system by its fluid condition, from sub-cooled flow (blue) to superheated flow (red). This is only representing one of the three loops linked with the three different azimuthal sectors in which the primary system has been divided.

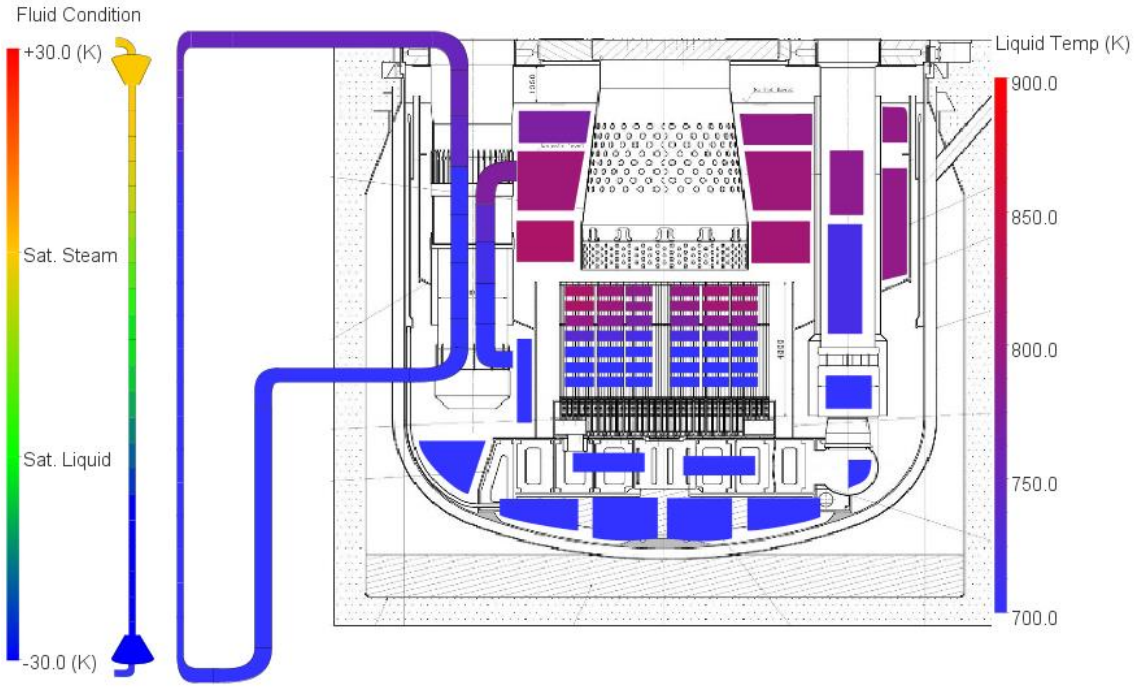

Figure 82: 3D systems representation – Steady state

The coupled TRACE-PARCS model has been demonstrated to perform simulations of symmetrical transients consistently with the results obtained using state-of-the-art one-dimensional model.

5.3. Asymmetrical transient Analysis

Once the 3D thermal-hydraulic and 3D neutronic coupled model has been benchmarked for symmetrical transients in the previous sections with high level of agreement, it is ready to be used to perform simulations of asymmetrical transients.

In the following sections, a selection of asymmetrical transients is considered. This selection includes the transients with highest potentially harmful consequences such as the loss of flow transients or reactivity initiating events. The loss of flow transients can be then compared with the symmetrical transients covering the same initiating events.

One of the main objectives of these studies is to analyse how the system accommodates this kind of asymmetrical transients and if there is any deficiencies of the design that may threat any design criteria based on the results provided by the model. It must be highlighted that an asymmetrical transients is much more likely to happen in probabilistic terms than the symmetric ones. The failure of one single primary pump is more likely to occur than the failure of three of them simultaneously. The same conclusion can be extended to loss of flow events in the secondary or tertiary circuits. The withdrawal of one control rod is an initiator that necessary should lead to an asymmetric transient, since there is no control rod position in the core where its removal would lead to a symmetrical transient. For these reasons, the study of asymmetrical transients is very justified. However, there was an important limitation for the state-of-the-art

based on the use of one-dimensional models, which overcomes the use of the coupled 3DTH+3DN model developed using TRACE-PARCS codes.

Unfortunately, due to the unique nature of this novel model capability and of the coupling scheme developed in this work, the results cannot be benchmarked against any other similar results or experimental data yet.

5.3.1. Coastdown of one single primary pump

The unprotected loss of primary pumps (ULOF) transient has been already analysed in paragraph 4.1.2.2. This transient is initiated by the simultaneous coastdown of all primary pumps. As it was shown, this transient has very severe consequences as it leads the reactor to a power excursion in a few seconds, considering no intervention of the protection systems.

However, the transient considered in this section consists of the coastdown of one single primary pump, what triggers an asymmetric transient. The other two pumps keep their nominal massflow. From a probabilistic point of view, this transient is more likely to happen than a complete primary loss of flow, so its potential consequences should be taken into account in the safety assessment of the design. Figure 83 shows the massflow evolution in the three primary pumps.

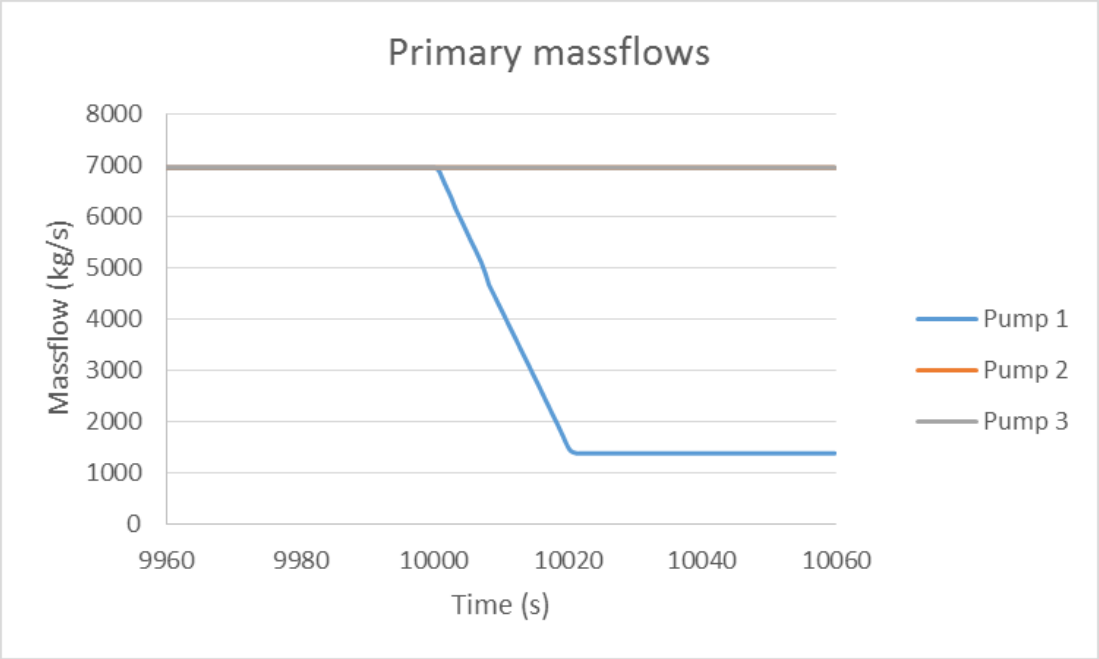

Figure 83: Massflow evolution in the three primary pumps – Coastdown of one single primary pump

This mass flow reduction of one single pump creates an asymmetric flow distribution in lower axial levels of the lower plenum.

Nevertheless, the large inertia of this pool is enough to accommodate this asymmetric distribution in such a way that the asymmetrical effects have almost disappeared close to the core inlet.

Figure 84 shows the vertical massflow distribution along the three azimuthal sectors of the inner ring of the vessel. It can be observed that the azimuthal sector of the tripped pump (Az.1) still has the lower massflow but the other azimuthal sectors (Az.2 and Az.3) are also affected.

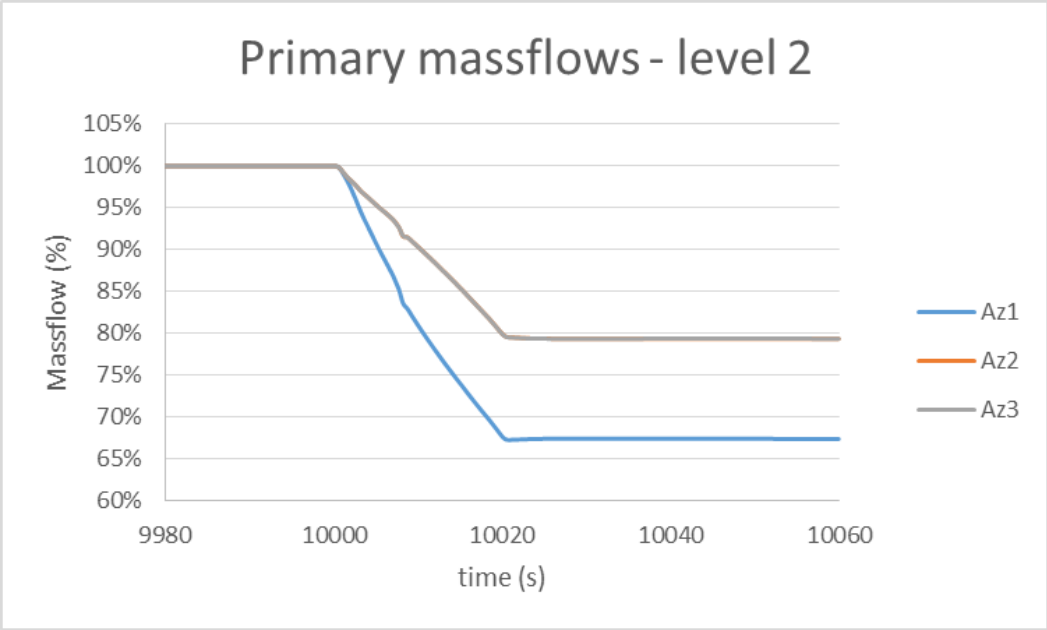

Figure 84: Massflow distribution at axial level 2 of primary VESSEL component

As the coolant flows towards the core, the asymmetrical effect vanishes. At the level 4, the core entrance, this effect is completely neglected. As Figure 85 shows, the flow is perfectly homogenous at the core entrance.

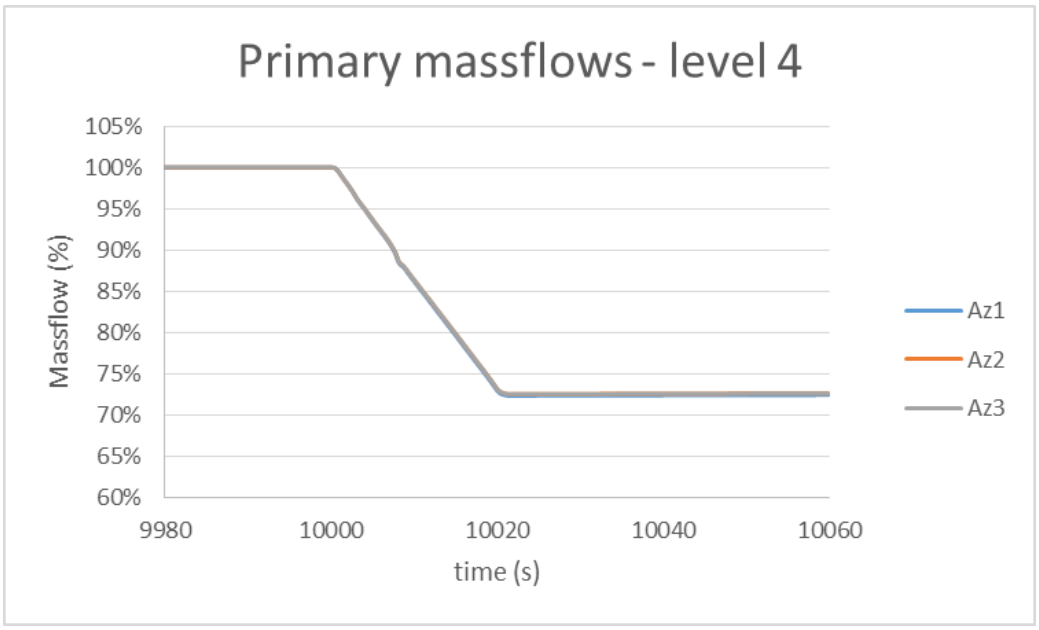

Figure 85: Massflow distribution at axial level 4 of primary VESSEL component

It can be appreciated that the three azimuthal sectors remain at a massflow level of 73%. This flow level is equivalent to the trip of one single pump taking into account the remaining flow that the pump keeps during natural circulation effects (~ 20%). This is to say that the trip of one single primary pump is equivalent to the effect of reducing the massflow by 27% in the three primary pumps simultaneously.

Figure 86 shows the power evolution of the asymmetrical trip of one single pump as compared with the symmetrical flow reduction of all primary pumps by 27%. As it can be appreciated the results are perfectly equivalent.

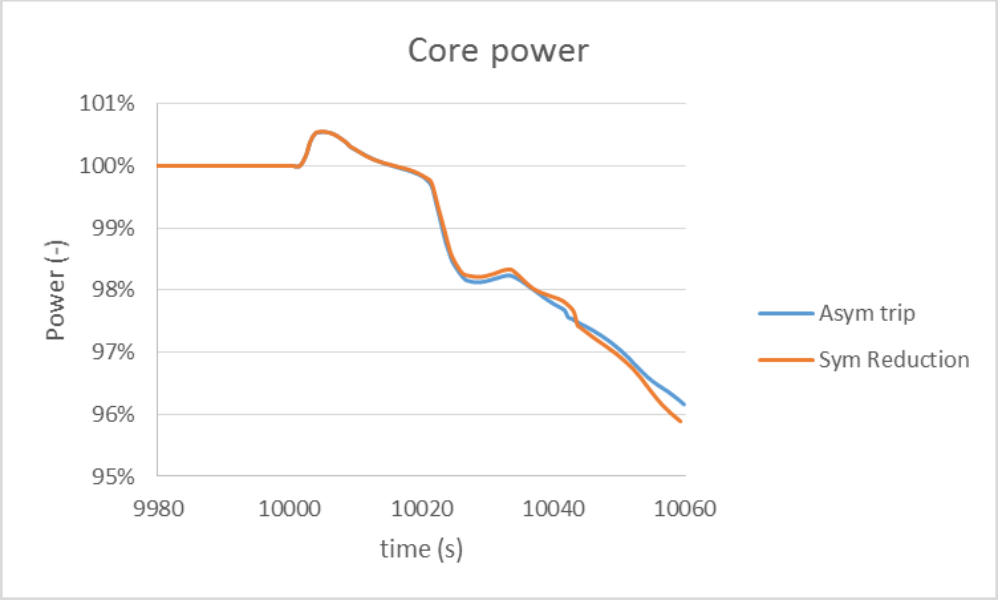

Figure 86: Core power – Coastdown of one single primary pump

Since this transient is completely driven by thermal parameters, this is the coolant heat up caused by the loss of flow, and the loss of flow is perfectly symmetrical, then, this transient does not present any asymmetrical behaviour. Figure 87 shows the radial power profile at the end of the transient. The profile keeps the shape of the steady-state conditions.

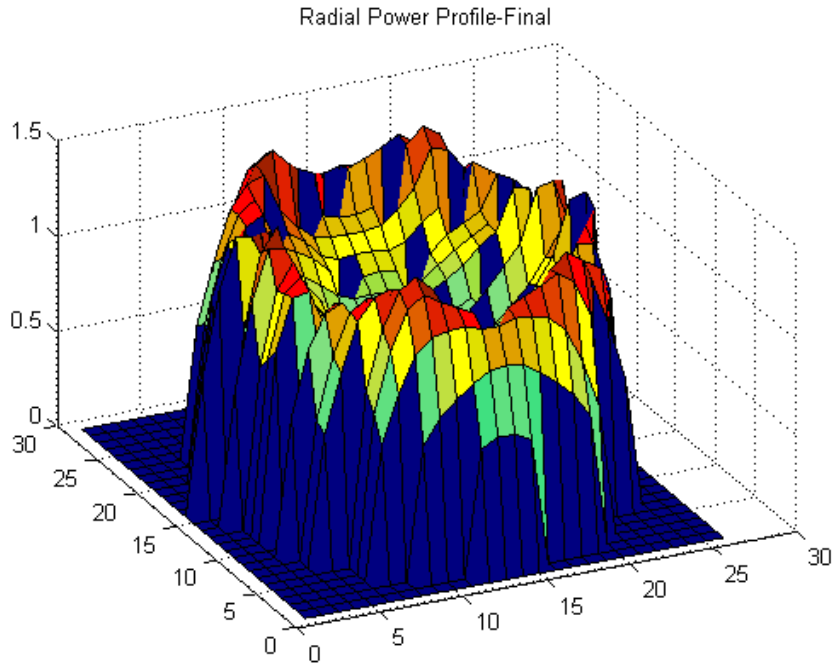

Figure 87: Radial core power profile – Coastdown of one single primary pump

The nodes that present a value of power close to zero (in blue) are the positions where the control rods are placed and slightly inserted due to the differential insertion caused by the temperature increase. Figure 88 shows the relative difference at the end of the transient with the steady state configuration. The differences are lower than 0.5%. These differences can be considered as just numeric effects.

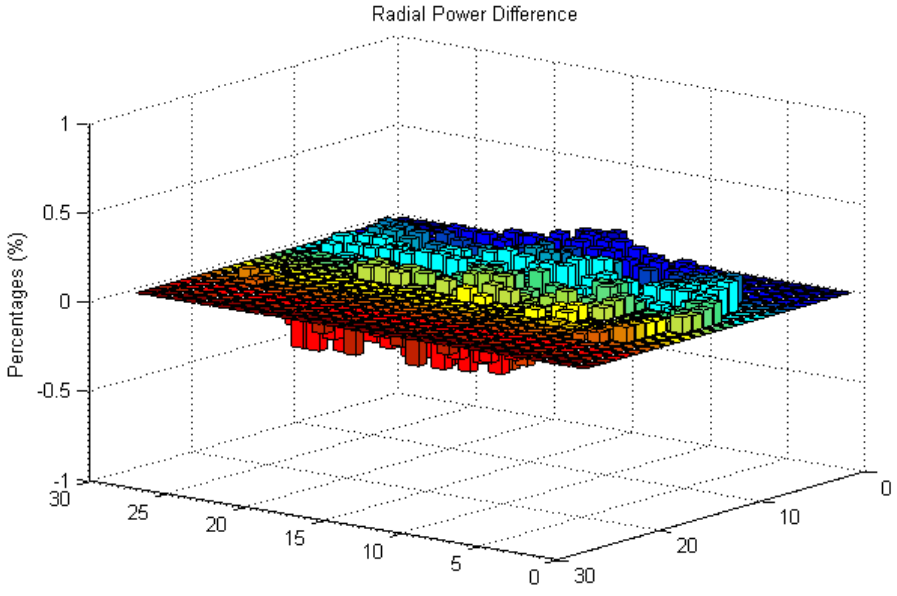

Figure 88: Radial core power differences – Coastdown of one single primary pump

Figure 89 shows the peak temperature distribution.

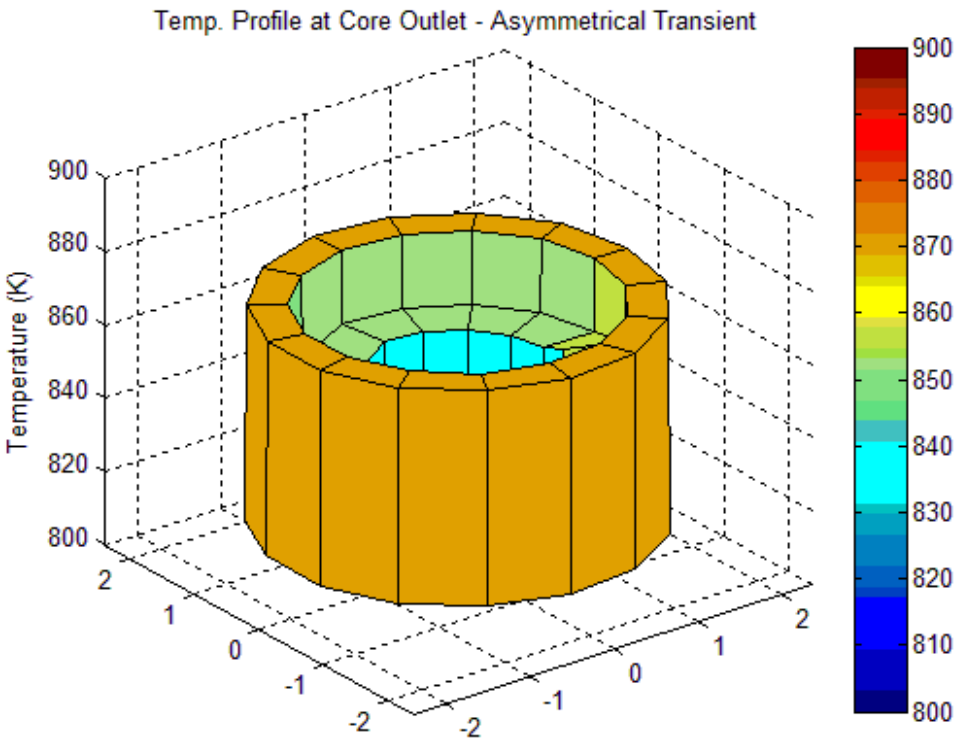

Figure 89: Radial core power differences – Coastdown of one single primary pump

The maximum temperature reached during the transient if 870 K, which gives a fair safety margin for the system to arrive to boiling conditions (~ 1150 K).

It can be concluded then, that this asymmetrical transient cannot be considered as a threat to the reactor integrity since the system is able to accommodate it even without any protection system acting. Now, consequences are completely under the ones already discussed in the loss of primary flow (ULOF) transient analysed with the one-dimensional model.

It should be noted that this beneficial effect (symmetric behaviour) may be reduced if a detailed model of the cold pool including all the different internals and its related pressure losses is implemented. The losses may affect the mixing capability reducing the ability of the system to accommodate the reduction of massflow in one single pump.

5.3.2. Coastdown of one single group of secondary pumps

The transient is initiated by the coastdown of one group of pumps in the secondary circuit. This loss of flow reduces the cooling capability of the secondary circuit and consequently affects the thermal cycle in the primary pool.

The transient was analysed within the CP-ESFR project [Dufour et al, 2012] considering the coastdown of all secondary pumps. The one-dimensional capability of the models bounded a

more detailed analysis. The analysis concluded that the system is able to sustain the coastdown of all secondary pumps without any major safety concern.

This transient is also analysed with the coupled model. However, now it is considered a reduction only in one single secondary pump flow rate from nominal value to 20% of its nominal value in 20 seconds. This is a conservative assumption. Thus, studies performed within the project task considered natural circulation level ranges 20% to 28%. Nevertheless, since there are uncertainties in the secondary system design it is assumed in this section the lowest natural circulation level.

Figure 90 shows the massflow profiles in the three secondary system pumps.

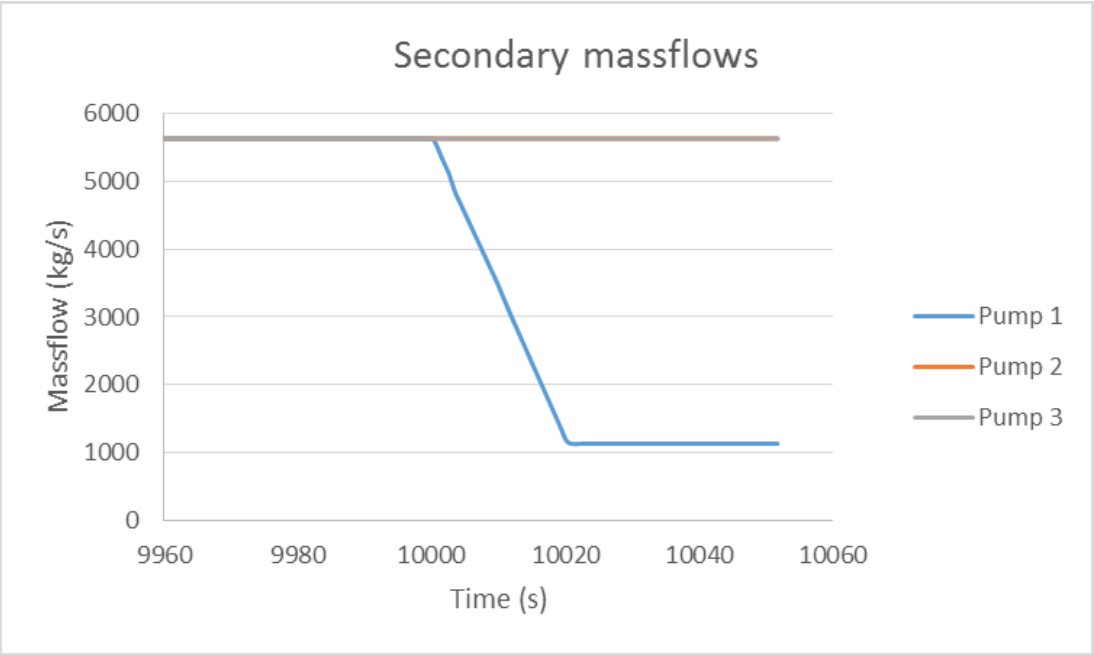

Figure 90: Massflow evolution in the three secondary pumps – Coastdown of one single secondary pump

The analysis of the simulation results of the coastdown of one single primary pump transient, presented in the previous section, has shown that the mixing effect in the large cold pool is enough to compensate the asymmetry caused by the flow reduction in one azimuthal sector, in such a way that the massflow profile at the core entrance presents symmetry. However, this mixing effect in the large cold pool does not take place in the current one single secondary pump transient, as there is no depression in the affected azimuthal sector.

Consequently, the coolant flow that comes from the intermediate heat exchanger outlet affected by the secondary circuit cooling shortage at a higher temperature than the other azimuthal sectors goes towards the core with a very small mixing effect.

Figure 91 shows the massflow profile at the core inlet for the three azimuthal sectors of the inner ring of the vessel.

It can be observed that the primary flow of the azimuthal sector affected by the secondary flow reduction (Az1) presents a slightly reduction (0.75%) in its massflow rate caused by the density change related with the temperature increase. The other two azimuthal sector increase their massflow rate but in a very limited amount (0.2%).

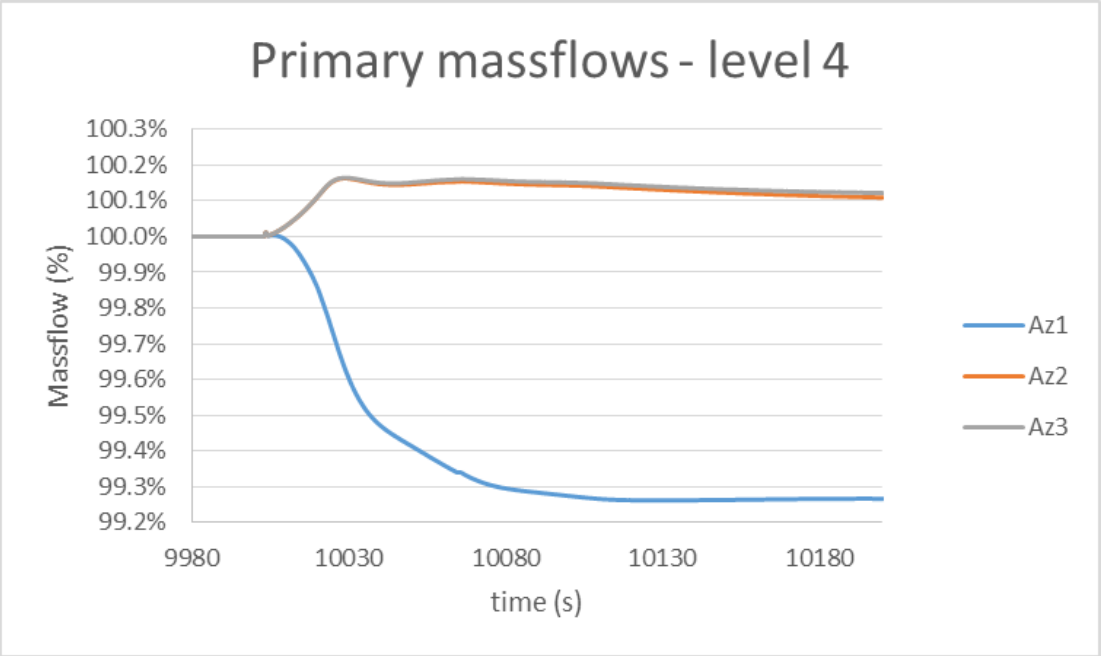

Figure 91: Primary flowrate profile at core inlet – Coastdown of one single secondary pump

Figure 92 shows the temperature profile of these three azimuthal sectors. It shows the strong increase of the inlet temperature in the azimuthal sector where the secondary system is providing a limited cooling capability. On the contrary, the other two azimuthal sectors present a very small temperature increase. This behaviour demonstrates the very small mixing effect taking place in the hot pool if the primary pumps keep working in a symmetric configuration. This asymmetric effect can only be seen with a three-dimensional thermal-hydraulic model, so it was overlooked in the state-of-the-art one-dimensional approach.

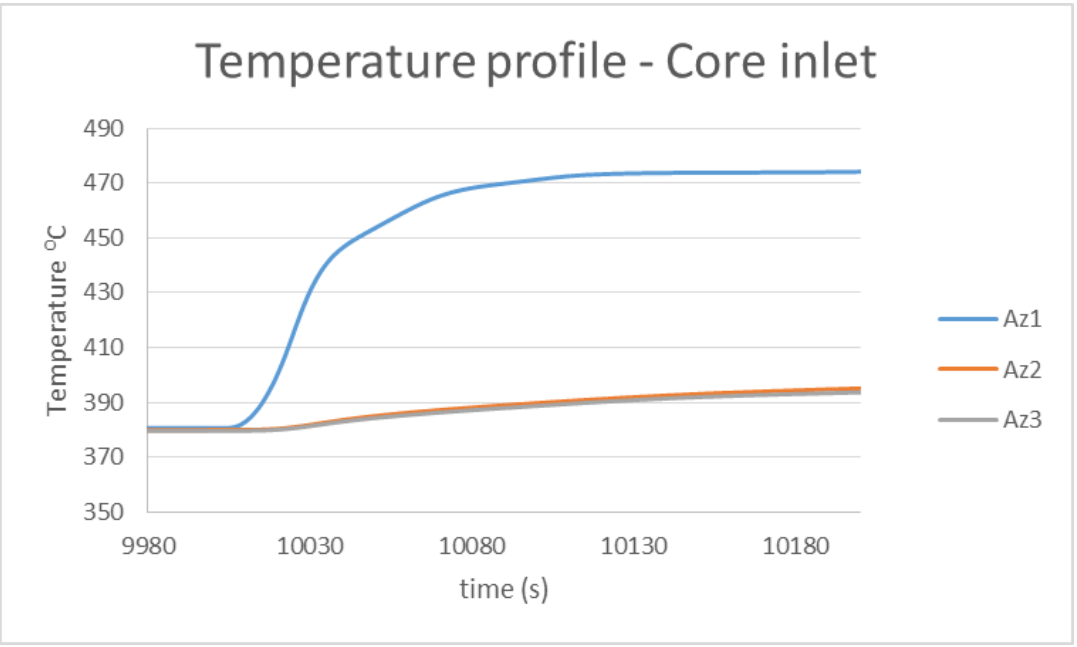

Figure 92: Temperature profile at core inlet – Coastdown of one single secondary pump

Figure 93 shows the temperature profile at the core outlet. It can be observed that the asymmetric temperature distribution is sustained in the coolant through the core. The core outlet coolant temperature in the azimuthal sector affected by the pump coastdown is close to 80 ºC higher than the other two azimuthal sectors. In those, the temperature variation is very limited (~ 5 ºC).

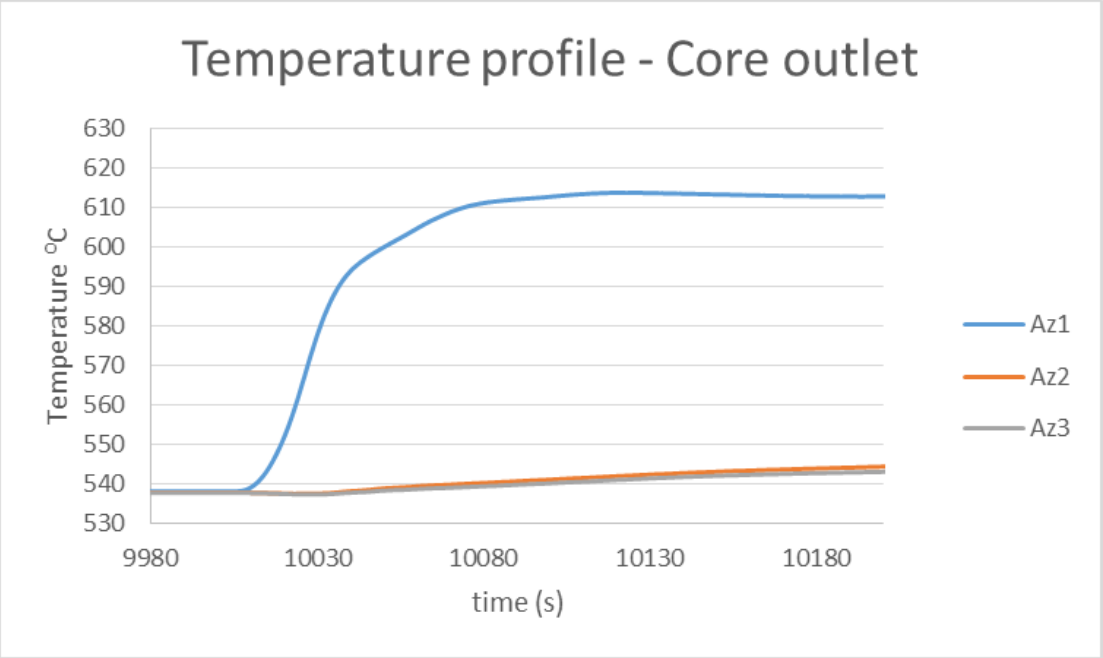

Figure 93: Temperature profile at core outlet – Coastdown of one single secondary pump

This asymmetric temperature profile at the core inlet triggers an asymmetric neutronic feedback shown in Figure 94 and Figure 95.

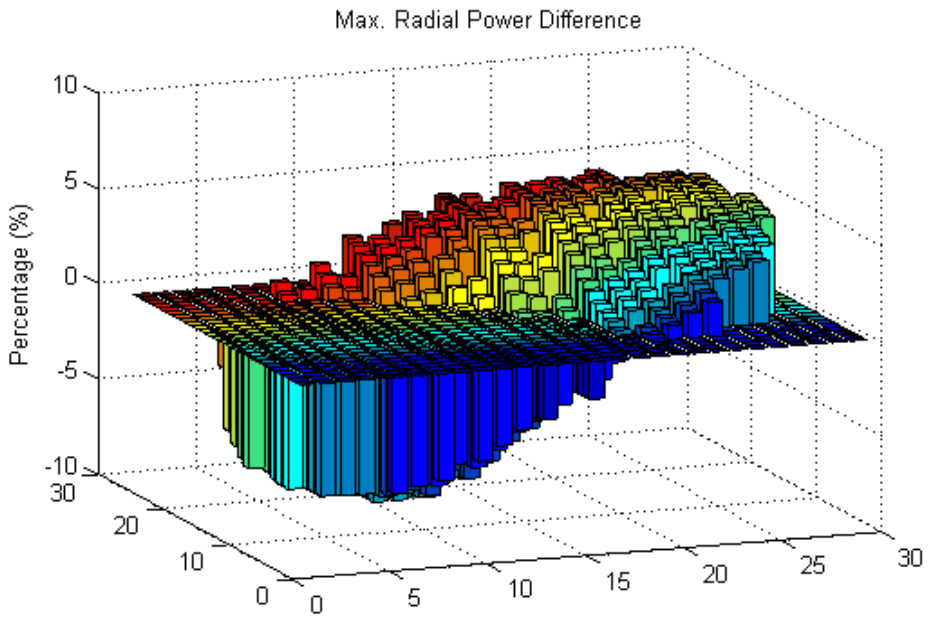

Figure 94: Maximum radial power profile difference (I) – Coastdown of one single secondary pump

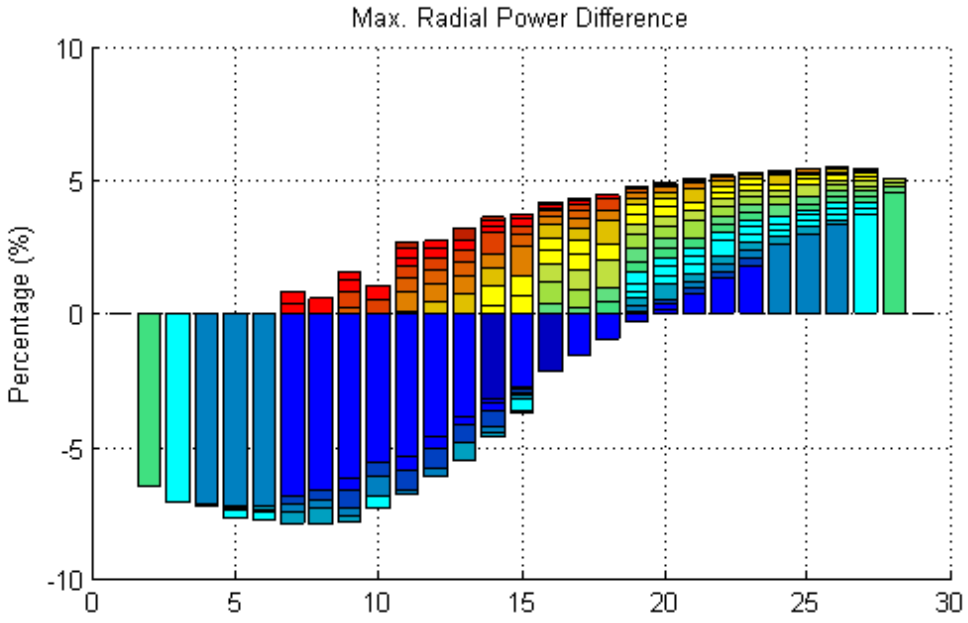

Figure 95: Maximum radial power profile difference (II) – Coastdown of one single secondary pump

Both Figure 94 and Figure 95 show the maximum power profile differences for the asymmetric transient. These differences go up to ~ 8%. The core area of the azimuthal sector affected by the secondary pump coastdown suffers a relative decrease in radial power. This is a very important fact, since the effect of the void effect caused by the remarkable increase of coolant temperature is counterbalanced by the negative reactivity effects, mainly, the control rod differential insertion. On the contrary, the azimuthal sectors unaffected by the secondary pump coastdown present a slightly increase of relative radial power profile since small effect of the coolant heat up and Doppler effect (Figure 96) is not counterbalanced by the limited control rod differential insertion.

The following figures show the evolution of the other main parameters that affect the core reactivity that justify the aforementioned conclusions. Figure 96 shows the peak fuel temperature, directly linked with the Doppler effect. It shows that the peak fuel temperature decreases in all the three azimuthal sectors, which indicates a generalised power decrease. The temperature decrease in the azimuthal sector affected by the secondary pump coastdown is higher than the temperature decrease for the other two sectors. This indicates that the power reduction is higher in the affected azimuthal sector, which is in line with the power profile results.

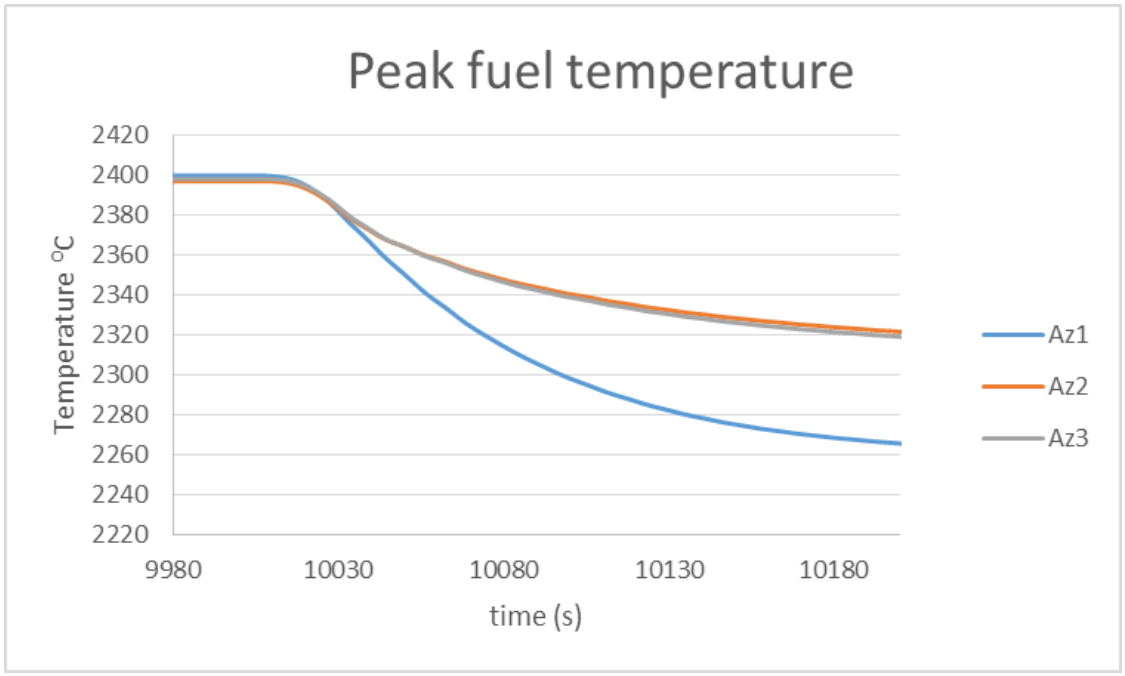

Figure 96: Peak fuel temperature – Coastdown of one single secondary pump

Figure 97 shows the control rod differential insertion of the three control rod banks.

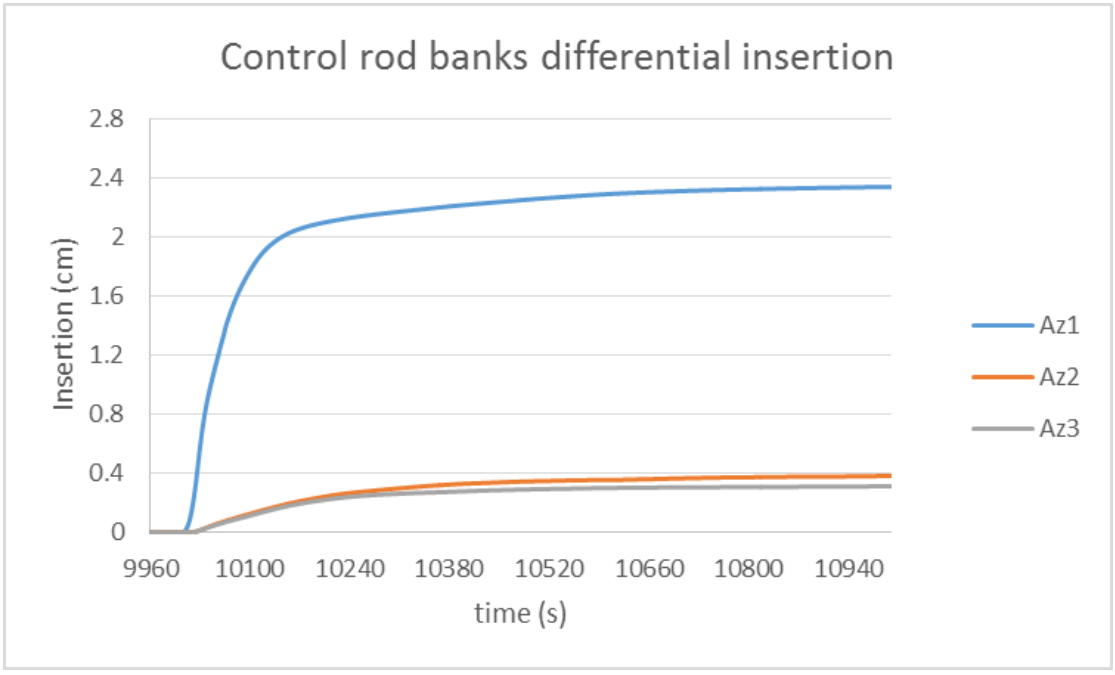

Figure 97: Control rod banks differential insertion – Coastdown of one single secondary pump

As described in paragraph 3.3.1.4, the control rod bank insertion is divided into three regions to take into account possible azimuthal temperature differences that develop a different insertion paths in different areas of the core. Figure 97 shows a strong insertion (~ 2.4 cm) in the azimuthal sector where the secondary pump stops caused by the strong structure temperature increase caused by the coolant heat up in that area. This insertion is what counterbalances the positive void effect, and consequently, the increase of power that the coolant heat up would trigger. The figure also shows the limited insertion appearing in the other two azimuthal sectors (~ 0.4 cm),

which is not enough to compensate the Doppler positive effect caused by the fuel temperature decrease in those azimuthal sectors.

The evolution of total power generated is shown in Figure 98. Consistently with the conclusions already obtained, the total generated power decreases around 10% as a consequence of the secondary pump coastdown.

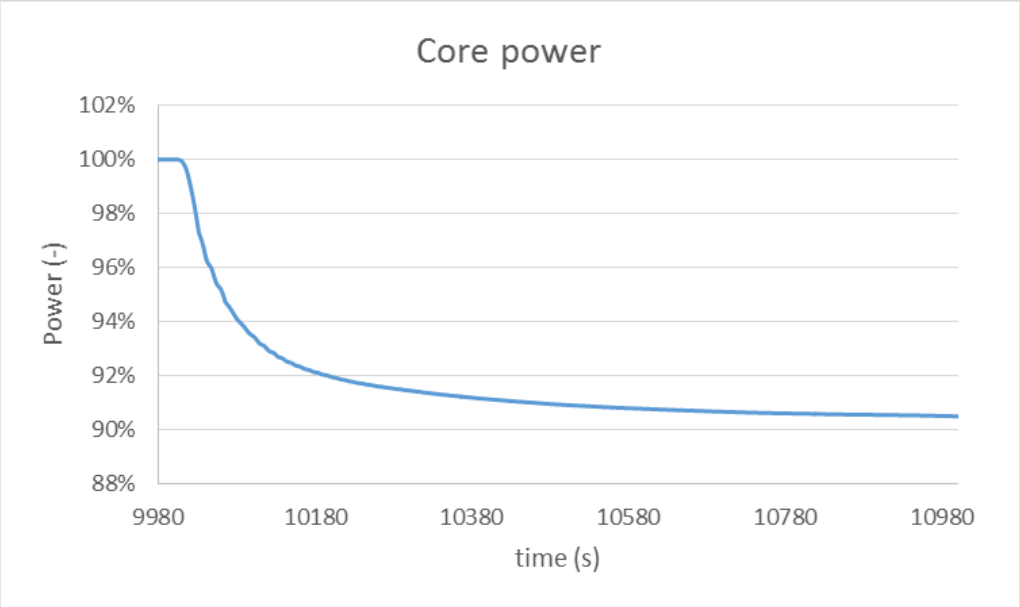

Figure 98: Total core power – Coastdown of one single secondary pump

It is important to highlight the temperature difference in the core support structure shown in Figure 99. The temperature difference in the azimuthal sector affected by the pump coastdown is ~ 100 ^{o}C higher than the ones for the other two azimuthal sectors. This value is remarkably higher than the one settled as a design criteria in the literature ($\Delta T = 30\ K$) [HNE-Sodium, 2010].

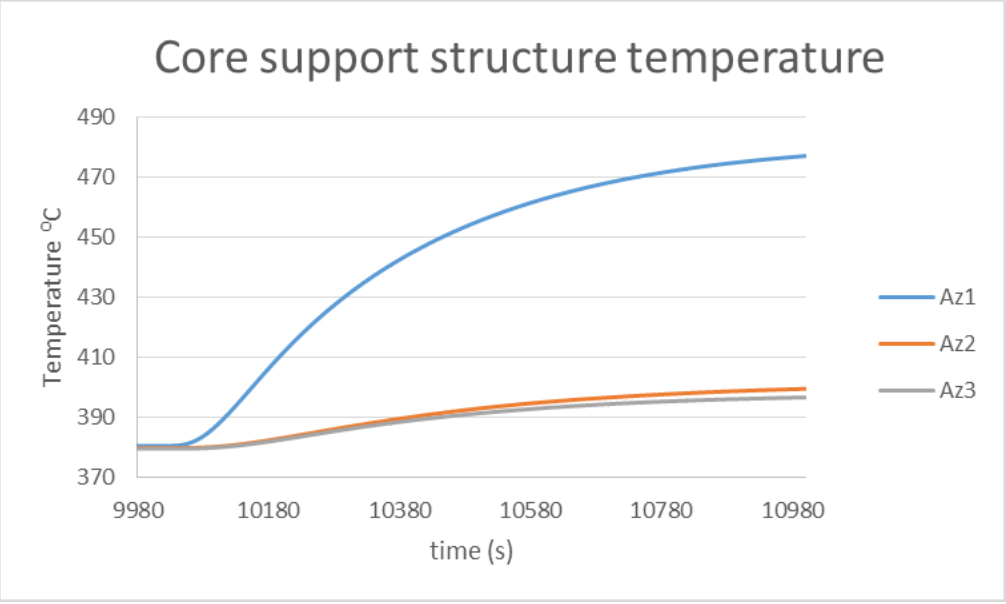

Figure 99: Temperature profile at the core support structure – Coastdown of one single secondary pump

The simulation results for this one single secondary pump coastdown transient demonstrate the importance of a 3DTH+3DN model in order to take into account asymmetric phenomena with an impact that should be considered as part of the safety analysis in the designing phase of the project.

This model also gives an overview of the thermal state of the complete system. Figure 100 shows a snapshot of the temperature profile of the primary, secondary and steam generator systems once reached the steady state conditions triggered by the coastdown of one secondary pump initiator.

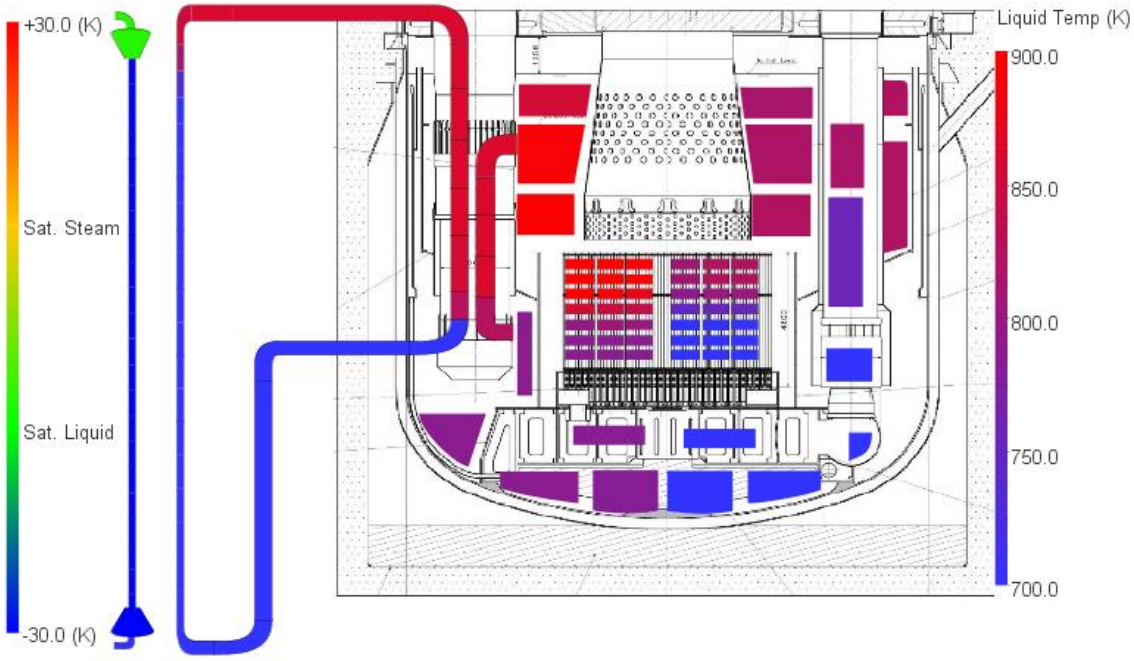

Figure 100: Temperature profile in the plant – Coastdown of one single secondary pump

5.3.3. Control rod bank withdrawal

The transient consists of the spurious withdrawal of one control rod bank. This transient is ascribed among the Unprotected Transient Over Power (UTOP) since the withdrawal necessarily increases core power.

It is assumed an asymmetric withdraw of a control rod bank in 1 second. Equivalent studies performed in light water reactors assume that this event occurs in an order of 0.1 sec. Nevertheless, this very short time is justified mainly by the high pressures reached in the core of those reactors triggering an ejection of the control rod bank. This assumption in not applicable to this design at it works at much lower pressures, so consequently the time for a control rod to be withdrawn should be longer. A detailed study of a realistic simulation of the withdrawal of a control rod is missing, which would help to make an estimation of a realistic timeframe for this event to happen.

The state-of-the-art one-dimensional models cannot simulate this transient, so there is no possible comparison available.

Figure 101 shows the control rod banks distribution. Banks 1 to 3 represent the control rod banks placed in the three azimuthal sectors. The bank number 4 is the bank that is withdrawn. It moves from its initial position to a complete withdrawal in 1 second.

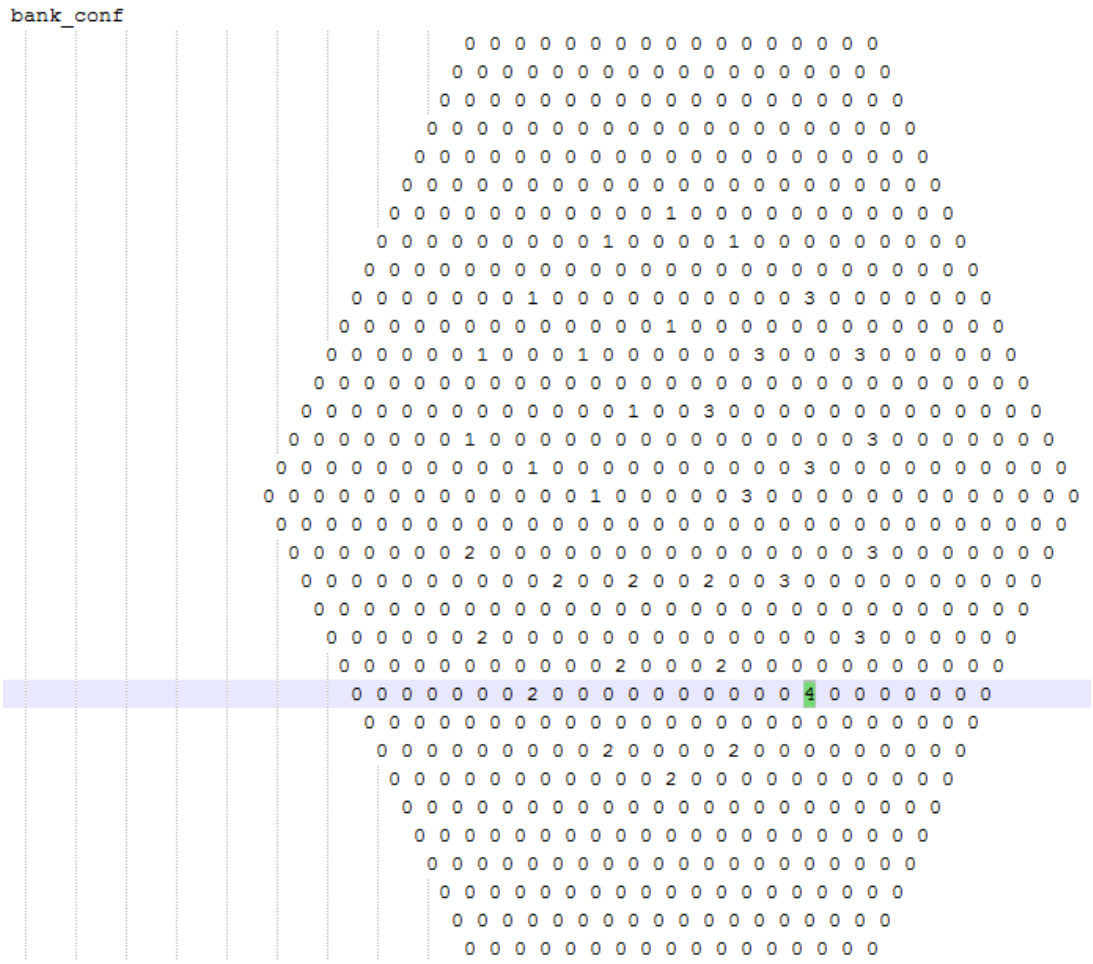

Figure 101: Control rod bank distribution – Control rod bank withdrawal

Figure 102 shows the total power evolution as a consequence of the asymmetric control rod withdrawal (control rod bank 4).

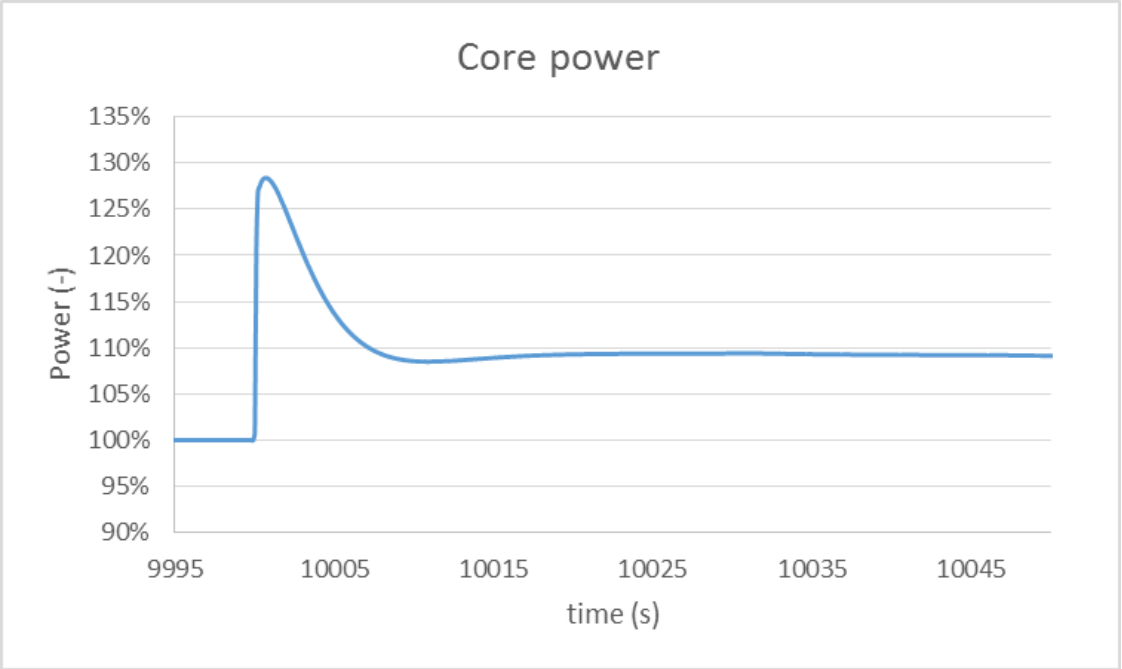

Figure 102: Total core power – Control rod bank withdrawal

The figure shows an initial overpower peak of ~ 128 %, afterwards the system evolves into a new equilibrium level at higher power than the nominal value (~ 110 %) as a consequence of the new position of the control rod (bank 4).

The total power evolution shown is not enough to see the possible local effect effects that this transient may trigger. The new 3DTH+3DN model is able to provide further details on the behaviour of the core during this transient.

Figure 103 and Figure 104 show the maximum difference radial power profile generated by this transient. The figures show a maximum power difference close to 40% in the area surrounding the control rod withdrawn. All this region suffers an strong overpower that is slightly counterbalanced by the negative reactivity feedbacks that predominate in the core areas unaffected by the transients, namely, void effect, Doppler effect and differential insertion of the control rods.

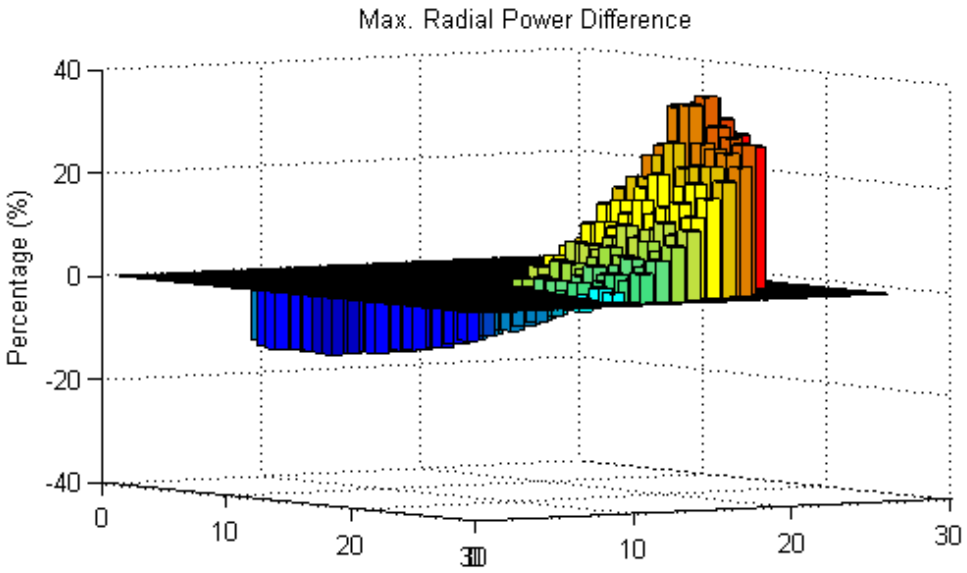

Figure 103: Maximum radial power profile difference (I) – Control rod bank withdrawal

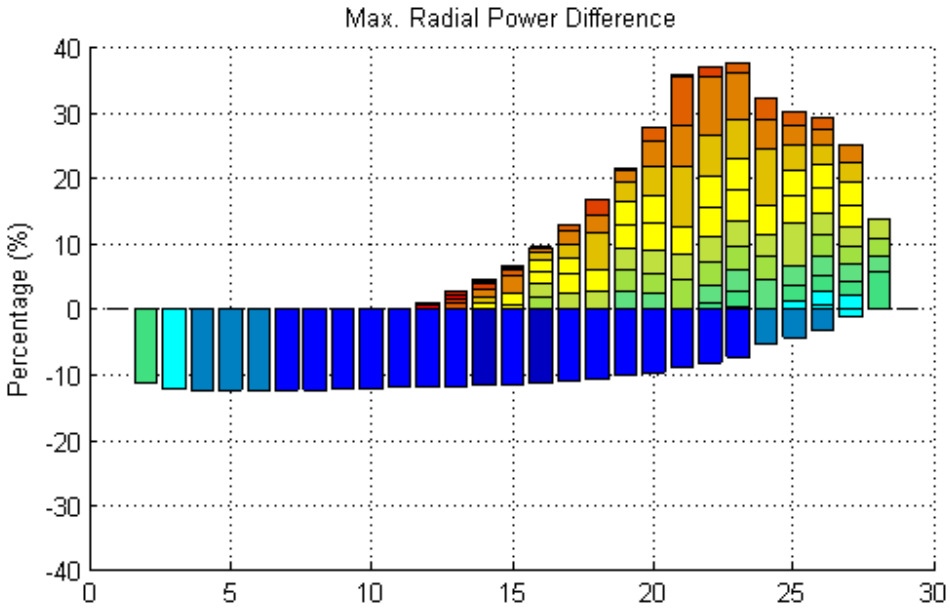

Figure 104: Maximum radial power profile difference (II) – Control rod bank withdrawal

Since the transient is reactivity initiated and the system does not go into a high overpower level (10% after 6 seconds) the variables that affect the effects that contribute to reduce the power generation does not remarkably change. For that reason the radial power profile of the regions not affected by the control rod withdrawal present a radial power difference of just 10% and consequently the system is not able to return to its nominal power value spontaneously.

In addition to the results shown, two additional different cases are also simulated. Both consider a withdrawal time of 10 seconds, corresponding to a controlled withdrawal of a control rod mechanism – this is at speed of ~ 2.37 mm/sec from a pre-insertion position of 2.4 cm – but in two different positions of the core. The first calculation keeps the position considered in the previous case and a second one considers the withdrawal in a central position (see Figure 105) in order to check the spatial effect of the transient.

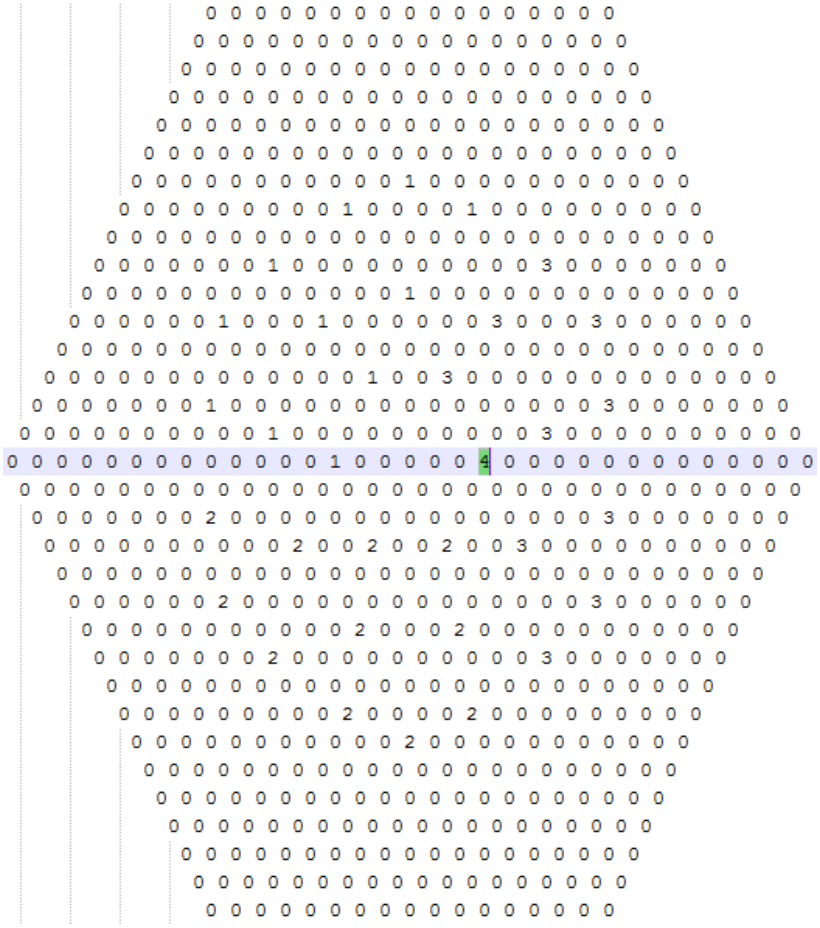

Figure 105: Control rod bank distribution (centred) – Control rod bank withdrawal

Figure 106 shows the power evolution comparison between the control rod withdrawal in a peripheral position and a centred one. The figure shows the power peak is reduced from ~ 130% appearing in Figure 102 to ~ 115% with a longer timeframe for the same control rod withdrawal (from 1 s to 10 s). The figure also shows that the power peak reduces its value up to ~ 105 % if the control rod withdrawal occurs in a central position of the core. This is due to the different worth (i.e. the different variation in reactivity created per cm inserted) of the control rod attending to its placement in the core.

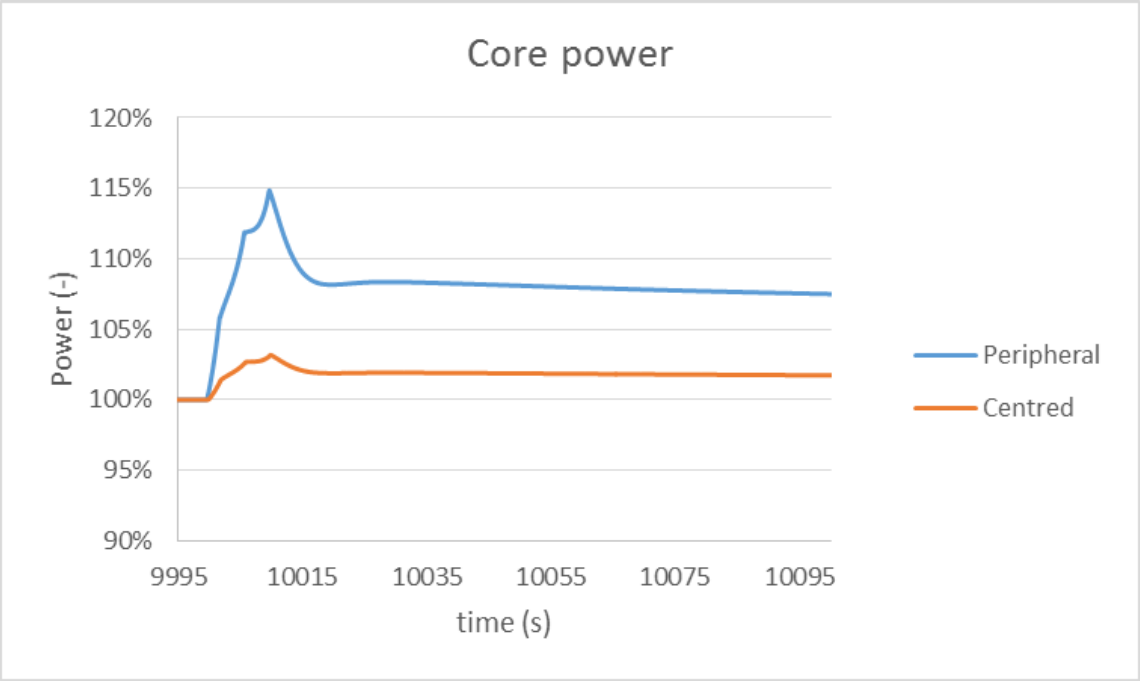

Figure 106: Total core power – Control rod bank withdrawal

Figure 107 shows the radial power profile difference for the 10 seconds control rod withdrawal on the periphery of the core.

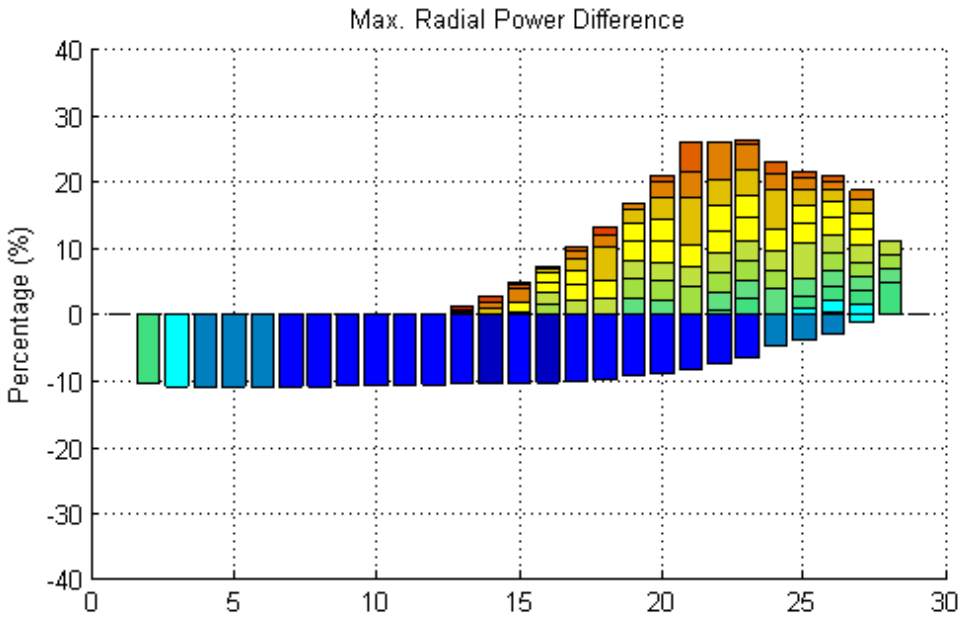

Figure 107: Maximum radial power profile difference (III) – Control rod bank withdrawal

The figure shows a reduction in the asymmetric component of the radial power profile from ~ 40% to ~ 28% caused by the longer time elapsed in the withdrawal. This reduction justifies the lower total power level reached during the transient.

Figure 108 and Figure 109 show the power profile difference created by the withdrawal of a centred control rod bank. It can be seen that the asymmetries are much reduced. The peak power is increased by ~ 12% in the fuel assemblies surrounding the affected control rod and this increase is progressively reduced towards the periphery of the core. The negative values of the radial power profiles are relatively small (limited increase in coolant and fuel temperatures implies low values of coolant void effect, Doppler effect and Control rod insertion differential insertion effect). This limited and localised power increase justifies the small influence in the total power evolution shown in Figure 106.

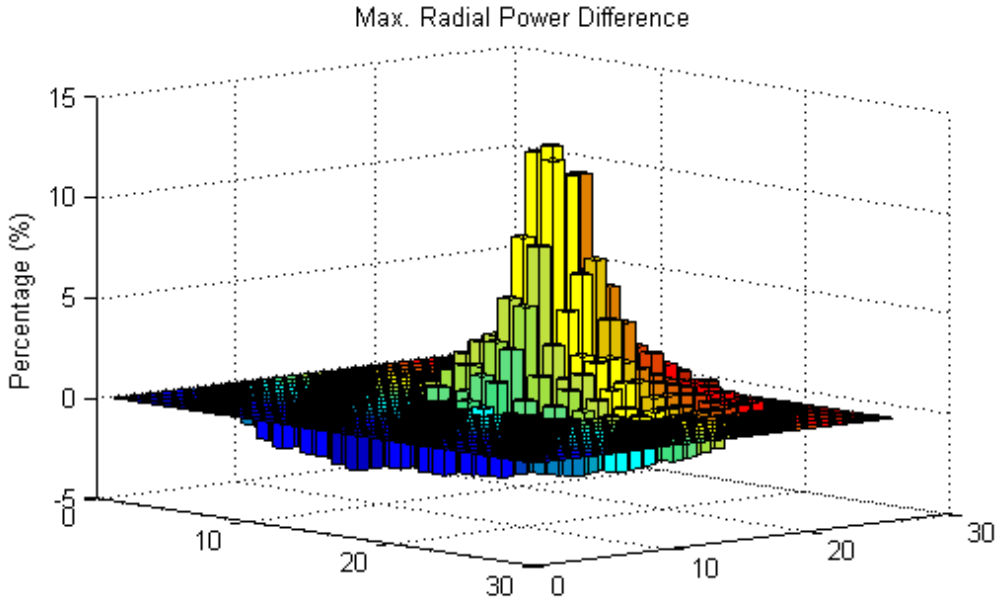

Figure 108: Maximum radial power profile difference (IV) – Control rod bank withdrawal

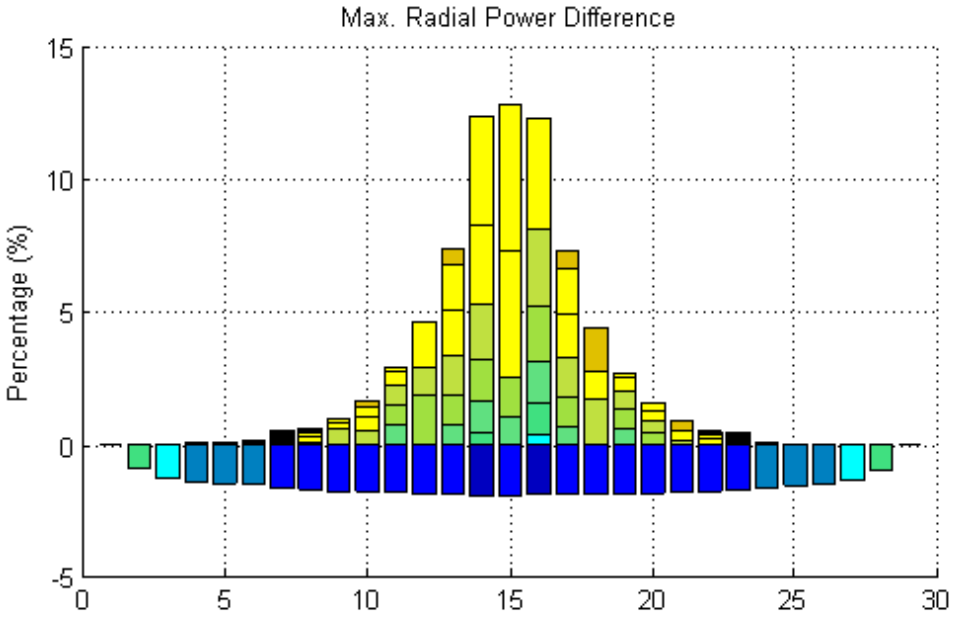

Figure 109: Maximum radial power profile difference (V) – Control rod bank withdrawal

6. Conclusion

This section presents the main conclusions of the research work developed in the framework of the PhD thesis within the field of coupled thermal-hydraulic and neutronic modelling of liquid cooled fast breeder reactors along with a brief summary of the methodology followed in each step towards its objective. In addition, the contributions of the research work to the state-of-art are cited and it is provided some guidance for further research envisaged for the near future.

6.1. Achievements

6.1.1. Study of the applicability of the code to be used in LMFBR safety analysis

The work starts with the study of the applicability of the computational tools selected to the LMFBR technology, in particular to a SFR-kind and a LFR-kind design.

Even though the results have shown that the selected codes are able to perform simulations in LMFBR technology, some considerations should be done:

Firstly, we identified the need to implement specific heat transfer correlations to substitute the ones hardcoded in the source code by the ones identified in the bibliography as the most convenient for LMFBR technology.

Pure lead properties are implemented in TRACE code in order to reduce the uncertainty created by using the built in lead-bismuth eutectic properties. These thermal properties are extracted from state-of-the-art experimental data provided by reference organisations in the field of Lead Fast Reactor technology (i.e. ENEA, ANSALDO).

In the neutronic code, PARCS, the formula used to evaluate the Doppler effect is modified from a square root to a logarithmic expression as a function of the fuel temperature to better evaluate the temperature contribution in LMFBRs' fuels.

6.1.2. One dimensional modelling of a SFR design

The modelling phase of the Sodium Fast Reactor technology starts in the framework of the FP7-CP-ESFR project.

A one-dimensional model of the European Sodium Fast Reactor (ESFR) design with point kinetic neutronic feedback has been developed (Paragraph 3.1.1) and its results have been compared with the equivalent model developed by the other organisations. A benchmarking exercise was settled with the peer research institutions involved in the Task 3.3.1 devoted to the development of tools and methods to assess the safety analysis of the ESFR design.

Globally, the benchmark demonstrated good agreement among the various codes in the various parameters calculated that are relevant for safety, considering the complexity of the different codes, their different origin, and quite different modelling approaches. The models were able to calculate the main output variables of the transient and demonstrated to be able to simulate the transient behaviour of SFR reactors under turbulent, forced flow conditions. The results provided by the one-dimensional model developed, as this thesis has shown, are in good agreement with all the other partners' calculations.

The main outcome of the study was that all codes used were able to analyse the transient behaviour of the ESFR plant design. In some cases, appropriate code specific modifications were made. In the benchmark case the code results were compared and the following deficiencies were identified:

- Even though its effect was limited, the use of static or dynamic fuel-cladding gap size model affects the calculation of the fuel temperature and thus the associated reactivity feedback effects (i.e., Doppler, axial expansion). So, its implementation is advisable for transient analysis where higher fuel temperature variations under different core states (specifically BOL, EOL) are observed.
- There is uncertainty about the time delay constant associated with the heat-up of the diagrid plate and the corresponding evolution of the core radial expansion reactivity feedback effect.
- There is uncertainty in the geometrical definition of the secondary systems that lead to different secondary circuit thermal inertias and consequently to differences in the transient temperatures of the primary/secondary/tertiary system configuration.
- There is need to harmonize methodologies to calculate mean values, such as fuel mean temperatures, that may affect some safety parameters such as the Doppler and axial fuel expansion reactivity feedback effects.

The benchmark was consequently a good basis from which to undertake the full set of calculations for representative transients. With the objective to assess the safety performance of the design a set of transients identified in the preliminary assessments as DBC4 or even DEC type of transients were analysed.

This PhD thesis included the results of one of these transients, namely the Unprotected Loss Of Flow (ULOF), which is triggered by the simultaneous coastdown of all primary pumps. This transient is considered as the most penalising case in the safety analysis.

The analysis of the ULOF transient using the one-dimensional modelling of the SFR developed in this PhD thesis points out that under unprotected conditions the coolant will inevitably reach saturation conditions, a situation of special concern for Sodium Fast Reactor technology.

The analysis identifies the grace time for the protection systems to act in order to avoid potentially limiting situations. This analysis has also shown the behaviour of the system after the core coolant reaches saturation, which may lead to a power excursion.

However, the discrepancies appearing among the partners' calculations pointed out the definitive need of further optimisation and harmonization efforts in the simulation approach of the considered transients and especially reviewing the different approaches for simulation of sodium boiling and its accuracy. This research should be focused not only to adequacies of the codes to simulate the particular phenomena (thermal-hydraulic, neutronic and fuel pin mechanics) that are involved in two-phase liquid metals transients, but also focused on the experimental validation of the different sodium boiling models to improve the consistency of the calculations. Extending the model developed in this thesis to handle biphasic sodium may contribute to such a purpose.

6.1.3. One-dimensional model of a LFR design

In a similar way as for the SFR, a one-dimensional model of the ALFRED design is developed in the framework of the LEADER project.

There was no formal benchmarking exercise to compare the results of the different models developed by the partners of the project. However, the results of the simulations of two transients included in the preliminary safety assessment of the design are compared in the corresponding project deliverable [Bandini et al, 2013]. These transients are, namely, the Unprotected Transient Over Power (UTOP), triggered by an insertion of reactivity representing the withdrawal of a control rod bank, and the ULOF transient, triggered by the simultaneous coastdown of all primary pumps.

The results shown in this work demonstrate the capability of the code to simulate transients in a LFR plant using the specific correlations of lead coolant implemented in its source. Nevertheless, pressure drop correlations specific of liquid metal coolants should be also implemented in order to reduce the uncertainty in the core pressure drop calculations.

The analyses indicate that the ALFRED design is, also thanks to the inherent characteristics of lead coolant, robust with respect to behaviour in postulated unprotected transients, ULOF and UTOP (both presented in the thesis), providing sufficient grace times for the implementation of adequate mitigating measures.

6.1.4. Three-dimensional modelling of SFR design

The methodology followed in order to build a thermal-hydraulic - neutronic coupled scheme is detailed in section 3.2.

This methodology starts with the upgrade of the thermal-hydraulic one-dimensional model into a three-dimensional model. This is done by replacing the primary system model by a TRACE VESSEL component. This component is able to take into account radial and azimuthal flows and consequently is able to simulate in detail a more realistic flow behaviour. In addition, this model has the advanced capability that allows simulating the thermal-hydraulic behaviour of asymmetrical transients. This is a differential upgraded feature with respect to the state-of-the-art one-dimensional modelling techniques, providing great potential to contribute to the safety assessments of LMFBR´s designs.

It must be noted that this version of the thermal-hydraulic three-dimensional model for TRACE still uses the point kinetic reactivity feedback model. Consequently, the asymmetrical capability is limited since the point kinetic scheme uses spatial averaged values to calculate the neutronic related system variables, such as the core power, with no space dependency.

In order to test this first version of the thermal-hydraulic three-dimensional model developed for TRACE, it is applied to simulate the benchmarking case already adopted in the one-dimensional model comparison stage, the simultaneous flow reduction in the primary, secondary and tertiary circuits. The results are shown in section 5.1. It can be observed the very high level of agreement between the 1D and the 3D thermal-hydraulic models for this symmetrical case in simulating the main system variables such as core power, coolant temperatures and reactivity feedbacks. The results achieved were consistent enough to perform the replacement of the point kinetic neutronic feedback model with a spatial kinetic neutronic response model of the ESFR design.

Consequently, a second version of the 3D thermal-hydraulic model for TRACE is developed by implementing the spatial kinetic neutronic model following the technical description of the core for the spatial kinetic code PARCS and using the neutronic cross section set generated with the Monte Carlo based code SERPENT.

Once the coupled TRACE-PARCS model is developed, it is applied to simulate the reference case benchmark where both the thermal-hydraulic and the neutronic models are able to exchange the required information during the transient simulation. As this is a symmetric transient, the results provided by the different versions of the model should be comparable.

In Chapter 5 (section 5.2) the results of the comparison between the one-dimensional and three-dimensional models with point kinetic feedback and the coupled model is shown. All models predict the same transient trend and the discrepancies between point kinetic and spatial kinetic are lower than 10%, which could be considered as acceptable taking into account the different

assumptions (i.e. approximations needed in the point kinetic approach) taken in the two neutronic feedback models.

The good behaviour shown by the models in simulating a symmetrical transient enforced the test of the capability of the coupled model to simulate asymmetrical ones. Three different transients are simulated among the ones identified in the safety analysis of the design with the most severe consequences. These transients are namely, the coastdown of one single primary pump, the coastdown of one single secondary pump and the spurious withdrawal of one control rod bank.

The coastdown of one single primary pump transient analysis shows that the asymmetric flow profile triggered by the initiator is quickly homogenized in the cold pool (lower vessel area) due to its large inertia. Indeed, it is shown that the flow at the core inlet (diagrid region) is completely homogeneous in all the three azimuthal sectors; so consequently, this transient does not trigger an asymmetric power profile in the core nor asymmetric distribution of temperatures. The transient is equivalent to the simultaneous reduction of the flow by 27% in the three pumps. The design is able to accommodate this transient without even the intervention of dedicated protection systems, so we can conclude that the design is robust to withstand the asymmetric initiating event.

It should be highlighted that a fine modelling of the lower vessel including internals may affect the mixing capability of the lower vessel and potentially avoid a complete mix of the flow. This could lead to a situation where an asymmetric effect could be triggered in the core. But, taken into account the excellent behaviour with the undetailed model, this asymmetric effect would be limited.

The analysis of the transient triggered by the coastdown of one single secondary pump shows that the asymmetric coolant temperature profile generated by the reduction of the cooling capability of one intermediate heat exchanger is kept all along the primary circuit. Indeed, since the primary flow keeps a quite symmetric profile only affected by the small differences in density related with the temperature difference between azimuthal sectors no mixing effect takes place.

This quasi-symmetric flow profile keeps a strongly asymmetric temperature distribution in the core inlet, and consequently it is kept all along the primary system. The asymmetric distribution of temperatures generates an asymmetric power profile. This power profile is lowered down in the azimuthal sector thermally linked with the secondary circuit affected by the pump coastdown. This effect prevents that the temperature asymmetry grows until reaching coolant boiling and it is provided by the differential insertion of the control rod in that azimuthal sector created by the increase of structures temperatures. The power profile in the other two azimuthal sectors relatively increases due to the positive Doppler effect created by the fuel temperature decrease due to the total power reduction. The conclusion of the analysis performed was that the coastdown of one secondary pump initiating event triggers an asymmetric transient that should be considered in the safety analysis of the design, as its consequences are not covered by the symmetric coastdown of all secondary pumps. For

instance, the calculation shows a strong temperature gradient (~ 100 K) in the core supporting structure that should be limited to 30 K according to referenced design criteria.

The last transient analysed is the withdrawal of one asymmetric control rod bank. This transient is ascribed among the Unprotected Transient Over Power (UTOP) classification. It is simulated taking into account different time to withdraw the control rod bank in different positions. Even if the reactor power increases and evolves into a new equilibrium at higher power level than nominal the system is able to accommodate the transient without the intervention of the dedicated protection system, since the total generated power and temperatures of coolant and structures (i.e. fuel and cladding) keep under safety conditions. Nevertheless, it is observed the strong asymmetric neutronic effects with radial power profiles differences that go up to 40% in short time transients. The outcomes of the analysis of this transient are twofold. On the one hand it is demonstrated the need to analyse the asymmetric component of a periphery control rod bank and on the other hand the ability of the code to calculate such a transient with the strong gradients generated with the control rod withdrawal.

6.1.5. General conclusions

The PhD thesis contents the details of the development of a computational tool able to contribute to the safety analysis of liquid metal cooled fast breeder reactor. The following generic conclusions can be extracted:

- State-of-the-art computer codes originally developed for LWR technology can be applied to advanced fast reactor technology designs with the adequate modifications and validation against experimental results.
- International efforts have been made to test the consistency of different codes for analysing the behaviour of LMFBR designs using one-dimensional models.
- The codes can also be applied to extend the models into multi-physics three-dimensional analysis tools.
- These tools can be applied to analyse asymmetrical effects that were assessed in the state-of-the-art modelling techniques by extrapolating the corresponding symmetric transients with additional conservative margins. It has been demonstrated that these asymmetrical effects do have a remarkable importance for the safety analysis of the designs.

6.2. Scientific contributions

The research work presented has contributed to the state-of-the-art of its scientific field with the following publications:

Journal papers:

1. A. Lázaro et al. "Code assessment and modelling for Design Basis Accident Analysis of the European Sodium Fast Reactor design. Part I: System description, modelling and benchmarking". Nuclear Engineering and Design, Volume 266, January 2014, Pages 1-16

2. A. Lázaro et al. "Code assessment and modelling for Design Basis Accident analysis of the European Sodium Fast Reactor design. Part II: Optimised core and representative transients analysis". Nuclear Engineering and Design, In Press. April 2014

3. A. Lázaro et al. "Three-dimensional Multi-Physics Design Basis Accident analysis of a Sodium Fast Reactor design". Nuclear Engineering and Design. Under revision

4. K. Tucek et al. "Generation IV Reactor Safety and Materials Research by the Institute for Energy and Transport at the European Commission's Joint Research Centre" Nuclear Engineering and Design. Volume 265, December 2013, Pages 1181–1193

International conference papers:

1. Development of a three-dimensional thermohydraulic-neutronic coupling scheme for transient analysis of liquid metal cooled fast reactor technologies using the system code TRACE-PARCS – A. Lazaro et al. NURETH15 – Pisa 2013

2. Implementation of thermodynamic properties of lead in the TRACE system code towards its integration in a full-scope platform for safety assessments. A. Lazaro et al. NURETH15 – Pisa 2013

3. Safety Analysis Results of Representative DEC Accidental Transients for the ALFRED Reactor. G. Bandini et al. FR13 – Paris 2013

4. Development of a thermohydraulic model of the European Sodium Fast Reactor (ESFR) using the system code TRACE. A. Lazaro et al. European Nuclear Conference – Manchester 2012

6.3. Future Work

As mentioned in the introduction to this PhD thesis, the new reactor concepts proposed in the Generation IV International Forum are conceived to excel in their safety standards. Furthermore, the recent "Technology Roadmap Update for Generation IV Nuclear Energy Systems" [GenIV, 2014] specify the R&D roadmap needed for SFR technology for the upcoming ten years in order to reach those challenging objectives. It can be highlighted the following R&D needs:

- Inherent safety features
    - Safety principles (reactivity feedback, core design goals, balanced safety approach)
    - Passive or self-actuated shutdown systems
    - Decay heat removal options
    - Reactor safety behaviour and testing experience
- Safety analysis tools
    - Validation and uncertainty qualification
    - Severe accident modelling
    - Probabilistic safety assessment techniques.

The three-dimensional thermal-hydraulics neutronic-coupled model developed in this research work is a potential contributor to most of these topics. It can be directly used to evaluate the design optimisation options (including decay heat removal systems) and its influence in the safety behaviour of the plant, it can test specific safety features that could be implemented in LMFBR designs. It can be also used to define the specifications for the protection systems to act. The work presented here has demonstrated the direct applicability of the models to evaluate the reactor safety behaviour during operation and accidental transient scenarios.

Consequently, the coupled scheme developed stands out for its potential applicability to face the identified upcoming R&D needs of SFR technology.

Future work to improve and refine the capabilities of the developed coupling scheme can be divided into two categories.

On the one hand, in order to reach a higher detail level in the results shown, some limitations identified in the analysis should be tackled. One of these deficiencies that could contribute to refine the results is to solve the identified modelling weaknesses such as the utilisation of a state-of-the-art pin fuel mechanic code to evaluate fuel structure variables or the fine modelling of vessel internals that may influence the flow patterns and systems hydraulic losses.

It has been shown the efforts developed by the different organisations involved in the international research project to give consistency to the code calculations by benchmarking the predicted results. Nevertheless, it is still necessary for all the codes involved in the safety assessments of the designs to be validated against experimental data. There are different initiatives to validate sodium fast reactor analysis tools with the experimental data extracted from past related projects. This validation process should be also applied to the models and tools that are supposed to contribute to the safety assessments of the advanced designs. This is not a straightforward activity since it requires not only a strong modelling effort to be able to reproduce real experimental conditions, but also to develop the experimental facilities for the required experiences to take place.

Further to the results refinement and validation, in order to extend the scope of the analysis shown, the prospective research topics can be envisaged:

- Extension of the thermal-hydraulic code to include multi-phase flow correlations: Currently, most of the system codes, including TRACE code, are limited to monophasic liquid metal coolants. The implementation of state-of-the-art properties and correlations would provide those system codes with the capability to extend the analysis beyond boiling conditions, which is a major safety concern in LMFBR designs.

- Extension of the system codes with more detailed calculation tools. The system codes are developed to analyse the transitory behaviour of a complete system design. However, there are specific features that need to be analysed with a higher detail level, such assembly localised thermal-hydraulic effects (caused by fuel assembly blockages) or detailed behaviour of sodium in large pools. For that reason, the coupling of the system code model with detailed calculation tools would provide the tool with the required definition in those areas where a detailed calculation is required.

- Uncertainty and sensitivity analyses. It is quite clear that models and data used to represent the LMCFBR behaviour under accidental scenarios incorporates uncertainty. Models such as the coupled model proposed in this PhD thesis could be adopted as Best Estimate models used in developing Uncertainty and Sensitivity analysis of the model results within a BEPU methodology. However, further research is envisaged yet to better characterize model and parameter uncertainties and their effect on the simulation results used for safety analysis purposes.

- Use of deterministic safety analysis results within probabilistic safety analysis. As it is proposed in several nuclear technological platforms, proposed designs of LMFBR should undertake Probabilistic Safety Assessment (PSA) as it is an excellent tool to analyse the plant behaviour in case of accident scenarios and the role of the safety systems that are

intended to manage such scenarios. Probabilistic Safety Analysis encompasses not only with DBE (Design Basis Accidents) but also Extended Design Basis Accidents (DBE). The proposed coupled model can be used to perform deterministic safety analysis as part of the input necessary to undertake probabilistic safety analysis, i.e. success criteria of safety systems, safety parameters evolution and core performance, etc.

Bibliography

[Bandini et al, 2013] Bandini G., Bubelis E., Schikorr M., Stempnievicz M., Tucek K., Lázaro A., Kudinov P., Köö K., Jeltsov M., Mansani L., Safety Analysis Results of Representative DEC Accidental Transients for the ALFRED Reactor, Proceedings of the International Conference on Fast Reactors and Related Fuel Cycles (FR13), Paper: CN-199/260, Paris, 2013.

[Blanchet et al, 2009] Blanchet D., Buiron L., ESFR Working horse description, European Sodium Fast Reactor Reactor Consortium - Deliverable SP2.1.2.D1, 2009.

[Becker et al, 2010] M. Becker, S. Van Criekingen, C.H.M. Broeders, The KArlsruhe PROgram System KAPROS and its successor the Karlsruhe Neutronic Extendable Tool KANEXT, http://inrwww.webarchiv.kit.edu/kanext.html, 2010.

[Bubelis E., 2012] Bubelis, E. - Schikorr, M., Personal communication, 2012.

[Buksha et al, 1997] Yu.K. Buksha, Yu.E. Bagdassarov, A.I. Kiryushin, N.G. Kuzavkov, Yu.L. Kamanin, N.N. Oshkanov, V.V. Vylomov, Operation experience of the BN-600 fast reactor, Nuclear Engineering and Design, Volume 173, Pages: 67–79, 1997.

[Chenu, A.-Th, 2011] Chenu A., Single- and Two-Phase Flow Modelling for Coupled Neutronics/Thermal-Hydraulics Transient Analysis of Advanced Sodium-Cooled Fast Reactors. Thesis num: 5172, 2011, EPFL, Switzerland, 2011.

[Chenu et al, 2011] Chenu A., Mikityuk K., Chawla R., Pressure drop modelling and comparisons with experiments for single- and two-phase sodium flow, Nuclear Engineering and Design, Volume 241, Pages: 3898–3909, 2011

[Chetal et al, 2006] S.C. Chetal, V. Balasubramaniyan, P. Chellapandi, P. Mohanakrishnan, P. Puthiyavinayagam, C.P. Pillai, S. Raghupathy, T.K. Shanmugham, C. Sivathanu Pillai, Design of Prototype Fast Breeder Reactor, Nuclear Engineering and Design, Volume 236, Pages: 852-860, 2006.

[Darmet et al, 2012] Darmet, G.; Massara, S., Dynamical analysis of innovative core designs facing unprotected transients with the MAT5-DYN code, Proceedings of ICAPP 2012, Paper num: 12245, Chicago, 2012.

[Dufour et al, 2011] Dufour Ph., Amirabile L., Bandini G., Darmet G., Gallego E., Mikityuk K., Schikkor M., Stempniewicz M., Tosello A., Comparison Case, European Sodium Fast Reactor Reactor Consortium - Deliverable SP3.3.1.D0, 2011.

[Dufour et al, 2012] Dufour Ph., Amirabile L., Bandini G., Darmet G., Gallego E., Mikityuk K., Schikkor M., Stempniewicz M., Tosello A., Representative Transient Analysis, European Sodium Fast Reactor Reactor Consortium - Deliverable SP3.3.1.D1, 2012.

[Ehster, S., 2009] Safety objectives and design principles, European Sodium Fast Reactor Reactor Consortium - Deliverable SP3.1.D1, 2009.

[ENEA-ANSALDO, 2012] Mansani, L., Private Communication, 2012.

[Eur, 2001] European Utility Requirements for LWR Nuclear Power Plants. Revision C, 2001

[Fiorini, 2009] Fiorini G., Description of the work, European Sodium Fast Reactor Reactor Consortium – Grant agreement – Annex I, 2009.

[Fridman et al, 2011] Fridman E., Leppänen J., On the use of the Serpent Monte Carlo code for few group cross section generation. Annals of Nuclear Energy, Volume 38, Pages: 1399–1405, 2011.

[Fridman et al, 2013] Fridman E., Shwageraus E., Modelling of SFR cores with Serpent–DYN3D codes sequence - Annals of Nuclear Energy, Volume 53, Pages: 354–363, 2013.

[Geffraye et al, 2011] Geffraye G., Antoni O., Farvacque M., Kadri D., Lavialle G., Rameau B., Ruby A., CATHARE V2.5: A single version for various applications, Nuclear Engineering and Design, Volume 241, Pages: 4456-4463, 2011.

[GenIV, 2002] A technology Roadmap for Generation IV Nuclear Energy Systems, GIF002-00, 2002.

[GenIV,2014] Technology Roadmap Update for Generation IV Nuclear Energy Systems. The Generation IV International Forum, 2014.

[Genot, 2009] “ESFR Working Horse Loop Concept Description”, European Sodium Fast Reactor Reactor Consortium - Deliverable D4.1.1., 2009.

[HNE-Sodium, 2010] Sodium Fast Reactor: Fuel, Neutronic, Thermal-Hydraulics, Structural Mechanics and Safety, Handbook of Nuclear Energy, Ed. Springer, 2010.

[HNE-Lead, 2010] Lead-Cooled Fast Reactor (LFR) Design: Safety, Neutronics, Thermal, Hydraulics, Structural Mechanics, Fuel, Core and Plant Design, Handbook of Nuclear Energy, Ed. Springer, 2010.

[IAEA, 2001] IAEA NS-G-1.2 – Safety Standards Series. Safety Assessment and Verification for Nuclear Power Plants, International Atomic Energy Agency, 2001.

[IAEA, 2007] IAEA SAFETY GLOSSARY. Terminology used in nuclear safety and radiation protection. International Atomic Energy Agency, 2007.

[IAEA, 2012] IAEA SSR-2/1 – Safety of Nuclear Power plant design. Specific Safety Requirements. International Atomic Energy Agency, 2012.

[Kondo et al, 2013] Kondo S., Deshimaru T, Konomura M, Recent Progress and Status of Monju, Proceedings of the International Conference on Fast Reactors and Related Fuel Cycles (FR13) Paper: CN-199-030, 2013.

[Lassmann et al, 1987] Lassmann K., Hohlefeld F., The Revised URGAP-Model to Describe the Gap Conductance between Fuel and Cladding, Nuclear Engineering and Design, Volume 103, Pages: 215-221, 1987.

[Lázaro et al, 2012] Lázaro A., Ammirabile L., Martorell S., Verdú G., Development of a thermohydraulic model of the European Sodium Fast Reactor (ESFR) using the system code TRACE. Proceedings of the ENC2012 Conference, Manchester, 2012.

[Lázaro et al - S, 2013] Lázaro A., Stanisz P.S., Ammirabile L., Tsige-Tamirat H., Martorell S., Verdú G., Development of a three-dimensional thermohydraulic-neutronic coupling scheme for transient analysis of liquid metal cooled fast reactor technologies using the system code TRACE-PARCS, Proceedings of NURETH15 Conference, Pisa, 2013.

[Lázaro et al - L, 2013] Lázaro A., Tucek K, Ammirabile L., Martorell S., Verdú G., Implementation of thermodynamic properties of lead in the TRACE system code towards its integration in a full-scope platform for safety assessments, , Proceedings of NURETH15 Conference, Pisa, 2013.

[Lázaro et al-I, 2014] Lázaro A., Ammirabile L., Bandini G., Darmet G., Massara S., Dufour Ph., Tosello A., Gallego E., Jimenez G., Mikityuk K., Schikorr M., Bubelis E., Ponomarev A., Kruessmann R., Stempniewicz M., Code assessment and modelling for Design Basis Accident Analysis of the European Sodium Fast Reactor design. Part I: System description, modelling and benchmarking. Nuclear Engineering and Design, Volume 266, Pages: 1-16, 2014.

[Lázaro et al-II, 2014] Lázaro A., Ammirabile L., Bandini G., Darmet G., Massara S., Dufour Ph., Tosello A., Gallego E., Jimenez G., Mikityuk K., Schikorr M., Bubelis E., Ponomarev A., Kruessmann R., Stempniewicz M., Code assessment and modelling for Design Basis Accident analysis of the European Sodium Fast Reactor design. Part II: Optimised core and representative transients analysis. Nuclear Engineering and Design, In Press, 2014.

[Le Coz et al, 2013] Sauvage J, Hamy j, Jourdain V, Biaudis J, Oota H, Chauveau T, Audouin Ph, Robertson D., Gefflot R., The ASTRID project: Status and Future Prospects, Proceedings of the International Conference on Fast Reactors and Related Fuel Cycles (FR13) Paper CN-199-261, Paris, 2013.

[LEADER, 2010] Lead-cooled European Advanced DEmonstration Reactor (LEADER) Euratom 7th Framework Programme Collaborative Project

[LEADER, 2012] Plant data for the safety analysis of the ETDR (ALFRED), LEADER consortium Deliverable 058, 2012.

[LEADER, 2013] Report on the Results of Analysis of DEC Events for the ETDR (ALFRED) – LEADER – Deliverable 022, 2013.

[Massara et al, 2005] Massara S., Tommasi J., Vanier M., Köberl O., Dynamics of critical dedicated cores for minor actinide transmutation, Nuclear technology, Volume 149, Pages: 150-174, 2005.

[Matsuura et al, 2007] Matsuura M., Hatori M., Ikeda M., Design and Modification of Steam Generator Safety System of FBR MONJU, Nuclear Engineering and Design, Volume 237, Pages: 1419-1428, 2007.

[Mikityuk, 2009] Mikityuk K., Heat transfer to liquid metal: Review of data and correlations for tube bundles, Nuclear Engineering and Design, Volume 239, Pages: 680-687, 2009

[Mikityuk et al -ESFR, 2009] ESFR core characterization for safety analysis and review of different design solutions from viewpoint of their impact on safety, European Sodium Fast Reactor Reactor Consortium - Deliverable 3.2.D3, 2012.

[Mikityuk et al, 2010] Specification of the BOL O-ESFR core model for transient analysis, European Sodium Fast Reactor Reactor Consortium, 2010.

[Mikityuk et al, 2011] Mikityuk K., Shestopalov A., FRED fuel behaviour code: Main models and analysis of Halden FA-503.2 tests. Nuclear Engineering and Design, Volume 241, Pages: 2455–2461, 2011.

[NRC, 1995] RELAP5/MOD3 Code Manual Vol2. NUREG/CR-5335-Vol II. Office for Nuclear Regulatory Research. Washington, 1995

[NRC, 2007] TRACE v5.0 Theory and User's manual. Office for Nuclear Regulatory Research. Washington.

[NEA, 2007] Handbook on Lead-bismuth Eutectic Alloy and Lead Properties, Materials Compatibility, Thermal-hydraulics and Technologies, Edition 2007, Chapters 2 and 3, NEA No. 6195, OECD, 2007.

[PARCS, 2010] PARCS v3.0 U.S. NRC Core Neutronics Simulator. User Manual. March 2010.

[Phillipponneau , 1992] Phillipponneau Y., Thermal conductivity of (u, Pu) O2-x mixed oxide fuel. Journal of nuclear materials. Volume 188, Pages: 194-197, 1992.

[RELAP, 1995] RELAP5/MOD3 Code Manual Vol2. NUREG/CR-5335-Vol II. Office for Nuclear Regulatory Research. Washington, 1995

[SARD3.5, 2012] ¨Proposal for a harmonized European methodology for the safety assessment of innovative reactors with fast neutron spectrum to be built in Europe¨ FP7-SARGENIV Consortium - Deliverable D3.5, 2012.

[Sackett, 1997] Sackett, K.I, Operating and test experience with EBR-II, the IFR prototype Progress in Nuclear Energy, Volume 31, Pages: 111–129, 1997.

[Schikorr, 2001] Schikorr, W.M., Assessment of the kinetic and dynamic transient behaviour of sub-critical systems (ADS) in comparison to critical reactor systems, Nuclear Engineering and Design, Volume 210, Pages: 95-123, 2001.

[Sauvage, 2005] Phenix, Une histoire de coeur et d'energie, Commissariat à l'Energie Atomique – CEA, 2005.

[Saraev et al, 2012] Saraev, O.M., Yu. V. Noskov, D. L. Zverev, B. A. Vasil'ev, V. Yu. Sedakov, V. M. Poplavskii, A. M. Tsibulya, V. N. Ershov, S. G. Znamenskii, BN-800 design validation and construction status, Atomic Energy, Volume 108, Pages:248-253, 2012.

[SNETP, 2009] Sustainable Nuclear Energy Technology Platform (SNETP) - Strategic Research Agenda, 2009.

[Stempniewicz, 2010] Stempniewicz M., SPECTRA Sophisticated Plant Evaluation Code for Thermal-Hydraulic Response Assessment, Version 3.60, April 2010, Volume 1 – Program Description, Volume 2 – User's Guide, Volume 3 – Subroutine Description, Volume 4 - Verification and Validation, Nuclear Research Group - NRG, 2010.

[Sunderland, 2012] ESFR cores with optimised characteristics, European Sodium Fast Reactor Reactor Consortium - Deliverable 2.1.5.D1, 2012.

[Takamichi et al, 1988] The Physical Properties of Liquid Metals. Oxford University Press 1988.

[Vasile et al, 2011] Vasile A., Fiorini G., European Commission - 7th Framework Programme, The Collaborative Project on European Sodium Fast Reactor (CP-ESFR), Nuclear Engineering and Design, Volume 241, Pages: 3461 – 3469, 2011.

[WalRe,1981] ¨Fast Breeder Reactors¨ A. Waltar, B. Reynolds. Pergamon Press, 1981.

[Wolfert et al, 1988] Wolfert Y., Brittain I., CSNI validation matrix for PWR and BWR thermal-hydraulic system codes. Nuclear Engineering and Design, Volume 108, Pages 107–119, 1988.

[Xu, M., 2000] "Chinese fast reactor technology development", The 5th Nuclear Energy Symposium on Energy Future in the Asia/Pacific Region—Research & Education for Nuclear Energy, Pages: 28–37, Beijing, 2000.